

Optoelectronic oscillators with time-delayed feedback

Yanne K. Chembo*

*University of Maryland, A. James Clark School of Engineering,
Department of Electrical and Computer Engineering,
and Institute for Research in Electronics and Applied Physics (IREAP),
8279 Paint Branch Drive, College Park, Maryland 20742, USA*

Daniel Brunner, Maxime Jacquot, and Laurent Larger

*FEMTO-ST Institute, CNRS and Université Bourgogne Franche-Comté,
15B Avenue des Montboucons, 25030 Besançon cedex, France*

 (published 25 September 2019)

Time-delayed optoelectronic oscillators are at the center of a large body of scientific literature. The complex behavior of these nonlinear oscillators has been thoroughly explored both theoretically and experimentally, leading to a better understanding of their dynamical properties. Beyond fundamental research, these systems have also inspired a wide and diverse set of applications, such as optical chaos communications, pseudorandom number generation, optoelectronic machine learning based on reservoir computing, ultrapure microwave generation, optical pulse-train synthesis, and sensing. The aim of this review is to provide a comprehensive survey of this field, to outline the latest achievements, and discuss the main challenges ahead.

DOI: [10.1103/RevModPhys.91.035006](https://doi.org/10.1103/RevModPhys.91.035006)

CONTENTS

I. Introduction	1	C. Phase noise of single-loop OEOs	25
A. Early architectures	2	D. Multiloop OEOs	28
B. Introducing the time delay	3	E. Multifrequency OEOs	29
C. Modern concept of optoelectronic oscillator	4	F. Tunable OEOs	29
D. OEOs in science and technology	5	G. Millimeter-wave OEOs	30
E. Outline	5	H. Optical-pulse OEOs	30
II. Broadband OEOs: Nonlinear Dynamics and Complexity	5	I. Whispering-gallery mode resonator OEOs	31
A. Modeling Ikeda-like OEOs	5	J. Other architectures of narrow-band OEOs	32
B. Low-pass filter OEOs	6	K. OEOs for signal processing	33
C. Broad bandpass filter OEOs	7	L. From ultrapure to ultrastable OEOs	33
D. Semiconductor lasers with optoelectronic feedback	10	VI. OEO Sensing Applications	35
E. Spatiotemporal systems	11	A. Magnetic field and refraction index sensing	35
F. OEOs in the quantum regime	12	B. Load and strain sensing	35
III. OEO-based Chaos Synchronization and Communications	13	C. Temperature and pressure sensing	35
A. Principles of chaos communications	13	D. Distance, rotation, and vibration sensing	36
B. OEO architectures for chaos communications	14	E. Multiphysics sensing	37
C. Performance evaluation and optimization	15	VII. Conclusion and Perspectives	37
D. Security analysis and enhancement	16	Acknowledgments	38
E. Synchronization in networks	17	References	38
F. Random number generation	17		
G. Chaotic radars, lidars, and radio communications	18		
IV. OEO-based Reservoir Computing	18		
A. The concept of neuromorphic photonic computing	18		
B. Principles of delay-based reservoir computing	19		
C. Basic architecture of OEO reservoir computer	19		
D. Other architectures of OEO reservoir computers	20		
E. Optimal processing for OEO reservoir computing	21		
F. OEOs as neuromorphic autaptic systems	21		
V. Narrow-band OEOs for Ultrapure Microwave Generation	22		
A. Deterministic dynamics of narrow-band OEOs	22		
B. Phase noise as a measure of spectral purity	24		

I. INTRODUCTION

Optoelectronic oscillators (OEOs) are nonlinear, dissipative, and autonomous systems characterized by a closed feedback loop that is formed with two concatenated optical and electronic branches. Energy alternatively flows in this loop under the electric and optical forms, and, in general, the overall round-trip time T in the loop is not negligible with regards to the other time constants of the system as represented in Fig. 1. For this reason, optoelectronic oscillators belong to the family of time-delayed dynamical systems.

Despite the conceptual simplicity of their architectures, optoelectronic oscillators have been at the root of major scientific advances in the last 50 years, from the fundamental, applied, and technological viewpoints. This can be explained

*ykchembo@umd.edu.

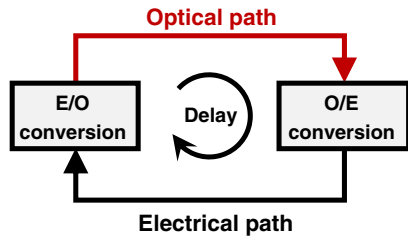


FIG. 1. Generic representation of an optoelectronic oscillator with time-delayed feedback. Energy flows alternatively in the optical and electrical forms, and conversion between both paths is performed by electrical-to-optical (E/O) and optical-to-electrical (O/E) converters. This closed-loop system is always *nonlinear*, *dissipative*, and *infinite dimensional* because of the time delay. The interplay between these three properties is the main source of dynamical complexity in OEOs. For metrological applications, a fourth property, *stochasticity*, becomes relevant as well.

by the fact that these oscillators can simultaneously output signals in both the electrical (~ 0 – 100 GHz) and the optical (~ 50 – 500 THz) spectral ranges. Access to such large bandwidths in these spectral domains has been enabled by the optical and wireless telecommunication industry, which has become a mature technological segment in the last 30 years. As a result, researchers have obtained access to a broad choice of commercial off-the-shelf components to process electrical and optical signals with unprecedented tunability, precision, and reliability. Moreover, optical-to-electrical conversion in optoelectronic oscillators is generally performed by a device that is insensitive to the optical phase or polarization state (e.g., a photodiode): consequently, the experimental constraints related to laser light coherence are relaxed and the system benefits from improved robustness and controllability. In the electrical domain, the signals can be accurately processed using devices such as phase shifters, amplifiers, filters, multipliers, or even software-based electronic modules. In the optical domain, the guided propagation of laser beams is facilitated by ultralow loss and ultrabroad bandwidth optical fibers. The light waves can be processed as well using all-optical devices such as filters, amplifiers, dispersion compensation modules, or nonlinear frequency converters. The transduction from the electrical to the optical domain (and vice versa) can be performed with a wide diversity of electro-optic or optoelectronic devices, with bandwidths as large as 100 GHz. Therefore, the dual-spectral-range property of optoelectronic oscillators has allowed them to benefit from key advantages inherent to signal processing in both the light-wave and microwave spectral domains and to become a paradigmatic system for optoelectronics and microwave photonics.

A. Early architectures

The inception of optoelectronic oscillators can be traced back to the late 1960s, that is, about 10 years after the invention of the laser. Researchers noted that many lasers were often displaying a time-varying optical output, modulated in the radiofrequency (rf) range. For all practical purposes, they

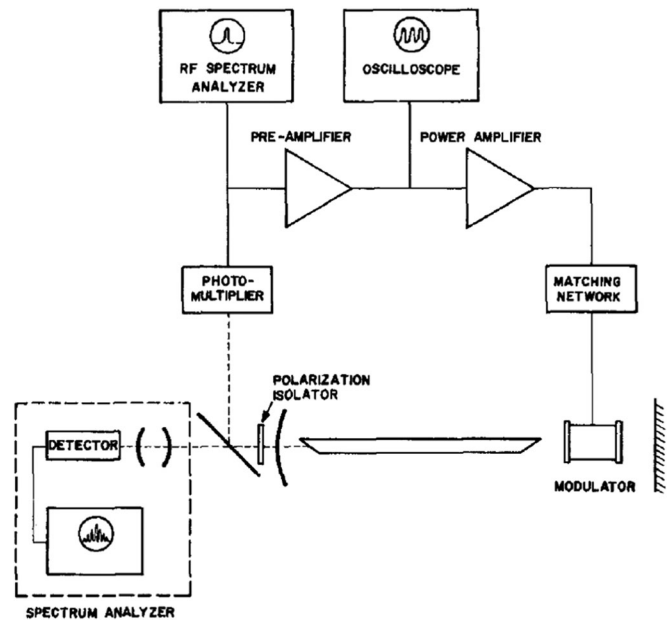


FIG. 2. One of the earliest architectures of the optoelectronic oscillator, consisting of an He-Ne laser with optoelectronic feedback. Analogously to the generic configuration displayed in Fig. 1, this system has an optical path (from the modulator to the photomultiplier) concatenated to an electrical path (from the photomultiplier back to the modulator). This feedback scheme permitted one to achieve stable mode locking between the longitudinal modes of the laser. From [Huggett, 1968](#).

classified this undesirable behavior as an “instability” and started to explore various methods to stabilize the lasers. They realized that photodetecting the laser output and feeding it back to the laser system itself could simultaneously stabilize both the optical and the radio-frequency signals, thereby foreshadowing the fundamental idea of optoelectronic oscillators—a closed-loop autonomous system featuring an optical and an electronic branch. One of the earliest architectures of optoelectronic oscillators along that line was proposed by [Huggett \(1968\)](#), who was working with a multimode He-Ne laser with 75 MHz longitudinal mode spacing; see Fig. 2. Interestingly, this early OEO was designed to operate in a regime where the oscillations were quenched, and stable mode locking was achieved by feeding back a portion of optical output to the laser using a potassium dideuterium phosphate (KD*P) longitudinal modulator placed in the laser cavity. [Paoli and Ripper \(1970a, 1970b\)](#) considered the case where the time-varying output was induced by pronounced relaxation oscillations in GaAs injection lasers (with frequency ~ 500 MHz), and they showed that feeding back a photodetected portion of the optical output to the pump current can efficiently stabilize these anharmonic relaxations oscillations, thereby yielding narrow pulse trains in the optical domain.

In these early versions of optoelectronic oscillators, the nonlinearity of the feedback loop was provided by the laser itself, and therefore, lacked both tunability and controllability. A major conceptual breakthrough was proposed by [Smith and Turner \(1977\)](#) from Bell Labs, in a pioneering article which explained how a nonlinear crystal placed in a Fabry-Perot

resonator can play this role of external, fully controllable nonlinearity. In their experimental setup, the nonlinear Fabry-Perot cavity was pumped by a He-Ne laser and the photodetected output was fed back to the intracavity lithium niobate (LiNbO₃) crystal. The system featured a bistable behavior that could be controlled by the laser pump power. The nonlinear behavior of this oscillator architecture was further investigated by the same group in a subsequent series of papers (Smith, Turner, and Maloney, 1978; Smith *et al.*, 1978; Smith, Turner, and Mumford, 1978). McCall (1978) later showed that similar systems were suitable to convert continuous-wave (cw) laser power into a stable train of short optical pulses.

An important innovation was provided by Garmire *et al.* (1978) and Garmire, Marburger, and Allen (1978) when they demonstrated that the same functionalities could be implemented by a simpler system, where the nonlinear Fabry-Perot resonator was replaced by a lithium niobate waveguide modulator. This mirrorless configuration opened the way for chip-scale integration, and it was moreover wavelength versatile as it could operate with either a monomode or a multimode pump laser. Interestingly, these modulator-based systems had the capability to operate beyond bistability and display multistability as well (Okada and Takizawa, 1979). Feldman (1978) also proposed similar mirrorless architecture where the modulators were replaced by Pockels cells.

The main drawback of the lithium niobate waveguide or Pockels cells architectures previously presented was the need for relatively high voltages (~50–100 V) in order to control the nonlinear transfer function. This problem was solved with the introduction of integrated lithium niobate Mach-Zehnder interferometers (Ito, Ogawa, and Inaba, 1979; Schnapper, Papuchon, and Puech, 1979) that allowed one to achieve full controllability of the nonlinearity with voltages of the order of only a few volts. Indeed, the relevance of Mach-Zehnder modulators had been theoretically discussed earlier by Kersten (1978) in the context of analog signal processing in optical telecommunication networks.

In the early 1980s, the first concrete applications of these pioneering architectures of optoelectronic oscillators started to emerge, following the trend of introducing nonlinear optoelectronic systems in electrical and communication engineering (Abraham and Smith, 1982). For example, microwave generation was demonstrated with frequencies ranging from 400 MHz (Schlaak, Neyer, and Sohler, 1980) to 1.5 GHz (Neyer and Voges, 1982b). The multistability induced by the electro-optical nonlinearity was used as well to implement novel architectures of multivibrators (Sohler, 1980; Neyer and Voges, 1982c), or as an enabling concept for clock generation in optical communications (Schlaak and Kersten, 1981).

In the research previously highlighted on optoelectronic oscillators, the dynamical effects induced by finite bandwidth and time delay were systematically disregarded. These systems were therefore essentially analyzed as nonlinear dipoles, in the approximation of null transient times. This simplistic approximation is correct when the system is static, but loses its accuracy in the oscillatory regime, where the high cutoff frequency of the oscillation loop, or equivalently its smallest transient response time, has to be accounted for. In this context, Garmire *et al.* (1979) studied the switching time of a bistable optoelectronic

oscillator with a Pockels cell as it evolved between two stable states; Okada and Takizawa (1980) considered the dynamics of optical regenerative oscillation and pulse generation in an optoelectronic oscillator with a lithium niobate waveguide modulator, and Kaplan (1981) proposed a nonlinear analysis of an optoelectronic oscillator with an electro-optically driven interface. As far as optoelectronic oscillators with Mach-Zehnder modulators are concerned, their nonlinear dynamics was initially investigated by Neyer and Voges (1981), in a work where they synchronized their optoelectronic oscillator to an external signal, thereby providing an experimental illustration of Adler theory on phase locking. Ito, Ogawa, and Inaba (1981) introduced quadrature phase-shift-keying (QPSK) Mach-Zehnder modulators in the oscillation loop and analyzed the nonlinear dynamics of the system as the operating parameters of the modulator were tuned.

B. Introducing the time delay

Accounting for the response times of the feedback loop was a fundamental requirement in order to analyze the oscillatory behavior of the early architectures of optoelectronic oscillators: however, this was initially not the case for the feedback time delay. This is because the feedback paths were relatively short (from a few cm to ~1 m), and accordingly the time delays were relatively small as well (a few ns at most). Therefore, time delay was negligible in these oscillators, which had a bandwidth far below the GHz range. This is why the earliest architectures of optoelectronic oscillators with time-delayed feedback generally featured a long delay line that was inserted *on purpose*.

The initial motivation to introduce an additional delay in the optoelectronic oscillator feedback loop originated from new theoretical insight in the area of nonlinear dynamics in time-delayed systems. Ikeda (1979) proposed an equation (now eponymous) to describe the complex dynamics of a laser field confined in a four-mirror ring optical cavity, where laser light was propagating freely with a small segment involving a nonlinear element. This class of optical systems was initially introduced by Bonifacio and Lugiato (1978a, 1978b), who theoretically investigated some of the related instabilities. The Ikeda equation can be written in the form

$$\varphi + \tau\dot{\varphi} = A^2\{1 + 2B \sin[\varphi(t - T) + C]\}, \quad (1)$$

where φ is the optical phase shift determined by the ring-feedback interference condition in the nonlinear element, the overdot denotes the derivative with regard to time, τ is the response time of the low-pass filtering feedback loop, T is the delay time corresponding to the intracavity round-trip time, while the sinusoidal transfer function of the feedback loop is defined by the real-valued parameters A , B , and C . The main impact of the Ikeda equation (1) has been to demonstrate that a simple model accounting for both time delay and nonlinearity in a dynamical system could lead to a rich and complex behavior. Indeed, shortly after, Ikeda, Daido, and Akimoto (1980) published a second article where they theoretically studied the bifurcation sequence of this equation from steady state to what they called “optical turbulence,” which corresponds to deterministic chaos in modern terminology.

The experimental confirmation of the theoretical ideas pioneered by Ikeda was provided by Gibbs *et al.* (1981) in a work where they demonstrated an optoelectronic oscillator that could be precisely modeled using the Ikeda equation. The nonlinear element of their optoelectronic oscillator was a Pb-based lanthanum-doped zirconate titanate piezoelectric crystal sandwiched between crossed polarizers, and the time delay was originating from an electrical feedback delay line. Strikingly enough, it should be noted that the original system proposed by Ikeda was not an optoelectronic oscillator because the feedback loop was all optical (Ikeda, 1979).

Shortly after the work of Gibbs *et al.*, the Ikeda dynamics was studied in two architectures of optoelectronic oscillators with integrated Mach-Zehnder modulators. Okada and Takizawa (1981) studied the case where the time delay is comparable to the response time of a low-pass filtering feedback loop ($T \sim \tau$). They experimentally and theoretically demonstrated various complex behaviors such as multiperiodicity and chaos. On the other hand, Neyer and Voges (1982a) investigated the asymptotic case where the delay is significantly larger than the response time of the feedback loop ($T \gg \tau$). In this regime, the response time τ can be neglected and the dynamical equation (1) degenerates then to the map $\varphi_{n+1} = A^2\{1 + 2B \sin[\varphi_n + C]\}$, where the discrete time steps n correspond to integer units of the time delay T . This system displays the typical period-doubling route to chaos as the feedback gain β is increased. The work of Neyer and Voges was a convincing demonstration that optoelectronic oscillators are ideal experimental benchmarks to investigate the fundamental concepts related to the complexity of iterated maps, mainly popularized by May (1976) and Feigenbaum (1980). From a broader perspective, the consideration of time delay has also opened as well a new field of research in relation to the complex dynamics of photonic systems with time delay (Soriano, García-Ojalvo *et al.*, 2013).

Beyond the nonlinear dynamics of time-delayed systems, there was another motivation to add a delay line in optoelectronic oscillators, and it was related to radio frequency and optical-pulse generation for engineering applications. Damen and Duguay (1980) introduced a system for pulse generation where the feedback loop cascaded a cw AlGaAs diode laser with adjustable dc bias current, an optical delay line, a fast photodiode, and a broadband amplifier whose output was used to close the loop onto the laser itself. In their system, which was named “optoelectronic regenerative pulser,” the delay time was not *per se* significantly large (~ 8 ns), but it was relevant because the intrinsic cutoff frequency of the feedback loop was far beyond a GHz, thereby allowing for pulse generation with pulse widths well below 100 ps. As far as the rf generation is concerned, Nakazawa, Tokuda, and Uchida (1981) proposed a system that included a few-km-long fiber delay line in a reflection configuration. They demonstrated that single-mode operation could be achieved when the high cutoff frequency of the loop bandwidth was set to 300 kHz, thereby generating signals in the low-frequency band. A multimode operation yielding square waves in the time domain was achieved when the bandwidth was increased to 400 MHz. Nakazawa, Nakashima, and Tokuda (1984) later on referred to this system as an “optoelectronic oscillator” and analyzed its stability. Shortly after, Grigor’yants *et al.* (1985)

emphasized the potential of optoelectronic oscillators for fiber sensing applications.

As it will appear later on, this quest for new methods to generate radio-frequency signals will play a key role in the development of novel architecture of optoelectronic oscillators and establish them as central systems in microwave photonics.

C. Modern concept of optoelectronic oscillator

A turning point for the science and technology of optoelectronic oscillators was the work of Yao and Maleki (1994) from the NASA Jet Propulsion Laboratory, where they introduced a narrow-band optoelectronic system for ultrastable microwave generation. Their idea was to perform energy storage in a fiber delay line instead of a high-finesse radio-frequency filter. Indeed, storing laser light energy instead of microwave energy was a conceptual breakthrough which provided a technological pathway toward improved purity and stability for radio-frequency signals at room temperature. A continuous-wave laser was used to seed a Mach-Zehnder modulator, whose output traveled in a few-km-long optical fiber delay line before being photodetected. The generated microwave beat note signal was then frequency filtered, amplified, and connected back to the modulator to close the feedback loop. In a subsequent series of three articles where they analyzed in detail the metrological performances of their microwave generator, they referred to it as an optoelectronic oscillator and introduced as well the acronym “OEO” (Yao and Maleki, 1996a, 1996b, 1996c). The broad appeal of this novel

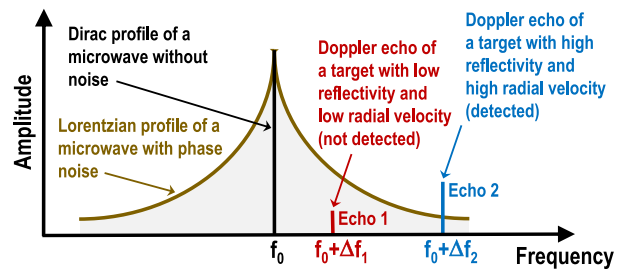


FIG. 3. Illustrative example of an application of OEOs (Doppler radars). In their simplest configuration, pulsed radars allow the determination of distances by monitoring the round-trip time of flight of a microwave pulse bouncing back from a target, while continuous-wave (or Doppler) radars are used instead to monitor the velocity of targets via the Doppler frequency shift of the reflected microwave (note that both distance and radial velocity can be measured simultaneously using pulse-Doppler radars). When a noiseless microwave (Dirac peak) of frequency f_0 is used as a radar probe, the target generates a Doppler echo of frequency $f_0 + \Delta f$, where the Doppler shift $\Delta f = [2v/c]f_0$ is proportional to the radial velocity v of the target, with c being the velocity of light in vacuum. However, radar probe microwaves are necessarily noisy (Lorentzian profile), so that targets with low reflectivity and/or radial velocity have a spectral signature like Echo 1 that might not be detected for being indiscernible from the microwave phase noise background (gray area). For this reason, ultralow phase noise microwaves are critically needed in aerospace engineering applications, and narrow-band OEOs provide a mature technological platform to generate such ultrapure signals, as discussed in Sec. V.

microwave oscillator was rooted in its simple architecture, its frequency versatility, and its competitive microwave phase noise performance (Maleki, 2011). As evidenced in Fig. 3 with the case of Doppler radars, these oscillators are now expected to provide novel technological platforms for many scientific and engineering applications.

In most scientific works, as well as in this review, the term optoelectronic oscillator and the acronym OEO are used in a broad sense to describe any autonomous oscillator that concatenates an electronic and an optical branch, as in Fig. 1. This nomenclature permits a unifying synthesis for the wide body of cross-disciplinary literature related to these hybrid systems, where the very same physical effects or concepts are frequently labeled with different names.

D. OEOs in science and technology

In the last 20 years, there has been a steady growth in the number of publications related to OEOs from both the scientific and the technological viewpoints. As a consequence, the OEO has become one of the most studied systems in optoelectronics and microwave photonics (Larger and Dudley, 2010).

From the fundamental side, OEOs permit one to investigate the properties of nonlinear time-delayed systems (Erneux, 2009). Such dynamical systems can be written under the form $\dot{\mathbf{x}} = \mathbf{F}(\mathbf{x}, \mathbf{x}_T)$, which corresponds to a flow where $\mathbf{x} = (x_1, \dots, x_N)$ is a N -dimensional real-valued vector, $\mathbf{x}_T \equiv \mathbf{x}(t - T)$ is its delayed counterpart, and \mathbf{F} is a N -dimensional algebraic function. Contrary to ordinary differential equations where the initial conditions are given by a discrete and finite set of values, initial conditions in delay-differential equations should be specified using a function $g(t)$ defined on the continuous interval $[-T, 0]$, so that an infinity of values has to be initially known to fully characterize a unique solution of the system. In this regard, delay-differential equations (DDEs) are mathematically infinite dimensional, exactly as spatially extended systems ruled by partial differential equations (Arecchi *et al.*, 1992; Yanchuk and Giacomelli, 2017). Because the timescales and delay time in OEOs can be distributed over up to 10 orders of magnitude, they emerged as excellent experimental benchmarks to investigate the rich bifurcation structure originating from the interplay between infinite dimensionality and nonlinearity, leading to complex dynamical states such as slow-fast relaxation oscillations, pulse-package trains, chaotic breathers, chimera states, or hyperchaos.

From the applied perspective, propositions for innovative technological systems have been remarkably plentiful and diverse. As highlighted in the preceding section, OEOs are used for ultrastable microwave generation and deliver some of the best phase noise performances at room temperature. OEOs are widespread in optical chaos communication architectures and have permitted successful demonstrations of multi-Gbit/s transmission in metropolitan optical fiber networks. Still in the hyperchaotic regime, they are proven to be efficient sources of entropy for ultrafast (gigasamples/s) random number generation, while passing some of the most stringent randomness tests. OEOs are a cornerstone in the emerging field of photonic reservoir computing and proved their potential in

established benchmarks such as spoken-digit recognition or time-series forecasting. OEOs also have been developed for high-speed and high-sensitivity sensing of magnetic fields, temperature, pressure, or distance.

The purpose of the present review is therefore to provide an extended survey of the latest theoretical, experimental, and state-of-the-art technological advances related to these OEOs.

E. Outline

This review is divided into five main parts, which cover the most active research areas in the field of time-delayed optoelectronic oscillators.

Section II is devoted to the nonlinear dynamics and complexity of broadband OEOs. The topic of optical chaos synchronization and communications is reviewed in Sec. III, while Sec. IV deals with optoelectronic reservoir computing. Ultrapure microwave generation using narrow-band OEOs is discussed in Sec. V, and Sec. VI provides an overview of the sensing applications. Research perspectives for OEOs are discussed in the last section, which also concludes this review.

II. BROADBAND OEOs: NONLINEAR DYNAMICS AND COMPLEXITY

Broadband (or wideband) OEOs are characterized by an electrical bandwidth that spans at least an octave, and typically more than a decade, in frequency. The combination of high gain, nonlinearity, broad bandwidth, and time delay permits the observation of a wide diversity of complex and high-dimensional dynamical behaviors in these systems, including multistability, excitability, chaotic breathers, pulse packages, chimera states, and fully developed hyperchaos. We outline in this section the main theoretical concepts related to broadband OEO models, along with the corresponding experimental demonstrations.

A. Modeling Ikeda-like OEOs

Ikeda-like OEOs have an architecture characterized by a feedback loop with four essential elements, namely, the linear gain β , the nonlinear function f_{NL} , the spectral linear filtering function $H(i\omega)$, and the time delay T . In the time domain, the dynamics of the system can be tracked by a scalar dynamical variable $x(t)$, and its counterpart $X(i\omega)$ in the Fourier domain obeys

$$H^{-1}(i\omega)X(i\omega) = \beta F_{\text{NL}}(i\omega)e^{-i\omega T}, \quad (2)$$

where $F_{\text{NL}}(i\omega)$ is the Fourier transform of the time-domain signal $f_{\text{NL}}[x(t)]$ (Larger, 2013). When the filter is passive, the linear filter $H(i\omega)$ is characterized by an impulse function $h(t)$, which is its inverse Fourier transform, fulfilling $h(t) = 0$ for $t < 0$ (causality) and $\int_0^{+\infty} |h(s)| ds < +\infty$ (stability). In general, the spectral filtering function can be explicitly expressed as $H(i\omega) = \sum_{k=0}^m [a_k \times (i\omega)^k] / \sum_{k=0}^n [b_k \times (i\omega)^k]$ with $m < n$, where a_k and b_k are constant coefficients. In the particular case where its inverse $H^{-1}(i\omega)$ can be expanded exactly as a truncated summation of the kind $\sum_k c_k \times (i\omega)^k$ with c_k being constant coefficients and $k \in \mathbb{Z}$, the inverse

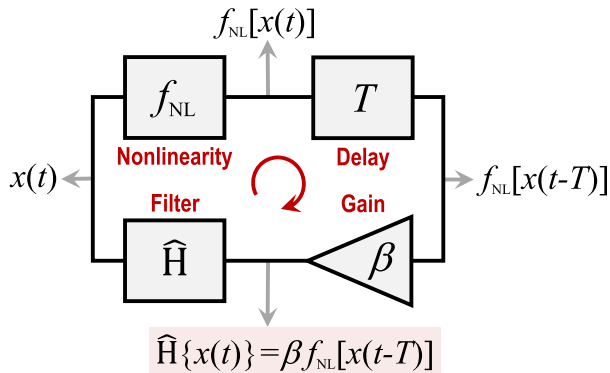


FIG. 4. Time-domain block diagram for an Ikeda-like OEO. The variable $x(t)$ circulates in the clockwise direction and is subjected to the four main elements of the loop, namely, the nonlinearity f_{NL} , the time delay T , the gain β , and the linear filter \hat{H} . The closure condition of the feedback loop yields Eq. (3) that governs the OEO dynamics.

Fourier transform on both sides of Eq. (2) yields the following equation in the time domain:

$$\hat{H}\{x(t)\} = \beta f_{\text{NL}}[x(t-T)], \quad (3)$$

where $\hat{H}\{x(t)\}$ is a linear integrodifferential operator, which can also be viewed as an input-output system obeying $\hat{H}\{x_{\text{out}}\} = x_{\text{in}}$. By definition, we refer to Eq. (3) as an *Ikeda-like* equation. The interplay between f_{NL} , T , β , and \hat{H} , which are the four elements of the oscillator block diagram, will rule the complex dynamical behavior of these OEOs, as schematically explained in Fig. 4. A typical example of Ikeda-like OEO architecture is presented in Fig. 5, and many versions of this experimental setup have been developed for both fundamental and applied research.

B. Low-pass filter OEOs

An important class of broadband OEOs corresponds to those involving a low-pass filter. The simplest way to model

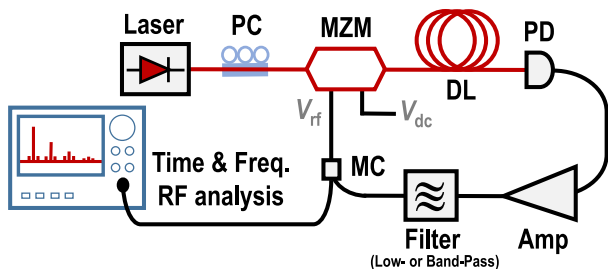


FIG. 5. Experimental setup for one of the most common implementations of Ikeda-like OEOs. The dynamical variable here is the voltage V_{rf} at the radio-frequency input of the Mach-Zehnder modulator, which induces a sinusoidal nonlinearity in the feedback loop with a constant offset phase proportional to V_{dc} . The filter can be of the low-pass or bandpass kind. In the latter case, it can feature either a narrow or a broad bandwidth. PC: polarization controller; MZM: Mach-Zehnder modulator; DL: delay line; PD: photodiode; Amp: rf amplification; MC: microwave coupler.

such systems is to consider a first-order filter with high frequency cutoff f_{H} . Therefore, one can rewrite Eq. (3) under the form

$$\hat{H}\{x\} \equiv x + \tau \dot{x} = \beta f_{\text{NL}}[x_T], \quad (4)$$

where $\tau = 1/2\pi f_{\text{H}}$ is the time constant related to the filter, and $x_T \equiv x(t-T)$ is the delayed dynamical variable.

This low-pass filter DDE actually degenerates to the original Ikeda equation (1) when f_{NL} is a sinusoidal function. In fact, this situation corresponds to most experimental implementations of low-pass filter OEOs because the nonlinear function f_{NL} generally originates from interferometric devices. Ikeda OEO architectures along this line are particularly versatile and allow for the variable x to stand for different electric (voltage, current) or optical (phase, wavelength, power, or coherence) signals in the feedback loop.

The pioneering experiment of Gibbs *et al.* (1981) described in Sec. IB considered the phase of a laser field as the dynamical variable, exactly as in the original Ikeda equation. The OEO architectures proposed by Okada and Takizawa (1981) and Neyer and Voges (1982a) used an integrated Mach-Zehnder modulator as a nonlinear element, and the Ikeda variable x was the rf voltage at the input of the modulator. Vallée and Delisle (1985) proposed an acousto-optical oscillator where the Ikeda variable was also a rf voltage, here needed to drive the modulated diffraction pattern of a Bragg cell. In other architectures, the Ikeda variable was the wavelength of a tunable laser: For example, Larger, Goedgebuer, and Merolla (1998) proposed a wavelength Ikeda oscillator using a distributed Bragg reflector (DBR) laser diode that was wavelength tunable via the injection current of the passive DBR section, and the nonlinearity was ensured by a birefringent plate placed between two crossed polarizers. Larger *et al.* (2001) implemented as well an OEO pumped by a superluminescent diode, where the dynamical variable x was the optical path difference controlling the temporal coherence of the broadband source. Recent work from Chembo *et al.* (2016) used an OEO to demonstrate Ikeda temporal chaos in the color-selection mechanism from the visible spectrum of a supercontinuum light source. In this work, the bandwidth of the chaotic acousto-optically driven dynamics was purposely set low enough in order to restrict the color-selection dynamics within the human-eye bandwidth (few Hz). This system was motivated by a broad audience dissemination project in the framework of the International Year of Light 2015, thus enabling the direct observation of chaotically changing colors over the full visible spectrum. It is worth noting that all the Ikeda OEOs previously highlighted feature a relatively low bandwidth, generally lower than 1 MHz.

Some of the key properties of the nonlinear dynamics associated with the Ikeda equation had originally been identified as soon as this equation was proposed, with a particular emphasis on its bifurcation diagram as a function of the feedback gain parameter β (Ikeda, 1979; Ikeda, Daido, and Akimoto, 1980). In general, the system has one or several stable fixed points when β is low. A primary Andronov-Hopf bifurcation (simply referred as ‘‘Hopf bifurcation’’ throughout this review) occurs as β is increased, leading to a limit-cycle

oscillation. Further increase of the gain leads to a period-doubling bifurcation sequence, and ultimately, to chaos.

The specific dynamical properties of this bifurcation sequence critically depend on the ratio T/τ . In the regime of long delay time ($T/\tau \gg 1$), the system is very high dimensional and displays a wide variety of complex behaviors, and most notably, high-dimensional hyperchaos. Indeed, [Vicente *et al.* \(2005\)](#) showed that the Kaplan-Yorke dimension of the Ikeda OEO asymptotically scales as $d_{KY} \propto \beta T/\tau$, while the Kolmogorov-Sinai entropy grows as $h_{KS} \propto \beta$, in agreement with previous theoretical predictions from [Dorizzi *et al.* \(1987\)](#). In experimental setups allowing for very high gain, this property has permitted the generation of fully developed hyperchaos with up to ~ 250 null and positive Lyapunov exponents, corresponding to ~ 500 dimensions ([Goedgebuer *et al.*, 1998](#)). On the other hand, in the regime of short delay time ($T/\tau \sim 1$), the system mostly displays multistability, quasiperiodic oscillations, and eventually low-dimensional chaos ([Yaowen *et al.*, 1999](#); [Udaltsov *et al.*, 2001](#)). A unified theory for the primary Hopf bifurcation in the Ikeda system was proposed by [Erneux *et al.* \(2004\)](#), and they showed that it featured a four-periodic sinusoidal solution in the limit of large delay, and a two-periodic square-wave solution in the limit of small delay.

Examples of low-pass filter Ikeda-like OEOs where f_{NL} is not a sinusoidal function are scarce. Notable exceptions are the works of [Liu and Ohtsubo \(1992\)](#) and [Takizawa, Liu, and Ohtsubo \(1994\)](#), who considered laser diodes with optoelectronic delayed feedback, with the Ikeda variable being the laser power. The nonlinearities were induced in the optical branch by a Twyman-Green interferometer in the first case, and by a Fabry-Perot interferometer in the second. In both cases, the oscillator displayed period-doubling routes to chaos in the limit of large delay, as the gain was increased. Another example is the wavelength Ikeda OEO introduced by [Chiang *et al.* \(2002\)](#), with a setup involving an externally tunable semiconductor laser diode and nonlinearity provided by the transfer function of a Fabry-Perot cavity.

C. Broad bandpass filter OEOs

Broad bandpass OEOs feature an electric path cascading a high-pass and a low-pass filter, characterized by low and high cutoff frequencies f_L and f_H , respectively. In the simplest configuration, both filters can be considered of the first order and in that case the Ikeda-like equation (3) can be rewritten under the form of an integrodifferential delay equation

$$\hat{H}\{x\} \equiv \left(1 + \frac{\tau}{\theta}\right)x + \tau\dot{x} + \frac{1}{\theta} \int_0^t x(s)ds = \beta f_{NL}[x_T], \quad (5)$$

where $\tau = 1/2\pi f_H$ and $\theta = 1/2\pi f_L$. Generally, the condition $\tau/\theta = f_L/f_H \ll 1$ holds for broadband OEOs. Accordingly, the simplification $(1 + \tau/\theta)x \simeq x$ is almost always considered in Eq. (5) and henceforth considered as well throughout this review.

As in the low-pass case, the dynamical variable x in broad bandpass OEOs can stand for various electrical or optical signals. The first architecture was implemented by [Goedgebuer *et al.* \(2002\)](#), where the dynamical variable was the rf voltage

at the input of an integrated Mach-Zehnder modulator in the 24–166 MHz frequency range. In the high-gain regime, this OEO was able to output a hyperchaotic signal with a Lyapunov dimension of ~ 3700 . A novel time-delayed OEO was proposed by [Blakely, Illing, and Gauthier \(2004\)](#) using a Mach-Zehnder interferometer as passive nonlinearity, and a semiconductor laser as a current-to-optical frequency converter. The dynamical variable was the output power of the laser, which had a base-band bandwidth in the 7–240 MHz range. [Gastaud *et al.* \(2004\)](#) developed a bandpass Ikeda-like OEO where the bandwidth was significantly expanded and spanned from 30 kHz to ~ 7 GHz for the base-band voltage variable. [Genin *et al.* \(2004\)](#) introduced a broad bandpass OEO where the dynamical variable was the optical phase of a laser signal, with a bandwidth ranging from a few tens of kHz to 5 GHz. A bandwidth improvement up to 13 GHz for a phase dynamics OEO was later on achieved by [Lavrov *et al.* \(2009\)](#), using a linear phase modulator cascaded to a differential phase-shift keying (DPSK) demodulator. A distinctive property of this nonlinearity is that it is nonlocal, because it involves two delayed variables x_T and $x_{T+\Delta T}$ with $\Delta T \ll T$ in the nonlinear function f_{NL} . A similar bandwidth performance was achieved as well by [Nourine, Chembo, and Larger \(2011\)](#) with an OEO based on an integrated QPSK modulator and involving two independent electro-optic modulation inputs. This oscillator was therefore characterized by a two-dimensional nonlinearity and was based on a dual-delay feedback dynamics for the two rf voltages of the QPSK modulator, which were the dynamical variables of the coupled Ikeda-like equations.

Compared to their low-pass filter counterparts, the nonlinear dynamics and bifurcations of broad bandpass Ikeda-like OEOs have many distinctive features. The most evident is that they have only a single fixed point (the trivial solution $x = 0$) because the bandpass dynamics asymptotically filters out the null spectral component in the dynamical variable. As a consequence, unlike low-pass filter OEOs, they cannot display multistability between constant solutions, even though multistability between time-dependent solutions is possible. However, although it might *a priori* appear as counterintuitive, the broad bandpass filtering actually provides increased complexity via the third timescale θ .

The first step for the bifurcation analysis of Eq. (5) is generally to rewrite it under the form of the following flow:

$$\varepsilon x' = -x - \mu y + \beta \{f_{NL}[x(s-1)] - f_{NL}[0]\}, \quad (6)$$

$$y' = x, \quad (7)$$

where the prime stands for the derivative with regards to the dimensionless time $s = t/T$ in units of delay, $\mu = T/\theta$, and $\varepsilon = \tau/T$ is a smallness parameter. The constant term $-\beta f_{NL}[0]$ has to be added in the right-hand side of Eq. (6) as the integral constant ensuring that the trivial solution $(x, y) = (0, 0)$ explicitly appears as a fixed point of the flow.

A bifurcation analysis for this set of equations was performed by [Koumou *et al.* \(2005a\)](#) for the case of a sinusoidal nonlinearity. It was shown that the trivial steady state is globally stable for small feedback gain and loses this local stability via a primary Hopf bifurcation as the feedback

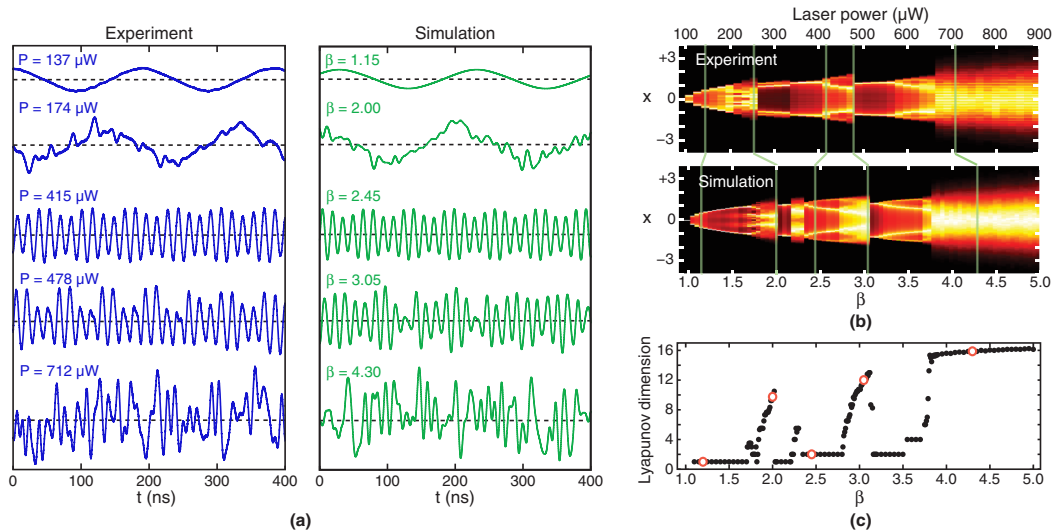


FIG. 6. Comparison between experimental measurements and numerical simulations with Eq. (5) for varying feedback strength in a broad bandpass Ikeda-like OEO. In the experiments, the feedback strength is controlled via the laser power P , while in the simulations it is controlled via β . (a) Measured and simulated time traces for five different values of the feedback strength. (b) Measured and simulated bifurcation diagrams. (c) Lyapunov dimension as a function of feedback strength. The vertical lines in (b) and open circles in (c) indicate the values of feedback corresponding to the five cases shown in (a). From [Cohen *et al.*, 2008](#).

gain is increased. More importantly, it was predicted that unlike in the low-pass filtering case, the Hopf bifurcations could here have frequencies that are not subharmonic to the free-spectral range $1/T$. A general bifurcation analysis was proposed by [Illing and Gauthier \(2005\)](#) for an arbitrary nonlinear function f_{NL} . They used the normal form theory to predict the supercritical or subcritical nature of the primary Hopf bifurcation, depending on the first three Taylor-expansion terms of the nonlinearity. They also evidenced double-Hopf bifurcations, thereby indicating the possibility of quasiperiodic oscillations. [Zheng and Wang \(2009\)](#) later on proposed a detailed bifurcation analysis using the Lindstedt-Poincaré method that can be simpler to implement than the usual center manifold reduction. More recently, normal form approaches have been used as well to investigate the existence and stability of Hopf bifurcations in bandpass Ikeda-like OEOs with sinusoidal nonlinearity ([Li and Wei, 2019](#); [Talla Mbé, Woafu, and Chembo, 2019](#)).

The main advantage of analyzing broadband Ikeda-like OEO dynamics with Eqs. (6) and (7) instead of the integro-differential Eq. (5) is that the smallness parameters ε and μ can appear explicitly. This permits one to perform a multiple-time scale analysis with a precision that increases as ε and μ decrease to 0. These asymptotic mathematical techniques have been successfully used to explain the asymmetric T -periodic square waves that are experimentally observed in broad bandpass OEOs with a rf voltage dynamical variable ([Weicker, Erneux, D’Huys *et al.*, 2012](#); [Weicker *et al.*, 2013](#)). The same methods have provided an analytical understanding of the fast-scale crenelated square-wave oscillations arising in Ikeda-like OEOs with nonlocal nonlinearity ([Weicker, Erneux, Jacquot *et al.*, 2012](#)).

Beside square-wave oscillations whose timescale solely depends on the delay time T , broad bandpass OEOs can display as well a slow-timescale dynamics. Indeed, when

$\tau \ll T \ll \theta$, a Hopf bifurcation of angular frequency $\Omega_s \approx (\theta T)^{-1/2}$ yields a slow-timescale limit cycle which morphs into a train of periodic and then chaotic breathers when the feedback gain is further increased ([Kouomou *et al.*, 2005a](#)). These breathers are hybrid states that have the singular property to simultaneously display slow-scale periodicity (timescale $\sim \Omega_s^{-1}$), along with fast-scale periodic (timescale $\sim T$) or chaotic (timescale $\sim \tau$) oscillations. [Cohen *et al.* \(2008\)](#) demonstrated that for all the resulting attractors, the Lyapunov dimension can be computed accurately as the feedback gain is increased, as shown in Fig. 6 where the full bifurcation sequence from steady state to fully developed hyperchaos is displayed.

[Peil *et al.* \(2009\)](#) specifically focused their research on the structure of periodic and chaotic breathers. They used wavelet analysis techniques to provide experimental evidence of τ -scale harmonic oscillations that could be theoretically explained by considering that the linear filters are of higher order, thereby requiring to add higher-order integrodifferential terms in the dynamical Ikeda-like equations. Chaotic breathers were also investigated in other architectures of broad bandpass OEOs, such as the system of [Romeira *et al.* \(2014\)](#) that included a phase modulator cascaded to a linearly chirped fiber Bragg grating. The route to breathing behavior was analyzed in detail by [Talla Mbé *et al.* \(2015\)](#), and typical time traces evidencing their birth, evolution, and destruction are presented in Fig. 7.

Broad bandpass OEOs can also display a distinctive pulsing behavior when certain specific conditions are met, as demonstrated by [Callan *et al.* \(2010\)](#). In particular, they highlighted the novel dynamical features that arise in the OEO dynamics when the amplifier saturation (in their case modeled with a hyperbolic tangent profile) is accounted for. Further theoretical and experimental research from [Rosin *et al.* \(2011\)](#) showed that the pulse widths can be controlled up to 3 orders

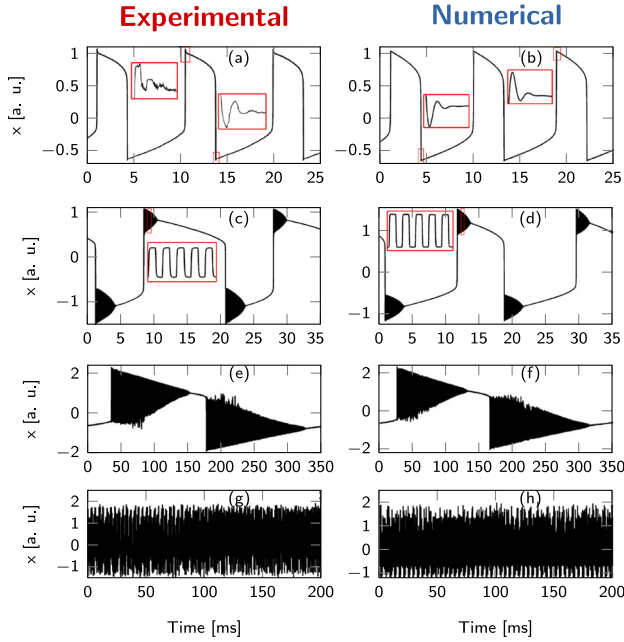


FIG. 7. Time-domain dynamics of an Ikeda-like OEO with broad bandpass filtering, as the feedback gain is increased beyond the oscillation threshold. The sinusoidal nonlinearity is provided here by an integrated lithium niobate Mach-Zehnder modulator. The numerical simulations are performed using a suitably normalized version of Eq. (5). (a), (b) Slow-fast (or relaxation) oscillations ($\beta \simeq 1.5$). (c), (d) Periodic breathers ($\beta \simeq 2$). (e), (f) Chaotic breathers ($\beta \simeq 3$). (g), (h) Fully developed chaos ($\beta \simeq 3.5$). Adapted from Talla Mbé *et al.*, 2015.

of magnitude (~ 100 ps–100 ns) via the low cutoff frequency, and that the Ikeda-like equations can be related to excitable models such as the FitzHugh-Nagumo equations with delayed feedback.

Complementary insight into the dynamics of broad bandpass OEOs is provided by a theory of Liénard equations, which requires one to rewrite the integrodifferential Ikeda-like equation (5) under the form

$$x' = y - F(x_R), \quad (8)$$

$$y' = -G(x), \quad (9)$$

where $F(x_R) = x - \beta\{f_{\text{NL}}[x_R] - f_{\text{NL}}[0]\}$ with $R = T/\tau$, $G(x) = \epsilon x$ with $\epsilon = \tau/\theta$ being the main smallness parameter, while the prime denotes the derivative with regards to the dimensionless time $\zeta = t/\tau$. In the case where the delay is null ($R = 0$), Eqs. (8) and (9) correspond to the so-called Liénard equations, provided that F and G are even and odd differentiable functions, respectively. Liénard equations have been thoroughly studied within the framework of nonlinear dynamics, and, in particular, they permit one to analyze the anharmonic properties of certain families of slow-fast limit cycles. In the limit of null delay, the Liénard analysis explains that the slow dynamics occurs when the system is in a layer close to one branch of the N-shaped x -nullcline $y = F(x)$, because $x' \simeq 0$ and $y' \propto \epsilon \simeq 0$. On the other hand, the fast dynamics occurs when the system horizontally exits the

neighborhood of that branch to jump to the other one [$|x'|$ is at least $\mathcal{O}(1)$]. This reasoning can be used to estimate the period of the slow-fast limit-cycle behavior in broad bandpass OEOs (Chengui *et al.*, 2014) or to understand the formation of multiscroll chaotic attractors (Márquez, Suárez-Vargas, and Ramírez, 2014). The Liénard analysis was also used by Talla Mbé *et al.* (2015) to show that this phenomenology is globally maintained when the delay is accounted for and can be used to explain the evolution from the slow-fast limit cycle to the breather behavior; see Fig. 7. Indeed, these breathers can also be viewed as resulting from a global bifurcation that merges the low-frequency Liénard dynamics with the high-frequency Ikeda dynamics (Marquez *et al.*, 2016).

Even though most of the research related to broad bandpass OEOs involves a sinusoidal nonlinearity originating from an electro-optic modulator, it is also possible to consider architectures where it is not the case. Chengui, Woafu, and Chembo (2016), for example, investigated the bifurcations and multi-scale dynamics of an OEO in the 0.5–6.5 MHz band, where the electrical-to-optical conversion in the feedback loop was performed by the pump semiconductor laser itself via its driving current electrode. In this oscillator, f_{NL} was therefore the power-intensity transfer function of the laser diode that is sometimes referred to as the *diode* or *elbow* function $D(x)$ that is null for $x < 0$ and equal to x otherwise. The specific case of multinonlinear OEOs has also been the focus of several research works, where their potential to enhance complex dynamical behaviors was explored in detail (Talla *et al.*, 2016; Chengui *et al.*, 2018; Talla Mbé, Kamaha *et al.*, 2019).

Broad bandpass OEOs have emerged as well as convenient benchmarks to investigate chimera states, which are self-organized patterns that can be sustained in high-dimensional networks. Larger, Penkovsky, and Maistrenko (2015)

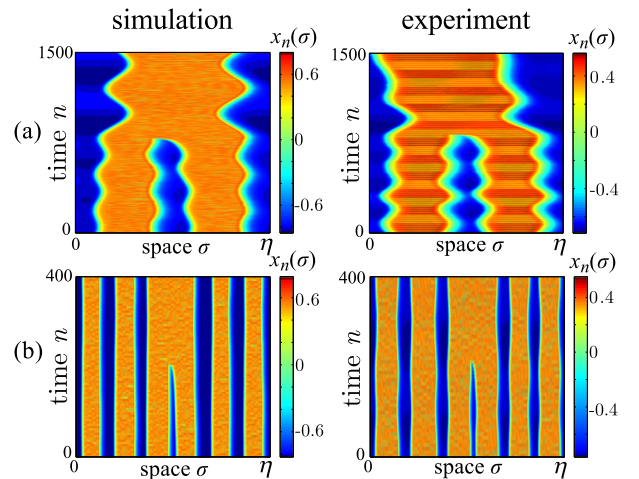


FIG. 8. Bifurcation transition at the border of a multistable chimera domain. When starting with a chimera state having the maximum number N of heads in a given domain, the crossing of the border toward the next domain leads to the vanishing of at least one head. Spacetime plots show the capture of such bifurcation events, both numerically and experimentally, as N -headed chimera becomes unstable being replaced by $N - 1$ heads. (a) 2-to-1 transition. (b) 6-to-5 transition. From Larger, Penkovsky, and Maistrenko, 2015.

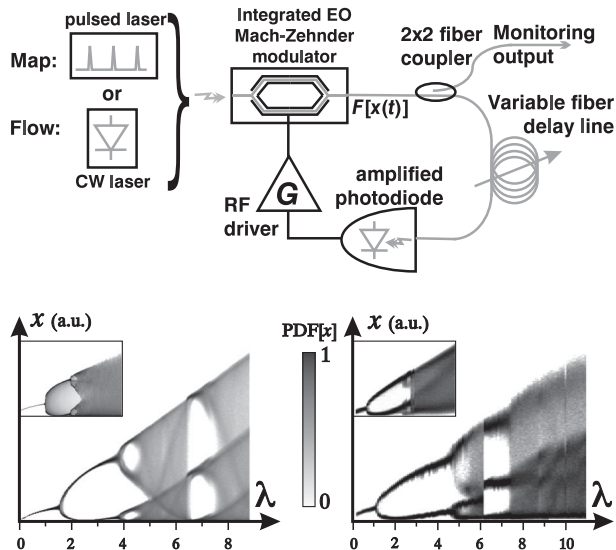


FIG. 9. (Top) Experimental setup to investigate the transition from flow (cw pump) to map (pulsed pump) in the broad bandpass Ikeda-like OEO. (Bottom) Numerical (left) and experimental (right) bifurcation diagrams of the map behavior as a function of the feedback gain λ ; the insets show the bifurcation diagrams obtained when seeding the oscillator with a cw laser. From Larger *et al.*, 2005.

investigated the excitation of laser chimeras using an Ikeda-like OEO with optical wavelength dynamics; see Fig. 8. As the gain was increased, they evidenced a cascade of pattern transitions to higher-order chimeras that ultimately led to turbulencelike chaos.

Another area of research is the study of the transition from the continuous flow of Eq. (5) to the discrete-time map $x_{n+1} = \beta f_{NL}[x_n]$. Indeed, this flow-to-map transition is sometimes investigated using the so-called adiabatic approximation (or *singular limit map*), by setting $x_n \equiv x(nT)$ in the limit $T \gg \tau$ (Neyer and Voges, 1982a). However, the validity of this procedure is generally restricted to the first sequences of periodic bifurcations, and significant discrepancies are observed for high gain in the chaotic regime. A more rigorous method relies on replacing the continuous-wave laser source by a pulsed one as explained in Fig. 9. This procedure allows for a better understanding of the flow-to-map transition in both the periodic and chaotic regimes (Larger *et al.*, 2005; Grapinet *et al.*, 2008a). Using a time-multiplexing scheme, Hart *et al.* (2017) also showed that they could create large complex networks of time-discrete coupled maps with arbitrary topology and display complex cooperative phenomena such as cluster formation and chimera states.

D. Semiconductor lasers with optoelectronic feedback

In an optoelectronic oscillator, the laser itself can be used to perform the electrical-to-optical conversion, via its pump current electrode, as shown in Fig. 10. If the high-cutoff frequency of the feedback loop is much lower than the laser relaxation frequency (which is typically a few GHz), the semiconductor laser responds adiabatically to the pump

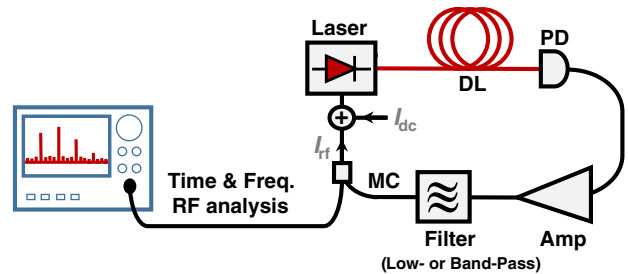


FIG. 10. Schematic view of an experimental setup for a semiconductor laser with optoelectronic feedback. The dynamics of this OEO essentially depends on whether or not the bandwidth of the feedback loop overlaps the relaxation oscillation frequency F_{RO} (\sim GHz) of the laser. DL: delay line; PD: photodiode; Amp: rf amplification; MC: microwave coupler.

current modulation and can be approximated as a quasi-instantaneous dipole with electrical input and optical output. In this case, the semiconductor laser with optoelectronic feedback still belongs to the family of OEOs modeled by Ikeda-like delay-differential equations [see, for example, Liu and Ohtsubo (1992), Larger, Goedgebuer, and Delorme (1998), Larger, Goedgebuer, and Merolla (1998), Chengui, Wofo, and Chembo (2016), or Chengui *et al.* (2018) as described in Sec. II.C].

However, when the bandwidth of the pump current signal becomes of the order of the semiconductor laser relaxation frequency, the current modulation can excite a nonlinear ns-scale dynamics inside the laser microcavity. Indeed, semiconductor lasers are generally of class B (Arecchi *et al.*, 1984), meaning that they have only 2 degrees of freedom (the intracavity photon and carrier densities). The delayed optoelectronic feedback drastically extends the dimensionality of the system, thereby allowing for a wide variety of complex dynamical behaviors. One should note that photon and carrier lifetimes are typically in the ps and ns ranges, respectively, so that even a delay of a few ns is already relevant.

Semiconductor lasers with optoelectronic feedback were initially studied for the purpose of short optical-pulse generation, as already highlighted in Sec. I.A. In particular, Damen and Duguay (1980) provided one of the earliest examples where the role and importance of the time delay in the pulse generation dynamics was unambiguously identified. Lau and Yariv (1984) demonstrated shortly after that the pulse width could be reduced down to 10 ps, and the repetition rate increased up to 5 GHz. Subsequent experimental work from other groups permitted one to achieve similar results (Paulus, Langenhorst, and Jäger, 1987; Nietzke *et al.*, 1990), and Lee, Shin, and Lee (1988) proposed a theoretical framework for the analysis of this ultrafast pulsed oscillator.

Giacomelli, Calzavara, and Arecchi (1989) experimentally focused on the effect of the delay for semiconductor lasers with optoelectronic feedback and proposed as well a theory that quantitatively agreed with experiments. Further theoretical insight was provided by the work of Grigorieva, Haken, and Kaschenko (1999), where a detailed bifurcation analysis was performed, explaining the emergence of periodic and quasiperiodic behavior. Pieroux *et al.* (2000) considered the asymptotic case of a large time-delayed feedback and

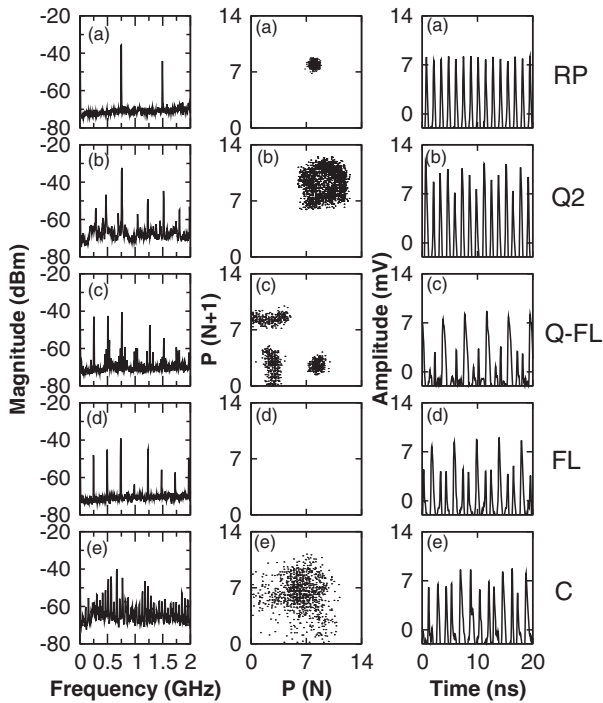


FIG. 11. Experimentally measured power spectra, phase portraits (with P and N being the normalized photon and carrier densities, respectively), and time series of different pulsing states for a semiconductor laser with optoelectronic feedback. (a) Regular pulsing (RP); (b) two-frequency quasiperiodic pulsing (Q2); (c) quasiperiodic frequency-locked pulsing (Q-FL); (d) frequency-locked pulsing (FL); (e) chaos (C). From Lin and Liu, 2003.

demonstrated the existence of both primary and secondary Hopf bifurcations.

Even though this distinction is not always highlighted, optoelectronic feedback in a semiconductor laser can be negative or positive, depending on if the feedback signal is inverted or not in the electric branch. Tang and Liu (2001a) investigated both experimentally and theoretically the route to chaos in semiconductor lasers with positive delayed optoelectronic feedback, while Lin and Liu (2003) investigated the opposite case of negative feedback; see Fig. 11. It was shown that in both cases there is a bifurcation route that successively generates regular, quasiperiodic, and finally chaotic pulsing behavior. However, frequency-locked pulsing states were found in the case of negative optoelectronic feedback, but not in the positive feedback case.

Vertical-cavity surface-emitting lasers (VCSELs) are characterized by a distinctive dual-polarization dynamics that displays many specific features when submitted to optoelectronic feedback. Zhang *et al.* (2007) performed a theoretical study of the polarization dynamics of VCSELs with negative optoelectronic feedback. They found that as the feedback delay and gain were varied, the VCSEL exhibited nonlinear behaviors such as polarization switching and mixed-mode polarization states. The work from Liao and Sun (2013) used the spin-flip model to show that negative optoelectronic feedback could also lead to mode competition and quasiperiodic routes to chaos. Y.-Y. Xie *et al.* (2014) investigated both

theoretically and experimentally the nonlinear dynamics of a VCSEL with positive optoelectronic feedback and they evidenced a rich diversity of behaviors, including regular, quasiperiodic, and chaotic pulsing. An experimental study was proposed by Marino, Giacomelli, and Barland (2014) in order to evidence front pinning and dissipative localized structures in a VCSEL with delayed positive optoelectronic feedback. Using a prototypical modeling methodology, they conjectured that these phenomena should be considered as generic features in time-delayed systems. The case of VCSELs with negative optoelectronic feedback was experimentally studied by J.-J. Chen *et al.* (2017). They found that the system displayed the regular, quasiperiodic, and chaotic pulsing states also observed in the positive feedback case and determined their permutation entropy as a function of the bias pump current and feedback strength.

Optoelectronic feedback can also be applied to other types of lasers such as Nd:YVO₄ microchip solid-state lasers (Uchida, Mizumura, and Yoshimori, 2006), multi-quantum well lasers (Lin, 2012), passively mode-locked semiconductor lasers (Drzewietzki, Breuer, and Elsasser, 2013), or semiconductor ring lasers (Kingni *et al.*, 2015), just to name a few. The dynamical states that have been observed and analyzed include multistability, quasiharmonic limit cycles, relaxation oscillations, pulse trains, and chaos. It was demonstrated that semiconductor lasers with optoelectronic feedback can even be used for small-span optical frequency comb generation (Chan, Xia, and Liu, 2007; Juan and Lin, 2009).

Finally, it is interesting to highlight research work where the laser, which emits coherent light, is replaced by an incoherent light source. Marino *et al.* (2011) considered the case where the optoelectronic feedback was applied to a light-emitting diode (LED). They reported theoretical and experimental evidence of slow-fast periodic oscillations and analyzed in detail the transition of these mixed-mode states to chaos. In the work of Joiner, Palmero, and Carretero-Gonzalez (2016), optoelectronic feedback was applied to a thermal light source, which was a simple night light bulb. They used a delay-embedding technique to reconstruct the attractor corresponding to the experimental time series. They determined that for certain parameters, this attractor was characterized by a fractional dimension and a positive Lyapunov exponent, two unambiguous signatures of chaotic behavior.

E. Spatiotemporal systems

Spatiotemporal optical systems with optoelectronic feedback have appeared as fruitful benchmarks to analyze complexity in the context of spatially extended systems.

The earliest studies on this topic are associated with architectures with a video feedback loop, where a camera looks at its own remote monitor as shown in Fig. 12. The one-dimensional acoustic equivalent of this setup, which is a microphone placed in front of its own loudspeaker, merely yields a loud screech (the so-called *Larsen effect*). However, in the video experiment, the monitor can display a rich variety of nonlinear spatiotemporal patterns. Häusler and Simon (1978) performed a theoretical and experimental analysis of the oscillating patterns arising when there is a mismatch between the camera and the monitor axis. The case where there is a

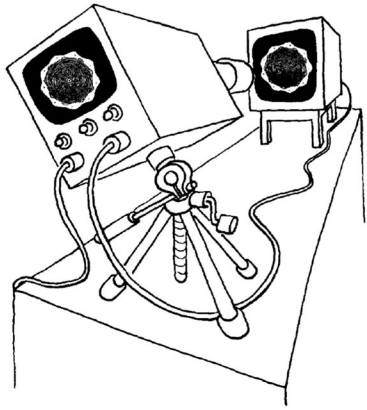


FIG. 12. Experimental setup for an analog video feedback experiment. Information flows counterclockwise through the electronic and optical pathways. Depending on the camera axis and the seed image, the monitor can display a wide variety of complex spatiotemporal behaviors, including periodic, labyrinthic, fractal, or chaotically turbulent patterns. Modern technology allows an easy implementation of such experiments using digital cameras and monitors. From [Crutchfield, 1984](#).

nonlinearity and a convolution in the electronic branch was investigated a few years later ([Häusler, Seckmeyer, and Weiss, 1986](#)), evidencing deterministic spatiotemporal chaos and labyrinthic patterns with long-range spatial correlations. The research of [Crutchfield \(1984, 1988\)](#) demonstrated that these video feedback systems can display almost entirely the textbook panoply of nonlinear phenomena in spatiotemporal systems: fixed points, limit cycles (including relaxation oscillations and flopping among fixed points), azimuthal patterns with $2\pi/n$ symmetry (n being an integer), homoclinic tangles, dislocations, spirals, lattices, and chaotic attractors. [Essevaz-Roulet *et al.* \(2000\)](#) investigated the dynamics of the azimuthal patterns in a setup where the mismatch between the camera and monitor axis was state dependent, and they evidenced the emergence of patterns with $2\pi/(p/k)$ symmetry (p and k being integers) following the hierarchy of a Farey tree. In the case of pixelated video feedback, [Courtial, Leach, and Padgett \(2001\)](#) evidenced the emergence of fractal patterns such as Koch snowflakes and Sierpinski gaskets.

Spatiotemporal optical systems with optoelectronic feedback have also been investigated in the case where the optical signal is the two-dimensional wave front of a laser beam. In that context, [Vorontsov, Carhart, and Dou \(2000\)](#) performed a theoretical and experimental study of a closed-loop system with an optical path featuring a liquid-crystal display (LCD) behaving as a large-scale array of phase modulators and a charge-coupled device (CCD) camera as a photo array. They implemented various types of nonlinearities in the feedback loop that allowed them to obtain many transverse optical structures, such as spatial solitons, lattice patterns (hexagonal and square), and spatiotemporal chaos. Further theoretical insight into this system was later on provided by [Lachinova and Lu \(2001\)](#), while [Hayasaki *et al.* \(2005\)](#) experimentally demonstrated the image processing potential of these architectures (distortion correction for fingerprint analysis).

A liquid-crystal spatial light modulator (SLM) with optoelectronic feedback was also proposed by [Rogers *et al.* \(2004\)](#)

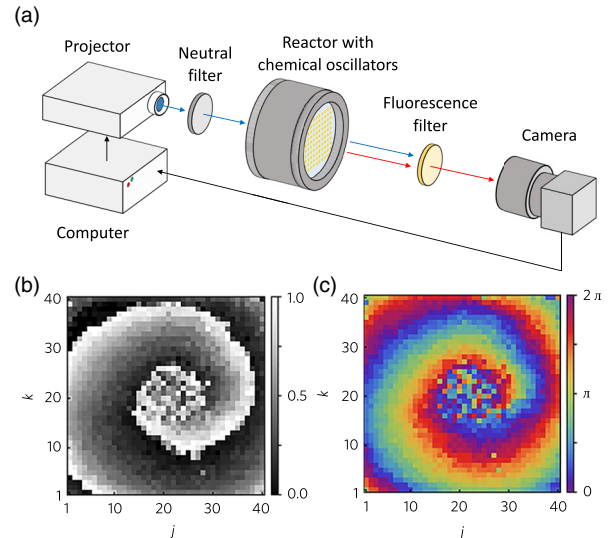


FIG. 13. Optoelectronic oscillator with spatiotemporal and time-delayed photochemical coupling. (a) Experimental setup. The camera records fluorescent light emitted by a large population of nonlocally coupled Belousov-Zhabotinsky (BZ) chemical oscillators. (b) Evidence of spiral-wave chimera in an array of 40×40 BZ oscillators. (c) Oscillator phases obtained from the gray-scale values in (b). From [Totz *et al.*, 2018](#).

as a platform to investigate spatiotemporal chaos in spatially extended systems, and particularly, the phenomenon of generalized synchronization. A similar architecture was used by [Hagerstrom *et al.* \(2012\)](#) to explore the spatiotemporal dynamics of nonlinear coupled maps, where optical nonlinearity was achieved using a liquid-crystal SLM. They demonstrated the emergence of spatially coherent and incoherent domains as a function of the coupling parameters and evidenced as well generalized chimera states.

The research works on spatiotemporal OEOs previously surveyed did not explicitly investigate the effect of the delay time, which was assumed to be much shorter than the response time of the two-dimensional optical systems. The role of delay time was however discussed in detail in the spatiotemporal OEO reported by [Totz *et al.* \(2018\)](#), where they studied the dynamics of a two-dimensional array of coupled Belousov-Zhabotinsky chemical oscillators submitted to optoelectronic feedback. Their experimental system is displayed in [Fig. 13](#), and it permitted one to demonstrate that these chemical oscillators could self-organize as spiral-wave chimera states depending on the strength and time delay of the feedback.

F. OEOs in the quantum regime

Optoelectronic oscillators with time-delayed feedback have been studied in regimes where quantum effects have to be accounted for, showing great promise to extend the relevance of such systems to quantum photonics applications.

One of the earliest results in this area was obtained by [Yamamoto, Imoto, and Machida \(1986\)](#), in joint theoretical and experimental research where they investigated photon number and the photocurrent noise levels in semiconductor lasers with optoelectronic feedback. Shortly after [Shapiro](#)

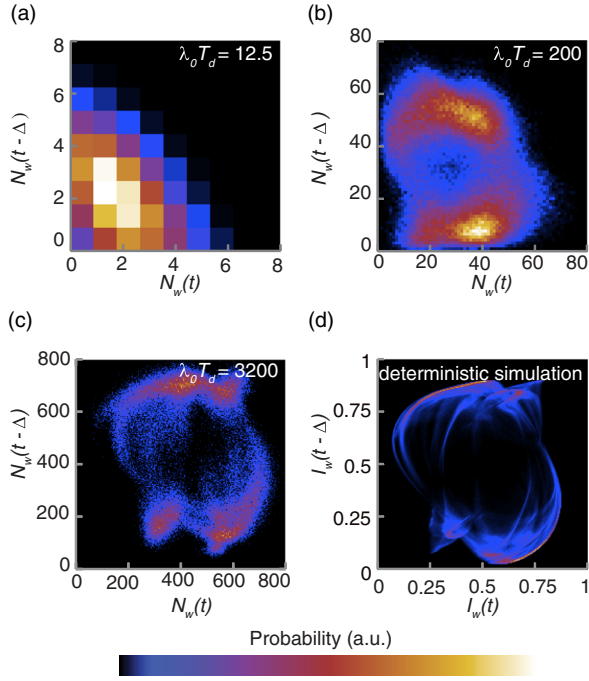


FIG. 14. Quantum behavior of an Ikeda-like OEO with feedback delay time T_d . The variable attenuation in the optical branch can be set to be so high that photons arrive sparsely in the photodetector following a Poisson process of rate $\lambda(t) = \lambda_0 I(t)$, where λ_0 is a proportionality coefficient and $I(t)$ is the output intensity of the Mach-Zehnder modulator. (a)–(c) Experimental data, and (d) the result of a deterministic simulation, with $N_w(t)$ being the number of photon arrivals in the interval $[t - w, t]$. These figures display the Poincaré sections as the OEO transitions from the quantum (Poissonian process) to the classical regime (chaotic attractor) when the normalized photon rate $\lambda_0 T_d$ is increased. The time-delay embedding is performed with a delay $\Delta = T_d/4$. From Hagerstrom, Murphy, and Roy, 2015.

et al. (1987) provided a detailed theoretical analysis valid for a large class of OEOs when driven by quantum fluctuations, with an emphasis on the open- versus closed-loop analysis. Later on, the understanding of OEOs in the quantum regime was strengthened by theoretical insights and experimental measurements provided by Youn *et al.* (1994) for semiconductor lasers with optoelectronic feedback, and by Taubman *et al.* (1995) for OEOs based on feedback loops with electro-optical modulators.

More recently, Hagerstrom, Murphy, and Roy (2015) considered an Ikeda-like OEO pumped by a continuous-wave semiconductor laser, but where a very strong attenuator is inserted in the optical branch, so that the photodetector witnesses the sparse arrival of single photons with a Poissonian statistics. They analyzed in detail the transition from single-photon shot noise to deterministic chaos, using Poincaré sections, Lyapunov exponents, and entropy; see Fig. 14.

The dynamical properties of a micropillar laser-detector assembly with optoelectronic feedback was investigated by Munnely *et al.* (2017), using the experimental setup displayed in Fig. 15. This OEO was held at the temperature of 15 K within a liquid helium-flow cryostat and operated in

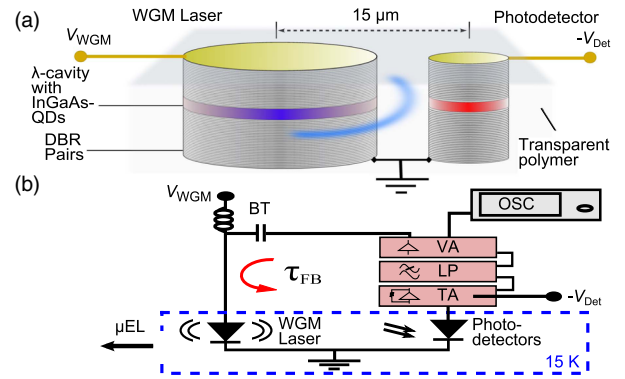


FIG. 15. OEO in the cavity quantum electrodynamics regime. (a) Sample layout. (b) Sketch of the setup. The extracted photocurrent is amplified by the transimpedance amplifier (TA) and is then passed through a 2 MHz bandwidth low-pass filter (LP) before being amplified at the main voltage amplifier (VA). The output voltage of the VA is coupled into the laser channel via a bias-T (BT) and monitored on an oscilloscope (OSC). The feedback delay is induced by the round-trip time τ_{FB} . The whispering-gallery mode (WGM) laser and the photodetector are helium cooled down to 15 K. From Munnely *et al.*, 2017.

the regime of cavity quantum electrodynamics (cQED). The oscillator displayed a MHz self-pulsing behavior, which was theoretically explained with a model taking into account both time-delay and cQED effects.

III. OEO-BASED CHAOS SYNCHRONIZATION AND COMMUNICATIONS

Optical chaos communications emerged as one of the first concrete applications of laser chaos. The main idea here is to ensure privacy in optical networks at the physical layer using a chaotic optical carrier and to retrieve the modulating message via chaos synchronization. The scientific literature reported a broad range of physical setups capable of performing these tasks [see, for example, Uchida *et al.* (2005), and references therein], and we discuss in this section the main results obtained with OEO architectures.

A. Principles of chaos communications

Chaotic systems are characterized by a positive maximal Lyapunov exponent, which determines the exponential divergence rate for two infinitesimally close trajectories in the state space. This sensitivity to initial conditions explains why these systems are unpredictable in the long term, despite being deterministic. In particular, since two independent chaotic oscillators do necessarily start from different initial conditions, it should always be impossible for them to oscillate synchronously, even if they are rigorously identical.

However, Pecora and Carroll (1990) demonstrated that when appropriately coupled, two identical chaotic systems can indeed be synchronized. They showed that synchronization occurs when the coupled system features a negative maximal conditional (or sub-)Lyapunov exponent, which determines the exponential convergence rate between the two chaotic systems in the state space when their trajectories

are infinitesimally close. This sub-Lyapunov exponent is coupling dependent: in fact, it is equal to the maximal Lyapunov exponent itself (and thus is positive) for uncoupled identical systems, thereby indicating the impossibility of synchronizing independent chaotic systems as stated earlier.

Chaos synchronization is therefore a counterintuitive phenomenon that finds its origin in the deterministic nature of the chaotic systems, and it opened the way for the concept of chaos communications (Cuomo and Oppenheim, 1993). In most chaos communication schemes, an information-bearing signal is masked within the noiselike output of a chaotic emitter, while a synchronous receiver recognizes the chaotic component (“chaos-pass filtering”) and extracts it to reveal the originally embedded signal. Within that framework, it can therefore be said that encoding relies on the unpredictability of chaotic oscillations, while decoding relies on their determinism. The possibility to synchronize chaotic laser light was theoretically investigated by Colet and Roy (1994), and later on, the concept of chaos communications was translated to the realm of optical fiber networks, where lasers are commonly used as transmitters.

B. OEO architectures for chaos communications

OEOs have emerged as versatile and particularly efficient systems for optical chaos communications.

Goedgebuer, Larger, and Porte (1998) first proposed an Ikeda OEO system for chaos communications, with which they successfully transmitted an audio signal hidden within a

chaotic wavelength carrier signal. Complementary experiments with the same setup were performed by Larger, Goedgebuer, and Delorme (1998). In both cases, the signal to be masked was added to the laser electrode controlling its emission wavelength, and the chaotic carrier had a 0–20 kHz bandwidth in the base band. Along with the all-optical fiber ring-laser system proposed by VanWiggeren and Roy (1998a, 1998b), this Ikeda wavelength oscillator has been one of the earliest experimental implementations of laser-based chaos communications.

Cuenot *et al.* (2001) implemented an alternative method called *chaos-shift keying* for binary transmission, which consists of modulating a parameter of the emitter, thereby creating a dynamical parameter mismatch. The quality of the chaos-pass filtering at the receiver end fluctuates accordingly, yielding a “1” in case of mismatch, and a “0” otherwise. The performance of this system was of the order of a kbit/s. Ikeda OEOs with coherence modulation have also been used for chaos communications and led to similar performances (Lee, Larger, and Goedgebuer, 2003). The various possibilities of encoding and decoding strategies using OEOs modeled by Ikeda equations were explicitly listed by Udaltsov *et al.* (2001). An emitter-receiver system where chaotic wavelength hopping was induced by delayed optoelectronic feedback was proposed by Liu, Davis, and Aida (2001), and their system achieved chaos communications at 1 Mbit/s.

A leapfrog improvement for the data rate was achieved by Goedgebuer *et al.* (2002), using a broad bandpass Ikeda-like OEO. They carried out a successful chaos communication

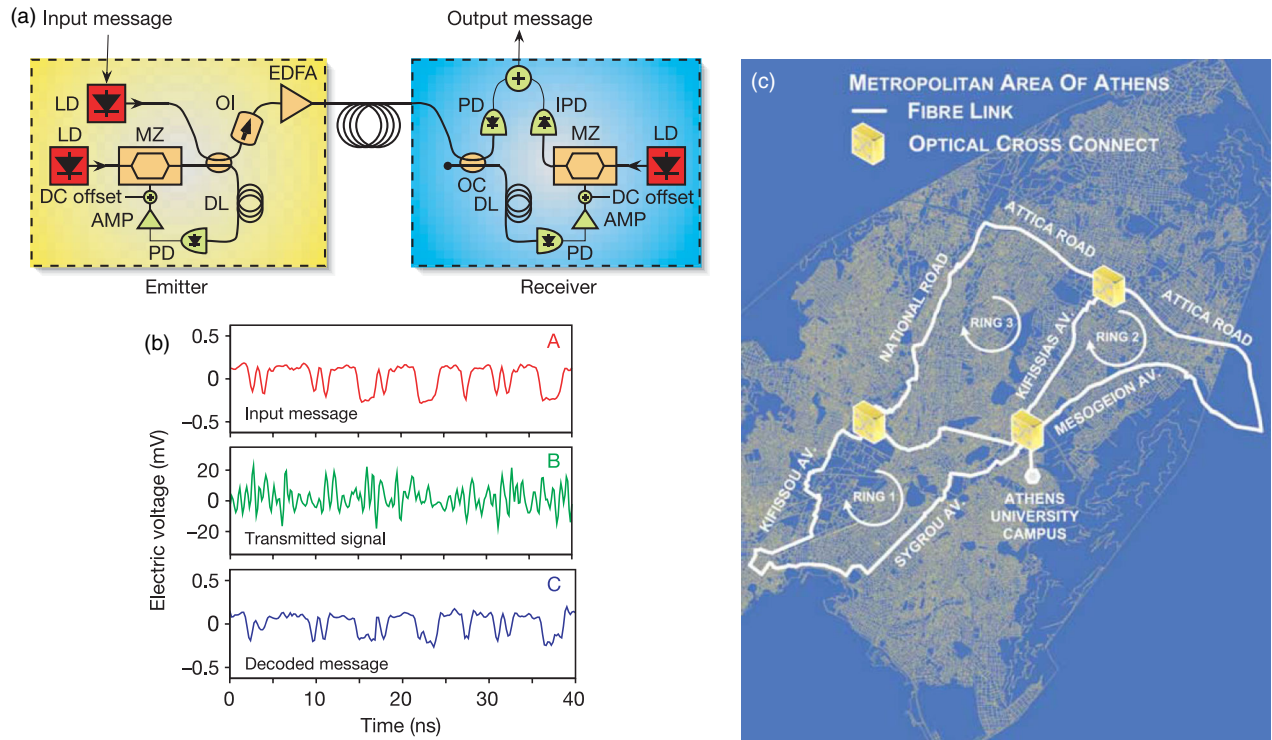


FIG. 16. Field experiment of chaos communication using an Ikeda-based optoelectronic oscillator. (a) Emitter-receiver system. The emitter uses a laser diode (LD) at 1550 nm to seed an integrated Mach-Zehnder modulator (MZ). An erbium-doped fiber amplifier (EDFA) boosts the power of the signal to be launched into the transmission line. (b) Time traces of the input, transmitted, and decoded signals after 120 km (at 1 Gbit/s). (c) Metropolitan optical fiber network of Athens, Greece, where the experiment was performed (total length of 120 km). Adapted from Argyris *et al.*, 2005.

experiment with a pseudorandom binary signal at 100 Mbit/s, over a 50-km-long optical fiber channel. The bit error rate (BER) was 2.4×10^{-3} without correction, and the message-to-chaos ratio was -10 dB. [Gastaud *et al.* \(2004\)](#) demonstrated a performance of 3 Gbit/s with a broadband chaotic carrier in a back-to-back configuration. The chaos-to-synchronization error ratio was equal to 18 dB, thereby permitting one to achieve BER of the order of 10^{-9} .

This architecture was deployed by [Argyris *et al.* \(2005\)](#) in a field experiment that allowed one to validate the chaos communication paradigm in commercial fiber-optic links; see Fig. 16. They encoded, transmitted, and decoded a 3 Gbit/s binary message over 120 km of optical fiber in the metropolitan area network of Athens, Greece. Successful transmission with a BER performance better than 10^{-7} was demonstrated. [Grapinet *et al.* \(2008b\)](#) considered a modified version of this system, where the continuous-wave pump lasers were replaced by pulsed ones, allowing the OEOs to output regularly clocked picosecond laser pulses with chaotically distributed amplitudes. They achieved successful back-to-back chaos communications with binary signals at 2.5 Gbit/s.

Another major field experiment was performed by [Lavrov, Jacquot, and Larger \(2010\)](#) using an optical phase chaos OEO. They first led an experiment in the *Frères Lumière* all-optical fiber network installed in the city of Besançon, France. The chaos communication experiment in this 22-km ring network yielded a BER as low as 3×10^{-10} at 10 Gbit/s. A second experiment was led in a 120-km-long optical fiber network in Athens, Greece: using optical amplifiers and dispersion compensation modules, they achieved a BER $\sim 10^{-6}$ at 10 Gbit/s, and a quasierror free transmission BER $< 10^{-9}$ when the data rate was lowered to 3 Gbit/s.

[Oden *et al.* \(2017\)](#) investigated a chaos communication system where optical phase chaos generated with customized three-wave imbalanced interferometers is used to achieve back-to-back transmission at a data rate of 3 Gbit/s, with BER $< 10^{-12}$. The main interest of this system is the high dimensionality of the physical key (defined by eight physical parameters), which nevertheless allows for excellent synchronization with a 15–20 dB chaos cancellation over a spectral range of 20 GHz around the laser carrier frequency. [Ai, Wang, and Wang \(2017\)](#) also recently performed chaos communication using a broad bandpass Ikeda-like OEO in intensity. They demonstrated a 5 Gbit/s carrierless amplitude-to-phase (CAP-4) modulation and a 10 Gbit/s on-off keying encoding, with a BER $\sim 10^{-3}$ after transmission in few-km-long multimode fiber. The most recent result on chaos communications using Ikeda-like OEOs is the work of [Ke *et al.* \(2018\)](#), where they experimentally demonstrated chaos communications over 100 km of optical fiber at a data rate of 30 Gbit/s. They used a duobinary modulation format with high spectral efficiency, so that the 30 Gbit/s signal could be embedded within a 10-GHz-wide chaotic carrier, with a BER $\sim 10^{-3}$.

Alongside Ikeda-like OEOs, semiconductor lasers with optoelectronic feedback also arose as excellent candidates for the purpose of optical chaos communications. [Tang and Liu \(2001b\)](#) proposed a chaos communication system that could transmit a pseudorandom nonreturn-to-zero (NRZ) bit

sequence at 2.5 Gbit/s, with a BER of the order of 10^{-4} . Their architecture used an additive chaos modulation scheme, with matched lasers emitting at 1299 nm. Later on, the possibility to increase the data rate to 10 Gbit/s was numerically investigated by [Liu, Chen, and Tang \(2002\)](#), and they confirmed the efficiency of additive chaos modulation for high-bit-rate synchronized chaotic communications.

Other groups theoretically explored alternative chaos communication systems based on semiconductor lasers with optoelectronic feedback. [Xia, Wu, and Liao \(2009\)](#) investigated a cascaded communication scheme based on negative optoelectronic feedback, capable of transmitting Gbit/s binary signals. Architectures with mutual coupling have been considered as well, providing the added advantage of simultaneous bidirectional message transmission ([Deng *et al.*, 2009](#)). The work of [Chiarello, Ursini, and Santagiustina \(2011\)](#) focused on wireless infrared optical chaos communications up to several hundreds of Mbit/s, with the goal of performing secure indoor transmissions in the presence of multipath reflections and ambient light noise.

C. Performance evaluation and optimization

One of the most active lines of research related to optical chaos communications is the improvement of both the performance and security of the existing systems, as well as the design of novel architectures aiming to circumvent the identified pitfalls.

A major concern is related to parameter mismatch. Indeed, two identical systems can be perfectly synchronized in the asymptotic limit, but unavoidable parameter mismatch between the emitter and receiver systems yields an imperfect synchronization, or equivalently, a mismatch noise that inherently degrades the quality of chaos communications. This problem of parameter mismatch rapidly started to be the focus of dedicated investigation, simultaneously with the demonstration of the first chaos communication systems based in Ikeda dynamics ([Goedgebuer, Larger, and Porte, 1998](#); [Larger, Goedgebuer, and Delorme, 1998](#)). A systematic analytical, numerical, and experimental study of mismatch noise in Ikeda-like OEOs was performed by [Kouomou *et al.* \(2004\)](#). They first investigated in detail the influence of each parameter considered individually and showed the relative root-mean-square amplitude of synchronization noise (or *noise-to-chaos* ratio) scales linearly with the absolute value of the parameter mismatch, even though some parameters such as the time delay are significantly more sensitive than others. This work also demonstrated that quite counterintuitively mismatches in different parameters can partially compensate for each other and reduce the overall synchronization noise. In a follow-up work, the effect of this mismatch noise was evaluated on a back-to-back chaos communication scheme with data rates up to 2.5 Gbit/s ([Kouomou *et al.*, 2005b](#)). The particular case of parameter mismatch in the Ikeda system with multiple feedback was theoretically studied by [Shahverdiev *et al.* \(2005\)](#). Shortly after, [Peil, Larger, and Fischer \(2007\)](#) showed that when bidirectional coupling is implemented, the stability basin increases significantly and large mismatches in time delay might still yield highly correlated dynamics, including generalized synchronization.

Recent research theoretically explored the effect of parameter mismatch for space-to-ground downlink laser chaos communications (M. Li *et al.*, 2018).

The problem of parameter mismatch was also investigated in systems involving semiconductor lasers with optoelectronic feedback. The main difficulty at the experimental level is that the parameters of the system are not tunable, except the time delay. Tang and Liu (2001c) performed a theoretical and experimental study of the synchronization of such lasers, when parameter mismatch is accounted for. They showed that robust synchronization with high emitter-receiver correlation (~ 0.9) can be achieved provided that the relative delay mismatch was kept typically below 1%. In subsequent work, Tang and Liu (2003) experimentally evidenced that when semiconductor lasers with delayed optoelectronic feedback are coupled unidirectionally, the interplay between the feedback loop and the transmission delay times can lead to either anticipated or retarded synchronization. Their research showed that both regimes feature the same stability against parameter mismatch. Tang *et al.* (2004) later on analyzed the case of two mutually coupled lasers with feedback and experimentally demonstrated that robust synchronization between the chaotic outputs can be obtained despite parameter mismatch. Depending on the coupling parameters, they also evidenced the phenomenon of *death by delay*, occurring when the coupling quenches the oscillations of the lasers.

Another important problem encountered in chaos communications is the detrimental effect of stochastic noise and fiber transmission impairments. Abarbanel *et al.* (2001) considered a chaos communication scheme using two semiconductor lasers with optoelectronic feedback, where the transmission was degraded not only by parameter mismatch, but also by spontaneous laser emission and channel noise. Their thorough numerical analysis permitted one to understand how the BER scales with these impairments. In particular, they explained how the open-loop receiver configuration could feature superior efficiency by eliminating the feedback loop mismatch. Bogris, Argyris, and Syvridis (2007) proposed a theoretical analysis to investigate the effect of the optical amplifier noise on the performance of optical chaos communications using a broad bandpass Ikeda-like OEO. They also considered specific fiber-induced distortions such as chromatic dispersion and evaluated the BER performance of the multi-Gbit/s communication system as a function of noise amplitude and transmission distance. Lin and Tsai (2007) numerically evaluated the performance of a chaotic communication system in a radio-over-fiber transmission based on semiconductor lasers with optoelectronic feedback. They compared the BER performances of additive chaos modulation and on-off shift-keying encoding schemes in a mismatched emitter-receiver system, when the chaotic carrier was propagated in a lossy, nonlinear, and dispersive transmission line, before being boosted with a noisy amplifier and transmitted in a wireless channel. Nguimdo *et al.* (2010) performed a theoretical and experimental study focusing on the detrimental effect of chromatic fiber dispersion on the synchronization of an optoelectronic phase chaos communication system. They evaluated the effect of dispersion management techniques to restore the integrity of the broadband chaotic

carrier after propagation in long-haul optical fibers. They also demonstrated that using dispersion shifted fibers matching the emitter carrier frequency is a pertinent strategy to avoid BER degradation, as it enables the chaos cancellation ratio to be almost the same as in the back-to-back configuration.

Finally, the problem of spectral optimization and multiplexing was considered by Rontani *et al.* (2011), as they proposed a dual-feedback Ikeda-like architecture to generate orthogonal chaotic codes. They numerically showed that when the feedback gain was high enough to ensure orthogonality, each of these codes could be used to simultaneously transmit 2.5 Gbit/s binary messages without cross talk.

D. Security analysis and enhancement

A critical challenge in chaos communications is to provide a quantitative evaluation of the level of security. Unlike digital software encryption schemes that are built on the solid bases of digital information theory, chaos communications are in principle fully analog. In consequence, assessing the level of security can hardly be performed unambiguously and therefore remains mostly qualitative. Assuming that the transmitted chaotic carrier is public, the main security key is determined by the values of the system parameters—the so-called *physical key*. Most security analyses are therefore geared toward making it difficult for an eventual eavesdropper to extract this physical key from the public transmitted signal. In particular, it is well known that one of the easiest parameters to extract from a chaotic time series is the delay time T , because of its strong signature in the Fourier spectrum in autocorrelation or in mutual information plots.

Udaltsov *et al.* (2003) demonstrated that the physical parameters of an Ikeda OEO could be extracted with high precision, provided that the eavesdropper has *a priori* knowledge of the system architecture. They also showed that if the eavesdropper does not know the nonlinear function f_{NL} , or if that function is characterized by several parameters, the physical key extraction task becomes significantly more difficult. Cheng *et al.* (2014) described a security enhancement method based on time-domain fractional Fourier transform in order to postprocess the optical chaotic carrier originating from a broad bandpass Ikeda-like OEO. This procedure was efficient to conceal the time-delay signature under certain optimal conditions, without modifying the chaotic source. Q. Zhao *et al.* (2016) considered the case of a wavelength Ikeda chaos oscillator and demonstrated that the time-delay signature vanished in the autocorrelation and mutual information plots for very high feedback gains ($\beta > 15$), while the offset phase appeared to have a negligible effect in this regime. Zhu *et al.* (2017) proposed a system built with three coupled phase-modulated electro-optic nonlinear loops. They described how time-delay signature was suppressed in the output chaotic carrier, when screened with autocorrelation and mutual information indicators.

Another method to enhance the security of chaos communication systems is to associate digital features to the basic analog architecture. Nguimdo *et al.* (2011) introduced a hybrid multi-Gbit/s encoding scheme that integrates a digital key in a phase-chaos Ikeda-like system. The idea was to mix a binary data stream within a chaotic carrier in a way that the

time delay and the binary signal mutually conceal each other. Cheng *et al.* (2015) proposed a chaos communication system based on orthogonal frequency division multiplexing, where the downstream and upstream were encoded in the optical and electrical domains, respectively. Here also the digital and analog signals were coupled in such a way that they mutually concealed the main features of their intrinsic temporal and spectral signatures.

Parameter modulation also provided a pathway to increase the complexity of the optical chaotic carriers. Along that line, Hu *et al.* (2014) studied a chaotic system based on an Ikeda-like bandpass OEO with varying parameters, allowing them to hide the time-delay signature. The security was also enhanced by the fact that the chaotic emitter featured higher Lyapunov exponents and dimension. Intermittent time-delay modulation (Gao, Xie, and Hu, 2015) or chaotic switching (Liu *et al.*, 2016) can be implemented as well to increase the complexity of the chaotic carrier of an Ikeda-like bandpass OEO and achieve time-delay concealment.

Multinonlinearity has emerged as a valid strategy to enhance the security of chaos communications and has been theoretically investigated by several research groups. Hizanidis *et al.* (2010) studied the case where an all-optical and chaotic external-cavity semiconductor laser was seeding an optoelectronic bandpass Ikeda loop with a phase modulator. They reported successful concealment of time delay and increased sensitivity to delay mismatches, thereby making it more difficult for an eventual eavesdropper to extract the encoded information. Elsonbaty, Hegazy, and Obayya (2015) analyzed a configuration where the chaotic carrier was generated using a polarization-resolved VCSEL with electro-optic feedback. The orthogonal polarization modes appeared to display uncorrelated dynamics, thereby allowing dual-channel Gbit/s chaos communications. Improvement of both complexity and security can also be achieved in bandpass Ikeda-like OEO via extra optical feedback (Hu, Shi, and Xie, 2017) or electrical mutual injection (Huang *et al.*, 2018).

The importance of preventing an eavesdropper from acquiring the physical key became even more critical since the work of Cohen *et al.* (2008), where it was demonstrated that once the physical key is known, it is possible to synchronize the experimental chaotic carrier with a numerical model, thereby eliminating the need to build a dedicated receiver with matched hardware parameters.

E. Synchronization in networks

The topic of chaos synchronization in networks of broadband OEOs is important from the viewpoint of fundamental nonlinear dynamics and pattern formation in complex networks (Murphy *et al.*, 2010). Particular focus has been devoted to the phenomenon of cluster chaos synchronization, which corresponds to the hybrid configuration where the chaotic oscillators synchronize with one another in groups, while there is no synchronization among the groups [see, for example, Hu *et al.* (2000) and Koumou and Wofo (2003a, 2003b)]. Various research groups have explored the occurrence and stability of this symmetry breaking in OEOs.

Illing, Panda, and Shareshian (2011) studied chaos synchronization in a network of three broadband Ikeda-like OEOs

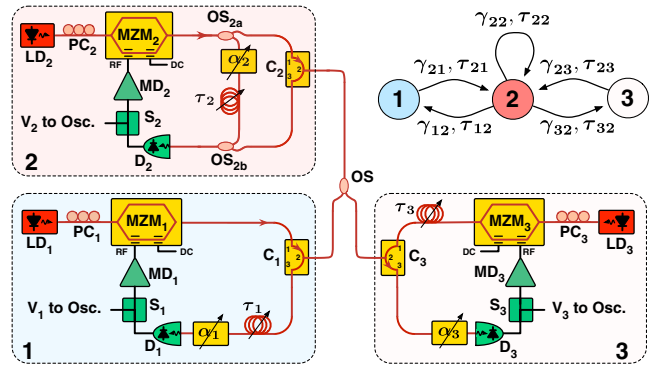


FIG. 17. Schematic of an experiment consisting of three coupled optoelectronic oscillators. LD: laser diodes; PC: polarization controllers; MZM: Mach-Zehnder modulators; C: optical circulators; OS: optical splitters; α : adjustable optical attenuators; τ : adjustable optical fiber delay lines; D: photodetectors; S: electronic splitters; MD: modulator drivers. (Inset) Coupling architecture. From Illing, Panda, and Shareshian, 2011.

with time-delayed mutual coupling and self-feedback; see Fig. 17. They obtained various patterns of cluster synchronization that were analyzed both theoretically and experimentally. The case with four OEOs was investigated by Ravoori *et al.* (2011). They analyzed the influence of the coupling topology on the synchronization dynamics and introduced the objective concept of *sensitive* and *nonsensitive* networks to determine the robustness of the network. Cluster synchronization was later on reported and analyzed for such four-node networks by Williams *et al.* (2013). This configuration is particularly interesting as it permits the formation of two asynchronous groups constituted with two synchronous chaotic OEOs, despite the fact that there is no intragroup coupling. Pecora *et al.* (2014) proposed a new framework and developed techniques for the analysis of network dynamics, in order to unveil the connection between network symmetries and cluster synchronization. Their experimental system was an OEO with a polarization-sensitive feedback loop involving a spatial light modulator. The specific case of large networks of star-coupled chaotic OEOs was numerically explored by Liu, Lin, and Miao (2017), and they evidenced random sequences of giant desynchronization that occur via the so-called *bubbling effect*. More recently, Hart *et al.* (2019) proposed a systematic investigation of the link between symmetry and synchronization stability in coupled networks of OEOs. One of their main findings was that quite counter-intuitively, synchronizability can be enhanced by breaking the network structural symmetry.

F. Random number generation

Random numbers are useful in several applications ranging from real-time random sampling to hardware cryptographic applications. By definition, truly random variables originate from probabilistic physical phenomena, such as radioactive decay or thermal noise. A high level of randomness can also be achieved by combining the complex dynamics of chaotic lasers with binary logic postprocessing (Uchida *et al.*, 2008), and this approach is expected to provide one of the most

efficient method for the ultrafast generation of pseudorandom numbers (Murphy and Roy, 2008).

OEOs can be used as well for ultrafast random number generation as demonstrated by Fang *et al.* (2014) with a broad bandpass phase-chaos architecture. In fact, OEOs can operate in a stochastic regime where entropy originates from pump laser and photodetection noise or in a deterministic regime where the source of entropy is the chaos generated in the OEO when the gain is sufficiently high. In the first case, the generated numbers are genuinely random, while they are only pseudorandom in the second case. They proved that regardless if the source of entropy was laser noise or laser chaos, the binary logic postprocessing allowed the pseudorandom output signals to equally pass some of the most stringent benchmark tests, such as the National Institute of Standards and Technology (NIST) and the DieHARD test suites. More importantly, they highlighted the fact that pseudorandom numbers obtained from OEO laser chaos had the potential to be synchronizable with high precision, and therefore, makes them particularly suitable for symmetric cryptographic schemes. Mu *et al.* (2015) used an intensity chaos from a broad bandpass OEO to perform ultrafast random number generation and validated the randomness of their source using the NIST suite. The latest experiments in this field were performed by Tian *et al.* (2018), with a system based on two chaotic OEOs with silicon Mach-Zehnder and microring resonator modulators. Their oscillator could output a pseudorandom bit data stream at 320 Gbit/s, with a randomness satisfying the NIST specifications.

G. Chaotic radars, lidars, and radio communications

Chaotic OEOs are characterized by unique spectrotemporal properties such as broad spectrum, synchronizability, or time-domain orthogonality for remotely distant time slots. For this reason, they found numerous technological applications for open-space light-wave and microwave engineering applications (Sciamanna and Shore, 2015).

Semiconductor lasers with optoelectronic feedback were proposed by Lin and Liu (2004) as suitable systems to perform chaotic lidar detection. In this context, the main appeal of chaos comparatively to periodically modulated lidars is that it lifted the echo ambiguity, and its broad bandwidth (>10 GHz around the optical carrier) increased accuracy without the need for expensive multi-GHz modulation systems. They reported subcentimeter resolution with a peak-to-side-lobe level of -27 dB, for a potential detection range of up to 7 km. Wu, Liao, and Lin (2010) numerically investigated the performances of a synchronized chaotic lidar architecture, which improved performance in the large noise regime ($\text{SNR} < 15$ dB) (signal-to-noise ratio).

Chaotic OEOs are also investigated as ultrawideband (UWB) carriers for short-range (<10 m) wireless communications. In this context, Wang *et al.* (2012) proposed an UWB chaotic system based on an Ikeda-like OEO. It featured a phase modulator seeded by a cw laser, and the optical phase-to-intensity conversion was performed by the chromatic dispersion of a 50-km-long optical fiber delay line. This oscillator could output multi-GHz rf chaos satisfying the indoor ultrawide band mask regulations. These UWB chaotic

signals also find applications for chaotic radars, which combine immunity to multipath fading, low-power consumption, and high-range resolution. In this context, Zheng *et al.* (2014) designed a fiber-distributed UWB radar based on an Ikeda-like chaotic OEO with a polarization-to-intensity modulation converter. Their system could achieve a cm-level resolution after propagation in 3 km of optical fiber. Yao *et al.* (2015) demonstrated a distributed multiple-input multiple-output chaotic radar based on wavelength-division multiplexing. In order to enhance the detection capability, multi-GHz chaotic signals generated by two broadband Ikeda-like OEOs were emitted through two different antennas. They induced target echoes that were processed by a central station performing the correlation analysis, thereby achieving target localization with cm-scale precision.

Another approach for chaotic radar is to use narrow bandwidth signals. The advantage here is that spectrum management is optimized, and the frequency selectivity permits one to use this technique in outdoor space without interference with other signals. Pallavisini *et al.* (2007) implemented an Ikeda-like OEO architecture based on a nonlinear rf interferometer for the generation of a 1.225 GHz microwave, with a chaos-induced spectral spreading of a few tens of MHz. Chembo (2017) proposed a joint theoretical and experimental study of a chaotic narrow-band OEO, intended for radar engineering and radio-communication scrambling applications. The chaotic signal had a central frequency of 3 GHz and a bandwidth of only 16 MHz.

IV. OEO-BASED RESERVOIR COMPUTING

In recent years, broadband OEOs have progressively emerged as a high-performance technological platform for the purpose of analog computation and machine learning. Research on neuronal networks has shown that high dimensionality, connectivity, and nonlinearity are key properties for analog computation: interestingly, these features can be emulated in OEOs, with the possibility to process information with an ultrahigh bandwidth. The research on the topic of OEO reservoir computing is still embryonic in comparison to other areas of artificial intelligence, but it has benefited from rapid growth and achieved remarkable performances in a diverse set of experiments, as discussed hereafter.

A. The concept of neuromorphic photonic computing

The quasitotality of modern computers is currently based on Turing–von Neumann machine software and digital electronics hardware. The analog photonic computer is, from that perspective, the result of a double paradigm shift.

On the one hand, the implementation of photonic computers is a topic that has been the focus of dedicated scientific research for decades. The strong, lasting, and cross-disciplinary interest for photonic computing is to some extent motivated by the elusive promise of computing “at light speed,” and optoelectronic computing appears as a natural path to transition from electronic and photonic computers. On the other hand, despite the ubiquitousness and ever-growing computational power of Turing–von Neumann machines, they remain surprisingly ineffective to solve some of the problems

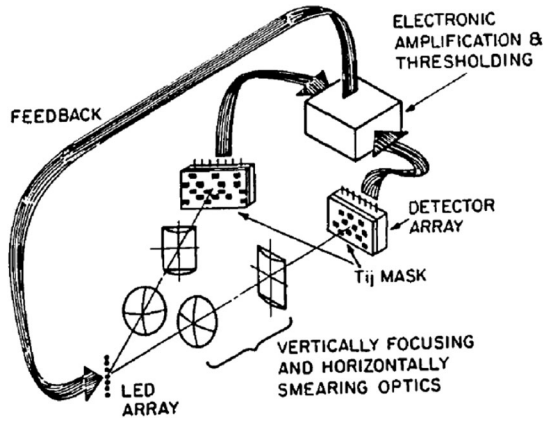


FIG. 18. An early architecture for analog optoelectronic computing, emulating the Hopfield neural model. From Farhat *et al.*, 1985.

that appear as rather simple for biological brains, such as pattern recognition, for example. Indeed, the best Turing–von Neumann computers generally need tens of megawatts to perform some of the tasks that the human brain can effortlessly achieve with few tens of watts. This is why bioinspired (or *neuromorphic*) computation paradigms have emerged as pertinent alternatives to solve certain classes of problems where Turing–von Neumann machines are known to fail or underperform.

Bioinspired computers are very often based on the concept of neural networks. The neurons are generally nonlinear nodes, while the coupling among themselves, also called connectivity, can at the same time be variable, random, and sparse in sections of the network. One of the earliest example of bioinspired computation based on a photonic system with optoelectronic feedback was provided by Farhat *et al.* (1985), with an experimental implementation of the Hopfield model for neural networks; see Fig. 18.

As in conventional neural networks, most neuromorphic computing schemes rely on optimizing the connection topology of a network comprising nonlinear elements. Topology optimization is typically carried out according to learning routines utilizing sample data and as such is fundamentally opposed to the *ad hoc* algorithmic coding for Turing–von Neumann machines. The dynamics of a neural network critically depends on its connectivity, and therefore, neuromorphic computing requires one to communicate the network state along with each of its connections, ideally in parallel. This bandwidth requirement provides an advantage to photonics over electronic substrates. From a broader perspective, photonic neural networks are expected to reach space-bandwidth products and energy efficiencies orders of magnitude beyond what is in principle achievable in electronics (Miscuglio *et al.*, 2018).

Novel paradigms for analog optoelectronic computation have recently emerged, and several of them can be implemented using time-delayed broadband OEOs.

B. Principles of delay-based reservoir computing

Training a neural network for a given task typically consists of finding the optimal connectivity between the neurons.

However, this procedure can be particularly difficult, time consuming, and computationally expensive, most notably when the number of neurons is large.

In order to overcome this difficulty, Maass, Natschläger, and Markram (2002) introduced the *liquid-state machine* (LSM), while Jaeger and Haas (2004) independently proposed the idea of *echo state network* (ESN). These two approaches for bioinspired computing are theoretically very close, and in their typical architecture, these neuromorphic computers have three layers that are, namely, the input layer, the reservoir containing the artificial neurons, and the output layer. The main conceptual innovation is that the input coupling and internal connectivity matrices are both fixed and initialized randomly, while the training and optimization procedure involves only the output (or readout) coupling matrix. It is this particular configuration of connectivity that makes this approach well suited for an implementation in nonlinear physical platforms. Verstraeten *et al.* (2007) showed that LSMs and ESNs can be unified and they proposed the term *reservoir computing* (RC) for this class of neuromorphic computers.

The first implementation of reservoir computing with time-delayed systems was proposed by Appeltant *et al.* (2011), using an electronic circuit modeling the Mackey-Glass dynamics. They demonstrated that instead of coupling a large number of discrete (individually discernible) and nonlinear neurons, one could just consider a feedback loop with time delay T that contains a single node with nonlinearity f_{NL} . Inside the feedback loop, a number N of *virtual* nodes with temporal separation $\delta T = T/N$ can be emulated in the system by multiplying the input signal by a time-domain mask $m(t)$, which is a T -periodic and multilevel step function with segments of equal duration δT ; see Fig. 19. Computation is therefore performed using the nonlinear transient dynamics, with no need to record remotely past states. Owing to the formal equivalence between delayed and spatially extended systems (Arecchi *et al.*, 1992), it can be considered that the input information is thereby spatiotemporally mapped within the time-delayed oscillator.

This idea was the breakthrough that led to subsequent proof-of-concept experiments of reservoir computing using OEO platforms, in particular, and photonic platforms in general [see, for example, Brunner *et al.* (2013, 2018) and Van der Sande, Brunner, and Soriano (2017), and references therein]. Most notably, reservoir computers implemented with photonic delay systems make use of a simple and elegant scheme: the network state is updated via communication along a single optical fiber. This communication is responsible for a large fraction of the inefficiency encountered when realizing neural networks in standard electronic architectures, while in principle, it is performed in photonic delay reservoirs only at the cost of a small optical power loss.

C. Basic architecture of OEO reservoir computer

The basic OEO reservoir computer is a single-loop Ikeda-like system where the main variable is the broadband input voltage of a Mach-Zehnder modulator. As for the architectures presented in Sec. II, the low or bandpass filtering is performed in the electric branch, while the time delay originates from an optical fiber feedback loop or from programmable electronic

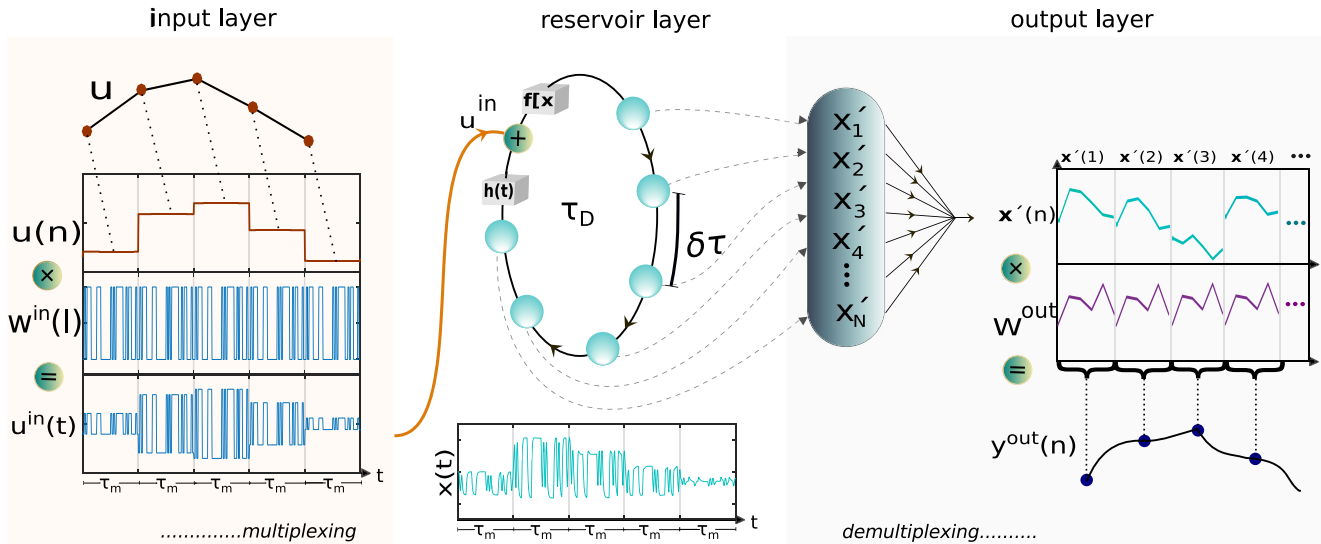


FIG. 19. Schematic illustration of the individual processes involved in a delay-reservoir computer, highlighting the input, reservoir, and output layers. The input layer is implemented by modulating the input $u(n)$ with the temporal mask $W^{\text{in}}(l)$ to create the input $u^{\text{in}}(t)$, with $l\delta\tau$ being the temporal position of node l within one delay. The reservoir response autonomously creates the state $x(n)$ within one delay τ_D . The readout weights correspond to temporal modulations of $x(n)$ according to W^{out} , and summing the resulting sequence over the delay length creates output $y^{\text{out}}(n)$. Some of the steps for OEO-based RC (such as training and testing, for example) are performed off-line. From Brunner *et al.*, 2018.

modules. It should be noted that the suitability of OEOs to perform reservoir computing tasks is strongly correlated to the consistency of Ikeda-like dynamics, as investigated by Oliver, Larger, and Fischer (2016).

The first implementations of the OEO reservoir computer were based on the low-pass configuration, and they were published almost simultaneously by two independent research groups. In the first contribution, Larger *et al.* (2012) used a low-pass Ikeda OEO for the spoken-digit recognition (TI-46 corpus, requiring the recognition of ten spoken digits from 1 to 10), and for the prediction of the Santa Fe time series, which originates from a far-infrared laser with Lorenz-like chaotic output. The word error rate (WER) for the spoken-digit recognition task was as low as 0.04% using 400 nodes. The second contribution from Paquot *et al.* (2012) showed that this OEO could perform as well tasks such as nonlinear channel equalization or a time-series prediction of nonlinear autoregressive moving average (NARMA) models. Results were also comparable to the state of the art, and they achieved a WER of 0.4% using 200 virtual nodes for the spoken-digit recognition task. For being based on conventional optical telecommunication hardware, these two contributions have provided an accessible blueprint for the subsequent versions of photonic reservoir computers (Woods and Naughton, 2012).

The single-loop bandpass OEO was later on used as a reservoir computing platform for other tasks. For example, Jin *et al.* (2015) numerically demonstrated that this Ikeda-like architecture could perform a handwritten numeral recognition task with the modified NIST database. This task consists of identifying ten kinds of handwritten numerals from 0 to 9, and they achieved a WER of about 15% with their numerical simulations. Qin *et al.* (2017) proposed a joint theoretical and experimental study where they used a bandpass Ikeda-like OEO for optical packet header recognition in

optical packet switching networks. They demonstrated that this OEO reservoir computer could correctly identify optical packet headers with lengths from 3 to 32 bits, with a WER of 1.25% for the 3-bit header recognition task.

Reservoir computing can also be unified in both hardware and software with extreme learning machines, as shown by Ortín *et al.* (2015). A distinctive advantage of their approach is that it showed the possibility of passing from one computation paradigm to the other with a simple switch that connected or disconnected the feedback loop.

D. Other architectures of OEO reservoir computers

Alternative configurations of OEO reservoir computers have been proposed to ameliorate the performances of the systems initially developed by Larger *et al.* (2012) and Paquot *et al.* (2012).

As far as hardware improvements are concerned, Martinenghi *et al.* (2012) introduced a novel architecture based on a bandpass Ikeda-like dynamics in wavelength and on multiple delay lines (up to 15) with randomly defined weights implemented via a field programmable gate array (FPGA) board; see Fig. 20. The system achieved a WER of 0.6% with 150 nodes for the TI-46 spoken-digit recognition task. Larger *et al.* (2017) drastically improved the bandwidth of the system by adopting a bandpass Ikeda-like OEO with phase modulation and DPSK optical phase-to-intensity conversion. They also adopted asynchronous write-in and a multilevel neuronal structure that permitted one to emulate ~ 1000 virtual neurons. These conceptual innovations allowed them to achieve a state-of-the-art speed performance of 1×10^6 words per second for spoken-digit tests, with a WER of 0.04% for the TI-46 test, and a WER of $\sim 6\%$ for the AURORA-2 test which is significantly more difficult.

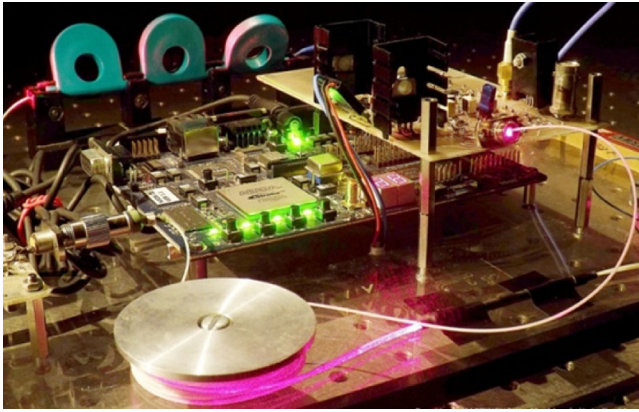


FIG. 20. Photograph of an Ikeda-like OEO reservoir computer built at the FEMTO-ST Institute, in Besançon, France. Multiple delay lines with random weights have been implemented using a FPGA board, thereby increasing the dimensionality and connectivity of the reservoir. Courtesy of R. Marinenghi.

Coupling OEOs have also emerged as an interesting strategy for optoelectronic reservoir computing. Tezuka, Kanno, and Bunsen (2016) numerically analyzed the performance of Ikeda-like bandpass OEOs with mutual coupling for the Santa Fe chaotic time-series prediction task, and they showed that this mutual coupling permitted one to slow down the modulation speed of the mask signal at no cost for computational performance. Zhao, Yin, and Zhu (2018) used a similar coupled OEO reservoir computer for the recognition of the optical packet headers. They numerically showed that under optimal conditions, the system could simultaneously recognize two different channels of optical packet headers, such as 3–6 bits and 8–32 bits, with a null WER.

E. Optimal processing for OEO reservoir computing

Improvements at the processing stage have been numerous and have allowed one to ameliorate the performances and practical attractiveness of OEO reservoir computers.

Soriano, Ortín *et al.* (2013) demonstrated that multilevel preprocessing masks permit one to optimize the performance of the reservoir computers in the presence of noise. This strategy was validated with the Santa Fe prediction task for which the use of a six-level mask contributed to decrease the error in the Santa Fe test to 2%, down from 12% with a binary mask. Antonik *et al.* (2017) proposed an online training scheme based on a gradient descent algorithm programmed on a FPGA chip. This approach aimed at circumventing the drawback of offline training that is standard for most OEO reservoir computers. They tested their system with a channel equalization task and reported error rates up to 2 orders of magnitude lower than previous implementations on this task. Duport *et al.* (2016a) implemented a stand-alone OEO reservoir computer, with analog input and output layers; see Fig. 21. The main innovation of this architecture is that it solved the problem of digital preprocessing and postprocessing, thereby allowing for a fully analog computation. This OEO reservoir computer

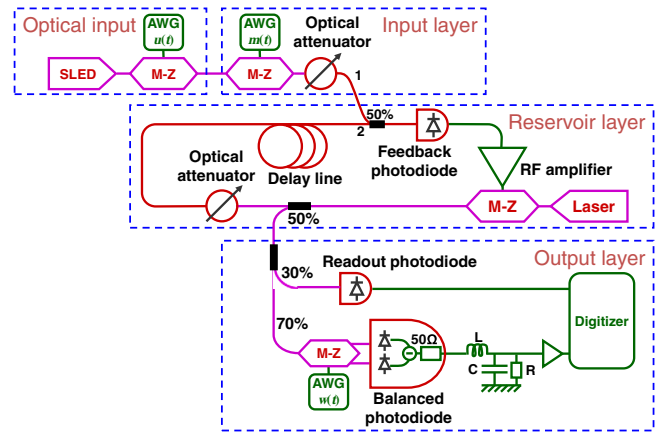


FIG. 21. Schematic of an experimental OEO reservoir computer. The reservoir layer is a delay dynamical system in which a Mach-Zehnder (M-Z) modulator acts as nonlinearity. The information is mixed to the signal using an arbitrary waveform generator (AWG). From Duport *et al.*, 2016a.

exhibited only limited degradation of performances comparatively to their conventional (hybrid) counterparts, when tested with nonlinear channel equalization, NARMA and radar signal forecasting tasks. The same tasks were successfully performed in another work of Duport *et al.* (2016b), where they showed that it is possible to optimize hardware bandwidth by time interleaving several reservoirs on the same physical setup. This procedure enables the OEO reservoir computer to process several tasks independently and simultaneously. Another recent processing improvement is the implementation of backpropagation algorithms (Hermans *et al.*, 2016). This approach allows one to obtain competitive performances, even for some of the most difficult benchmark tasks, such as the acoustic-phonetic continuous speech corpus TIMIT (~35% error rate with 200 nodes). Antonik, Haelterman, and Massar (2017) proposed an OEO computer where the output signals are fed back to the reservoir. This strategy permitted one to enhance the predictability performance of the system and was tested for the prediction of a chaotic time series from the Lorenz and Mackey-Glass oscillators.

F. OEOs as neuromorphic autaptic systems

Different approaches for OEO neuromorphic computing can be developed outside of the reservoir computing paradigm. For example, an excitable oscillator with delayed feedback can provide an ideal platform to model the dynamics of self-coupled, or *autaptic*, neurons.

Romeira *et al.* (2016) demonstrated a proof-of-concept system for optoelectronic neuromorphic computing using a laser driven by a nanoscale nonlinear resonant tunneling diode and submitted to delayed feedback; see Fig. 22. This OEO is characterized by dynamical properties similar to those of the FitzHugh-Nagumo neuron model with delayed feedback. They performed an extended theoretical and experimental analysis showing that their OEO has regenerative memory properties, enabling optical buffering, storage, and reshaping of data. This neuromorphic computing approach where

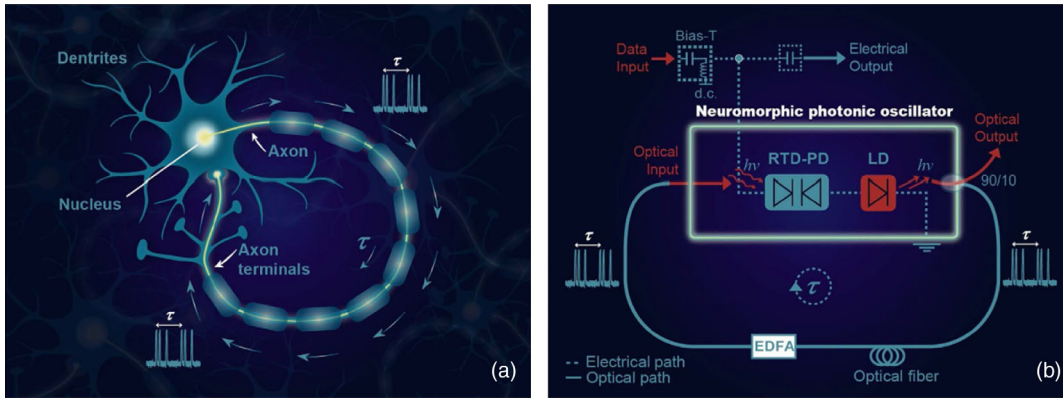


FIG. 22. Neuron-inspired regenerative memory with autaptic connection. (a) Diagram of a neuron with a self-feedback effect due to the presence of an autapse. (b) Schematic of the equivalent time-delayed neuromorphic photonic resonator in which the optical output is reinjected after a time delay due to the propagation into an optical fiber. RTD-PD: resonant tunneling diode photodetector; LD: laser diode; EDFA: erbium-doped fiber amplifier. From [Romeira *et al.*, 2016](#).

modulatorless OEOs are mimicking autaptic neurons could provide competitive solutions for ultrafast analog processing in optical telecommunication networks ([Romeira, Figueiredo, and Javaloyes, 2017](#)).

V. NARROW-BAND OEOs FOR ULTRAPURE MICROWAVE GENERATION

A narrow bandpass OEO is mainly characterized by a feedback loop that is highly frequency selective in the rf spectral domain. The filtering process is generally performed in the electric branch, using a narrow-band rf filter with quality factor $Q_{\text{rf}} = F_0/\Delta F \gg 1$ (typically > 100), with F_0 being the center frequency of the filter, and ΔF its 3 dB bandwidth.

The main application of these narrow-band OEOs is ultrapure microwave generation. As highlighted in the general Introduction, optoelectronic oscillators had been rapidly identified as pertinent systems for radio-frequency synthesis [see, for example, [Schlaak, Neyer, and Sohler \(1980\)](#), [Nakazawa, Tokuda, and Uchida \(1981\)](#), [Neyer and Voges \(1982b\)](#), [Grigor'yants *et al.* \(1985\)](#), or [Lewis \(1992\)](#)]. However, it is the work of [Yao and Maleki \(1994\)](#) with the archetypal architecture displayed in Fig. 23 that popularized them as a major platform for microwave engineering applications. Nowadays, OEOs have reached the highest level of technological maturity, as they have led to proof-of-

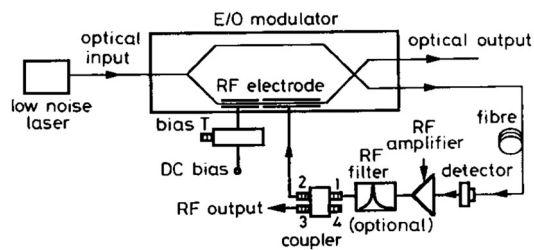


FIG. 23. Basic single-loop OEO architecture for ultrapure microwave generation as initially proposed by [Yao and Maleki \(1994\)](#). They used this OEO to generate a 9.22 GHz signal with a laser emitting at 1310 nm.

concept experiments and commercial products with competitive performances ([Maleki, 2011](#); [Maleki, Eliyahu, and Matsko, 2011](#)).

The purpose of this section is to present the various scientific and technological concepts related to ultrapure radio-frequency synthesis using these microwave photonic systems.

A. Deterministic dynamics of narrow-band OEOs

Before analyzing the detrimental effect of noise on the metrological performances of narrow-band OEOs, it is important to understand their deterministic dynamics, which corresponds to the system's behavior when stochastic effects are disregarded.

[Chembo *et al.* \(2007\)](#) introduced a time-domain approach based on delay-differential equations in order to investigate the nonlinear dynamics of narrow-band OEOs. The fundamental idea is that these OEOs are bandpass Ikeda-like systems, which can be described by the block diagram of Fig. 4. Therefore, exactly as the broad bandpass OEOs described in Sec. II.C, their time-domain dynamics has to be ruled by an integrodifferential delay equation like Eq. (5), with appropriately modified delay and filter timescales. In particular, the proportional, derivative, and integral prefactors of the linear operator \hat{H} have now to be defined analogously to the parameters of a resonant resistor-inductor capacitor filter following

$$\hat{H}\{x\} \equiv x + \frac{1}{\Delta\Omega} \dot{x} + \frac{\Omega_0^2}{\Delta\Omega} \int_{t_0}^t x(s) ds = \beta f_{\text{NL}}[x_T], \quad (10)$$

where $\Omega_0 = 2\pi F_0$ and $\Delta\Omega = 2\pi\Delta F$ are, respectively, the angular center frequency and bandwidth of the narrow-band filter.

The integrodifferential delay equation (10) contains all the information needed to perform the nonlinear dynamics study, but interestingly, it can be further simplified. Indeed, owing to the narrow-band nature of the filter, the microwave variable can be rewritten as

$$x(t) = A(t) \cos[\Omega_0 t + \varphi(t)] = \frac{1}{2} \mathcal{A}(t) e^{i\Omega_0 t} + \text{c.c.},$$

where $A(t)$ and $\varphi(t)$ are the amplitude and phase of the microwave, $\mathcal{A}(t) = A(t)e^{i\varphi(t)}$ is its complex envelope, while c.c. denotes the complex conjugate of the preceding term. The microwave output $x(t)$ is perfectly sinusoidal with frequency Ω_0 if both A and φ are constant. However, in the general case, both variables will be time dependent, even though they are bound [together with $\mathcal{A}(t)$] to vary slowly at timescale $\sim 1/\Delta\Omega$, while the original microwave variable $x(t)$ varies rapidly at timescale $\sim 1/\Omega_0$. Therefore, the slow and fast timescales are exactly split by a factor $\Omega_0/\Delta\Omega = Q_{\text{rf}}$, and the slowly varying envelope condition $|\dot{\mathcal{A}}(t)| \ll \Omega_0 |\mathcal{A}(t)|$ is automatically fulfilled.

In the case of an OEO with a sinusoidal nonlinearity $f_{\text{NL}}[x_T] \equiv \cos^2(x_T + \phi)$ originating from a Mach-Zehnder modulator, it can be shown that the complex slowly varying envelope $\mathcal{A}(t)$ obeys the following equation:

$$\dot{\mathcal{A}} = -\mu e^{i\vartheta} \mathcal{A} - 2\mu\gamma e^{i\vartheta} e^{-i\sigma} \text{Jc}_1[2|\mathcal{A}_T|] \mathcal{A}_T, \quad (11)$$

where $\vartheta = \arctan[1/2Q_{\text{rf}}]$ is a filter-induced phase shift, $\mu = [\Delta\Omega/2]\{1 + [1/(2Q_{\text{rf}})]^2\}^{-1/2}$ is the effective half bandwidth of the rf filter, $\sigma = \Omega_0 T$ is the microwave round-trip phase, and $\gamma = \beta \sin 2\phi$ is the effective gain of the feedback loop. The Bessel-cardinal function $\text{Jc}_1(x) = J_1(x)/x$ is qualitatively similar to the sinus-cardinal function, except its maximum at $x = 0$ is $1/2$ instead of 1 . In the limit $\Delta F \gg 1/T$ where several ring-cavity modes fit into the rf bandwidth (almost always fulfilled with km-long delay lines), this equation can be further simplified by setting $\vartheta \simeq 0$, and $\sigma \simeq 0 \pmod{\pi}$ with $\gamma e^{-i\sigma} \simeq -|\gamma|$.

It is interesting to note that in nonlinear photonic systems with feedback, several models are based on the hypothesis that the nominal frequencies of the light-wave signals are known, while only their amplitudes and phases are the variables of interest, as in the Lang-Kobayashi equations [Lang and Kobayashi (1980); also see Soriano, García-Ojalvo *et al.* (2013) and references therein]. The envelope Eq. (11) is essentially based on the same idea, except the carrier frequency is a microwave instead of a light wave.

The microwave envelope approach was successfully used to investigate the time-domain dynamics of narrow-band OEOs. Unlike the frequency-domain methods (based, for example, on the Barkhausen oscillation criteria), the time-domain models are the proper tools to explore transient, multiperiodic, multimode, or chaotic dynamical states, and to accurately perform higher-order bifurcation analysis (Chembo, Larger, and Colet, 2008). This formalism naturally identified the primary Hopf bifurcation at $|\gamma| = 1$ and allowed as well to determine the amplitude of the single-mode microwave oscillations beyond that point. But most importantly, as shown in Fig. 24, this model predicted a secondary Hopf bifurcation for higher gain, also referred to as a Neimark-Sacker (or *torus*) bifurcation. It occurs at the asymptotic critical value $\gamma_{\text{cr}} = \{2\text{Jc}_1[\text{J}_0^{-1}(0)]\}^{-1} \simeq 2.31$ when $\Delta F \gg 1/T$, but for narrower rf filters or shorter delay lines ($\Delta F \sim 1/T$), this torus bifurcation occurs at higher gain

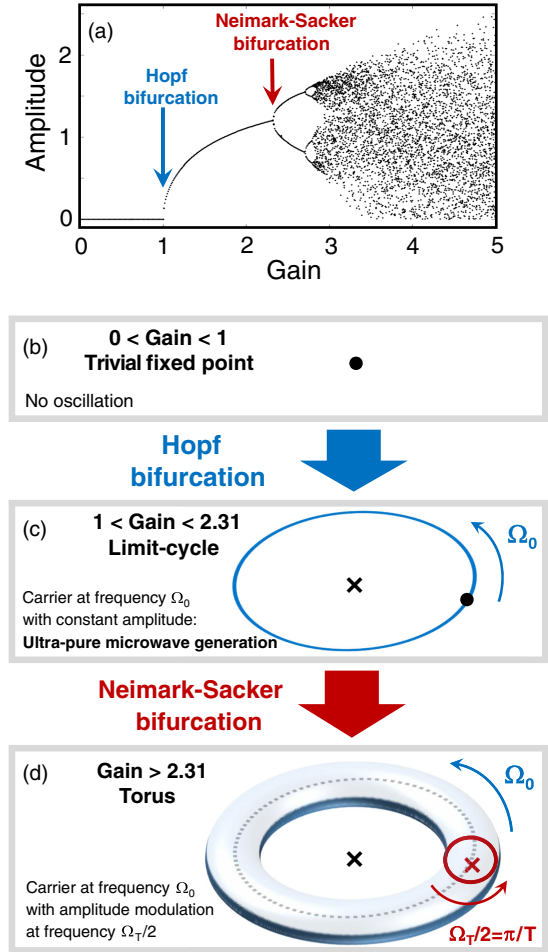


FIG. 24. Bifurcation sequence in single-loop OEOs as the feedback gain $|\gamma|$ is increased in Eq. (11), in the conventional configuration where $F_0 \gg \Delta F \gg 1/T$. (a) Bifurcation diagram of the microwave amplitude as a function of gain $|\gamma|$. (b)–(d) Topological changes in the state space. Further increase of the gain beyond (d) leads to a chaotic torus [Gain $\gtrsim 3$, as shown in the bifurcation diagram (a)]. Note that this full bifurcation sequence is totally deterministic and unrelated to phase or amplitude noise.

values (Chembo, 2017). This theoretical prediction of a secondary bifurcation was in complete agreement with experimental measurements, as evidenced in Fig. 25. It should be noted that the torus bifurcation intrinsically limits the output power that can be delivered by a single-loop OEO, as it destabilizes the microwave when the gain is increased beyond the critical gain value γ_{cr} . A similar secondary bifurcation was reported as well by Liu *et al.* (2014), in a theoretical and experimental work where they considered an OEO based on a polarization modulator. More recently, Bao, Banyas, and Illing (2018) used OEO architectures based on intensity modulators to perform a detailed analysis of both the Hopf and Neimark-Sacker bifurcations, demonstrating an excellent agreement between theoretical predictions and experimental results.

Figure 24 also shows that from a topological point of view, the complex envelope variable $\mathcal{A}(t)$ can be considered as a projection of the microwave variable $x(t)$ onto a Poincaré

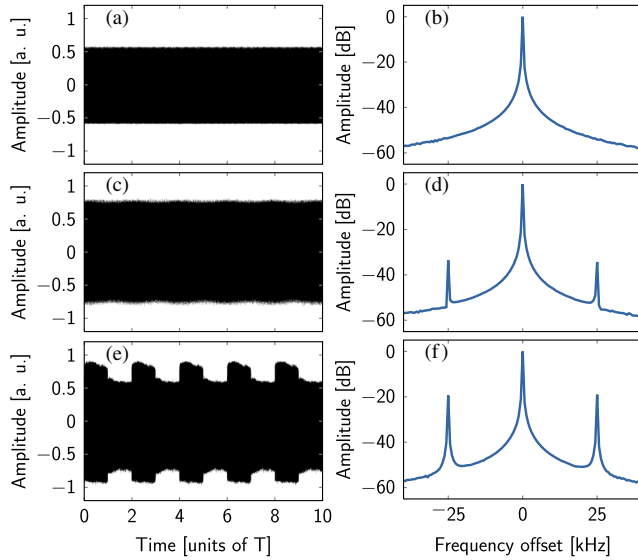


FIG. 25. Experimental evidence of the Neimark-Sacker bifurcation as the gain is increased in an OEO with a carrier at $\Omega_0/2\pi = 3$ GHz, a bandwidth $\Delta\Omega/2\pi = 20$ MHz, and a delay $T = 20$ μ s. (a), (c), and (d) are time traces, while (b), (d), and (f) are the Fourier spectra of the corresponding reconstructed envelopes (relatively to the carrier). (a), (b) Before the bifurcation, the signal has a constant amplitude and an angular frequency Ω_0 [see Fig. 24(c)]. (c), (d) At the onset of the Neimark-Sacker bifurcation, the amplitude starts to be sinusoidally modulated at angular frequency $\Omega_T/2 = \pi/T = 2\pi \times 25$ kHz. In the Fourier spectrum, deterministic modulation side peaks appear at ± 25 kHz around the carrier; they are unrelated to the noisy peaks that appear instead at multiples of $1/T = 50$ kHz. The normalized gain value is 2.42, to be compared to the theoretical prediction of 2.31 [see Fig. 24(d)]. (e), (f) Beyond the bifurcation, the small sinusoidal modulation morphs into large square-wave relaxation oscillations with the same frequency. The torus in Fig. 24(d) now has a rectangularlike cross section. Adapted from Chembo *et al.*, 2007.

section: therefore, when x consecutively undergoes a Hopf and a Neimark-Sacker bifurcation as the gain is increased, the envelope \mathcal{A} undergoes a pitchfork and a Hopf bifurcation, respectively.

B. Phase noise as a measure of spectral purity

The purity of a microwave is generally evaluated in terms of phase noise spectra. In noise-free oscillators, the amplitude and phase of the output signal are constant: therefore, the corresponding Fourier power spectrum is a collection of Dirac peaks, standing for the fundamental frequency and its harmonics. In most cases, the microwave oscillations originate from a limit cycle, which appears to be stable against amplitude perturbations, while there is no mechanism able to stabilize the phase to a given value: in other words, the amplitude of the oscillations is exponentially stable, while the phase is only neutrally stable. This neutral stability of the phase is a direct consequence of the phase invariance that characterizes autonomous oscillators.

In the presence of noise, both the amplitude and the phase become stochastic variables. In the time domain, amplitude

noise remains bounded owing to the transverse stability of the limit cycle and is therefore inconsequential in most applications. However, the neutral stability in the longitudinal direction allows the phase noise to grow unboundedly and to become the leading source of uncertainty in the oscillator. Indeed, in the simplest case, it can be shown that the phase dynamics is a Wiener process that obeys a stochastic differential equation of the kind $\dot{\varphi}(t) = \xi(t)$ [with $\varphi(0) = 0$], where $\xi(t)$ is a Gaussian white noise with an autocorrelation proportional to the power of the external noise source and inversely proportional to the power of the carrier. In an ideal noiseless oscillator, the phase would remain null, but in the presence of noise, it randomly drifts along the limit cycle, with variance $\langle \varphi^2(t) \rangle \propto t$: it can be considered in fact that the phase of the oscillator undergoes a diffusion process, in all points similar to a one-dimensional Brownian motion on a ring.

In the spectral domain, the main effect of phase noise will be to widen the zero-linewidth Dirac peaks, as explained in Fig. 3. Under the simplistic assumptions considered previously for the noise excitation, the power spectrum around the fundamental tone can be normalized to a Lorentzian $\mathcal{L}(f) \propto D/(D^2 + f^2)$ in units of dBc/Hz (dB relative to the carrier), where f is the offset frequency relatively to that carrier, and D is a constant proportional to the power of the white noise that is driving the phase. However, in real-world oscillators, the sources of noise display a wide diversity of spectral and statistical properties, so that in general the phase noise spectra $\mathcal{L}(f)$ substantially deviate from the theoretical Lorentzian profile (Rubiola, 2010).

Figure 26 displays the phase noise spectra of some of the best oscillators around 10 GHz at room temperature, along with the spectra of some commercial oscillators. It appears that under optimal conditions, OEOs significantly outperform

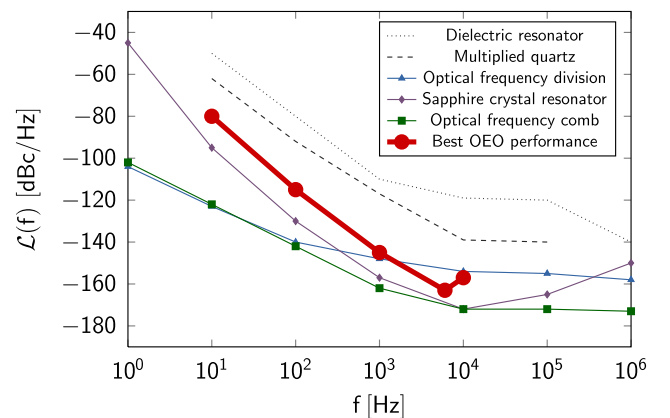


FIG. 26. Phase noise comparison between the best OEO performance (Eliyahu, Seidel, and Maleki, 2008) and other oscillators operating at room temperature in the X band (8–12 GHz). The OEO oscillates at 10 GHz and the other oscillators considered here are the following: a commercial dielectric resonator oscillator at 10.8 GHz (Miteq PLDRO-10-10800-5P), a commercial multiplied ($\times 80$) quartz oscillator at 10.24 GHz (Wenzel GMXO-FR), a 10 GHz optical frequency division oscillator (Fortier *et al.*, 2011), a 9 GHz sapphire oscillator (Ivanov and Tobar, 2009), and a 12 GHz fiber-based optical frequency comb oscillator (Xie *et al.*, 2017).

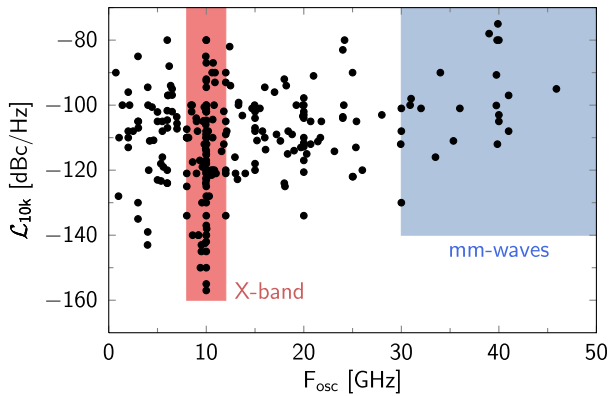


FIG. 27. Phase noise performance at 10 kHz offset [$\mathcal{L}_{10\text{k}} \equiv \mathcal{L}(f = 10\text{ kHz})$] for all the OEOs reported in this review with an oscillation frequency in the 0–50 GHz range. Two frequency bands of particularly high technological interest are highlighted, namely, the X band (8–12 GHz) and mm waves (30–300 GHz).

commercial solutions, while offering a competitive spectral purity when compared to the state of the art for microwave oscillators. It should be emphasized that beyond phase noise performance the appeal of a microwave oscillator for a particular application strongly depends on size, weight, and power (SWAP) constraints, to which is sometimes added the constraint of cost (SWAP-C). Other features such as tunability, agility, output power, or interoperability with other microwave photonics systems can also arise as well as decisive advantages depending on the technological context. From this perspective, OEOs emerge as one of the most versatile and promising microwave generation platform.

For practical purposes, it is convenient to assess the spectral purity of an oscillator with a single value, instead of the full spectral profile $\mathcal{L}(f)$. For that reason, the phase noise performance is generally given for a particular offset frequency that depends on the targeted application. For the quasitotality of OEOs, the phase noise performance is characterized by its value at an arbitrary offset of 10 kHz from the carrier. This particular offset reference finds its origin in the Doppler radar application of ultrapure microwaves, as explained in Fig. 3 (it is actually the Doppler shift induced by a typical plane flying at 540 km/h when probed by a 10 GHz microwave). Therefore, in order to avoid repetitiveness, it should be assumed that the phase noise performance of the OEOs discussed throughout this section is always indicated for a 10 kHz offset, unless otherwise specified. In Fig. 27, the phase noise performance of all the OEO microwave generators reported in this review is displayed as a function of the oscillating frequency in the 0–50 GHz band. This figure offers a visual representation of the spectral purity that can generally be achieved by OEOs. It appears that most of them are developed in the X band (8–12 GHz), which is prevalent in most aerospace and telecommunication engineering applications.

All the OEO microwave generators reported in this section are also classified in Table I, with respect to their spectral purity and frequency range. The various architectures and main properties of these oscillators are discussed in the following sections.

C. Phase noise of single-loop OEOs

The simplest architecture of narrow-band OEOs for microwave generation corresponds to Fig. 23, when it includes a narrow-band rf filter and a few-km-long fiber delay line, yielding a delay time T in the 1–100 μs range (Yao and Maleki, 1994). In most studies, the filter has a multi-GHz center frequency and a bandwidth of the order of a few tens of MHz. However, these values can vary largely depending on the bandwidth of the various elements of the feedback loop and thereby provide a great frequency versatility for the OEO. Some single-loop OEOs also include a phase shifter in the rf branch for a fine-tuning of the oscillation frequency.

The first detailed analysis for this oscillator was proposed by Yao and Maleki (1996a, 1996b, 1996c), and it was based on a frequency-domain approach. Their quasilinear study permitted one to understand the benefit of a long-delay line in order to improve phase noise performance and to determine the microwave signal amplitude as a function of the feedback gain when it is increased beyond the normalized oscillation threshold of 1. Yao and Maleki also projected that OEOs could achieve a phase noise better than -140 dBc/Hz for oscillation frequencies as high as 75 GHz. It should be emphasized that oscillation frequencies in the mm-wave range are difficult to achieve using conventional rf-only oscillators (electromechanical resonators, quartz devices, etc.) because the output signal generally results from high-order frequency multiplication and features severe spectral purity degradation ($20\log M\text{ dB}$ in the best case, with M being the multiplication factor).

The deterministic envelope equation (11) was a prerequisite in order to perform a phase noise analysis based on stochastic differential equations, also referred to as Langevin equations (Chembo, Volyanskiy *et al.*, 2009). The idea here is to add noise terms to the deterministic equation (11), which permits one to obtain stochastic equations for the amplitude $A(t)$ and the phase $\varphi(t)$. In the approximation where amplitude noise is neglected, the phase equation is linear and the spectral density of phase fluctuations $S_\varphi(f) \equiv |\tilde{\varphi}(f)|^2$ (in units of dBrad^2/Hz) can be straightforwardly determined using the Fourier transform. The single-sideband phase noise spectrum (in units of dBc/Hz) is subsequently obtained via the relationship $\mathcal{L}(f) \equiv (1/2)S_\varphi(f)$, leading, for example, to the spectrum displayed in Fig. 28.

This Langevin formalism permits one to fully characterize the OEO phase noise spectrum above the oscillation threshold. In particular, the main characteristics of the parasitic ring-cavity peaks in the phase noise spectrum have been analytically determined with great precision, such as, for example, the position of the n th order parasitic peak relative to the carrier ($= n/T - n/\pi T^2 \Delta F$), their height relative to the phase noise floor [$= 40\log(T\Delta F/n)$ in dB], and their linewidth [$= n^2(2/\pi T^3 \Delta F^2)$]. As explained in Fig. 28, these theoretical predictions are in excellent agreement with the experimental measurements. The long delay line therefore appears to be beneficial for phase noise, but, however, it was demonstrated by Levy *et al.* (2010) that flicker noise limits the performance of long-cavity OEOs ($>5\text{ km}$) close to the carrier ($<500\text{ Hz}$), as it contains a strong component that linearly depends on the loop length. It should also be noted that the ring-cavity

TABLE I. Recapitulative table of the phase noise performance at 10 kHz offset [or $\mathcal{L}_{10\text{ k}} \equiv \mathcal{L}(f = 10\text{ kHz})$] for all the OEOs reported in Sec. V. All frequencies are rounded to the nearest integer in GHz. The attributes in brackets after each reference are as follows. [x, C]: single-frequency OEO recovering a clock signal at frequency x ; [x, P]: optical-pulse OEO with repetition rate x ; [T_{x-y}]: OEO continuously tunable from frequencies x to y ; [z, M_{x-y}]: multifrequency OEO emitting on a discrete set of frequencies between x and y , with phase noise evaluated at frequency z .

Frequency band	$\mathcal{L}_{10\text{ k}} \leq -140\text{ dBc/Hz}$	$-140 < \mathcal{L}_{10\text{ k}} \leq -120\text{ dBc/Hz}$	$-120 < \mathcal{L}_{10\text{ k}} \leq -100\text{ dBc/Hz}$	$\mathcal{L}_{10\text{ k}} > -100\text{ dBc/Hz}$
L band (1–2 GHz), S band (2–4 GHz), or C band (4–8 GHz)	Ustinov <i>et al.</i> (2018) [T ₃₋₁₂]	Bogataj, Vidmar, and Batagelj (2016) [3], Z. Chen <i>et al.</i> (2017) [5, M ₅₋₂₁], Jin <i>et al.</i> (2019) [5], Li, Li, and Yao (2012) [T ₀₋₁₀], Y. Liu <i>et al.</i> (2018) [4], Liu <i>et al.</i> (2019) [T ₆₋₁₈], Loh <i>et al.</i> (2012) [3], Nguimdo <i>et al.</i> (2015) [6], Saleh <i>et al.</i> (2014) [6], Xie <i>et al.</i> (2016) [T ₁₋₁₅]	J. Chen <i>et al.</i> (2018) [2, M ₂₋₁₉], Devgan <i>et al.</i> (2006) [2, P], Huang <i>et al.</i> (2015) [T ₂₋₁₀], Li, Liu, and Zhu (2015) [T ₄₋₁₉], C. Li <i>et al.</i> (2016) [4, M ₄₋₂₄], Liao <i>et al.</i> (2017) [T ₂₋₂₄], Liu, Zou, and Chen (2013) [T ₁₋₇], Maxin <i>et al.</i> (2013) [T ₂₋₆], Poinot <i>et al.</i> (2002) [3], Romeira <i>et al.</i> (2011) [1], Shang <i>et al.</i> (2017) [T ₆₋₄₀], Shi <i>et al.</i> (2018) [T ₁₋₄₀], Tang <i>et al.</i> (2012) [T ₆₋₁₂], W. Yu, Wang <i>et al.</i> (2015) [5, M ₅₋₂₇], Wishon <i>et al.</i> (2018) [T ₆₋₁₂], T. Wu <i>et al.</i> (2016) [5, M ₅₋₁₅], Xiong <i>et al.</i> (2013) [T ₄₋₉], Ye <i>et al.</i> (2019) [7], Zhang, Gao, and Yao (2014) [T ₁₋₁₂], Zhang, Hou, and Zhao (2014) [3], Zhang <i>et al.</i> (2016) [4, M ₄₋₁₃], J. Zhao <i>et al.</i> (2016) [3]	Banejee, de Britto, and Pacheco (2019) [2], C. Li <i>et al.</i> (2018) [T ₄₋₁₃], Pan and Yao (2010) [6, C], Saleh, Lin, and Chembo (2015) [6], J. Tang <i>et al.</i> (2018) [7], Zhang and Yao (2018) [T ₂₋₈]
X band (8–12 GHz)	Chembo, Hmima <i>et al.</i> (2009) [10, P], Chembo, Volyanskiy <i>et al.</i> (2009) [10], Eliyahu, Seidel, and Maleki (2008) [10], Fleyer <i>et al.</i> (2016) [T ₉₋₁₀], Hong <i>et al.</i> (2016) [10], Lelièvre <i>et al.</i> (2017) [10], Okusaga <i>et al.</i> (2013) [10], Salik, Yu, and Maleki (2007) [9, P], Yao and Maleki (2000) [10], Yu, Salik, and Maleki (2005) [9, P], Zhang and Yao (2018) [10], Zhenghua <i>et al.</i> (2016) [10], Zhou and Blasche (2005) [10]	Bagnell, Davila-Rodriguez, and Delfyett (2014) [T ₆₋₆₀], Dai <i>et al.</i> (2015) [10, P], Dai <i>et al.</i> (2018) [10], Fan <i>et al.</i> (2019) [11], Fleyer and Horowitz (2018) [10], Fu <i>et al.</i> (2017) [10], Hao, Cen <i>et al.</i> (2018) [T ₈₋₁₂], Hosseini, Banai, and Kartner (2017) [11], Ji, Yao, and Maleki (1999) [10], Jia, Yu, Z. Wang <i>et al.</i> (2015) [10, P], Kaba <i>et al.</i> (2006) [10], Liu <i>et al.</i> (2012) [10, P], Liu, Liu <i>et al.</i> (2018) [10, M ₁₀₋₄₀], Mutgala <i>et al.</i> (2017) [10], Peng <i>et al.</i> (2017) [T ₇₋₄₀], Romisch <i>et al.</i> (2000) [11], Saleh, Llopis, and Cibiel (2013) [10], Ustinov <i>et al.</i> (2018) [T ₃₋₁₂], Volyanskiy, Chembo <i>et al.</i> (2010) [10], Xiao <i>et al.</i> (2019) [T ₈₋₁₄], Xie <i>et al.</i> (2013) [T ₅₋₃₈], Xu, Jin, and Chi (2013) [10, M ₁₀₋₂₀], Zhu <i>et al.</i> (2016) [10], Zhu, Du, and Pan (2018) [10, P]	G. Chen <i>et al.</i> (2018) [T ₉₋₁₅], Chen, Liu, and Pan (2018) [T ₈₋₄₀], J. Chen <i>et al.</i> (2018) [8, M ₂₋₁₉], Chen <i>et al.</i> (2019) [12, M ₁₂₋₂₄], Chi, Peng, and Lin (2011) [10], Cho and Sung (2012) [8], Dahan, Shumakher, and Eisenstein (2005) [10, P], Dai <i>et al.</i> (2017) [10], Devgan <i>et al.</i> (2009) [10], Eliyahu <i>et al.</i> (2013) [T ₂₋₁₅], Gao <i>et al.</i> (2013) [T ₆₋₁₃], Gao <i>et al.</i> (2017) [T ₄₋₁₂], Huang <i>et al.</i> (2014) [10, P], Huang <i>et al.</i> (2017) [10], Jiang <i>et al.</i> (2007) [10, P], F. Jiang <i>et al.</i> (2013) [T ₇₋₁₃], Lasri <i>et al.</i> (2002) [10, P], Lasri <i>et al.</i> (2004) [10, C], Lee <i>et al.</i> (2008) [11], Lee and Song (2017) [10, M ₁₀₋₂₀], Li and Yao (2012) [T ₃₋₂₈], Li <i>et al.</i> (2014) [T ₃₋₁₀], Li, Liu, and Zhu (2015) [T ₉₋₃₈], Liao <i>et al.</i> (2017) [T ₂₋₂₄], Ma <i>et al.</i> (2018) [10], Pan and Yao (2009) [10, C], Poinot <i>et al.</i> (2002) [9], Qu <i>et al.</i> (2015) [9], Shang <i>et al.</i> (2017) [T ₆₋₄₀], Shi <i>et al.</i> (2018) [T ₁₋₄₀], Shumakher and Eisenstein (2008) [10], Sun <i>et al.</i> (2014) [10], Tang, Zhang, and Pan (2014) [11], H. Tang <i>et al.</i> (2018) [T ₀₋₄₀], Teng <i>et al.</i> (2016) [8, M ₃₋₂₄], Tong <i>et al.</i> (2017) [10], Vallet <i>et al.</i> (2016) [12], Wang <i>et al.</i> (2011) [10, M ₁₀₋₂₀], Wang and Yao (2013) [T ₇₋₁₅], Wang, Li, and Zhu (2014) [10, M ₁₀₋₄₀], P. Wang <i>et al.</i> (2015) [T ₆₋₁₅], Wei <i>et al.</i> (2013) [T ₆₋₁₁], Wishon <i>et al.</i> (2018) [T ₆₋₁₂], Xu <i>et al.</i> (2015) [10], Yang <i>et al.</i> (2007) [12], Yang <i>et al.</i> (2013) [10], Zhang <i>et al.</i> (2014) [10], C. Zhang <i>et al.</i> (2018) [10, M ₁₀₋₂₀], Zheng <i>et al.</i> (2015) [10, M ₁₀₋₂₀], Zhou <i>et al.</i> (2016) [10, P]	Chen, Li, and Wen (2013) [10, M ₁₀₋₈₀], Hasegawa, Oikawa, and Nakazawa (2007) [10, P], Koizumi, Yoshida, and Nakazawa (2010) [10, P], Lee, Jeon, and Song (2019) [10], Liu, Zheng, and Shu (2017) [11], Lu <i>et al.</i> (2011) [10, C], Mei <i>et al.</i> (2014) [T ₉₋₁₁], Merklein <i>et al.</i> (2016) [T ₅₋₄₀], Saleh and Chembo (2017) [12], J. Tang <i>et al.</i> (2018) [9], Volyanskiy, Salzenstein <i>et al.</i> (2010) [11], Yang <i>et al.</i> (2012) [9, M ₉₋₁₉]

(Table continued)

TABLE I. (Continued)

Frequency band	$\mathcal{L}_{10\text{ k}} \leq -140$ dBc/Hz	$-120 < \mathcal{L}_{10\text{ k}} \leq -100$ dBc/Hz	$\mathcal{L}_{10\text{ k}} > -100$ dBc/Hz
Ku band (12–18 GHz)	G. Chen <i>et al.</i> (2018) [T ₉₋₁₅], Peng <i>et al.</i> (2017) [T ₇₋₄₀], Xiao <i>et al.</i> (2019) [T ₈₋₁₄], Xie <i>et al.</i> (2013) [T ₅₋₃₈], Xie <i>et al.</i> (2016) [T ₁₋₁₅]	Charalambous <i>et al.</i> (2017) [15], Z. Chen <i>et al.</i> (2017) [16, M ₅₋₂₁], J. Chen <i>et al.</i> (2018) [14, M ₂₋₁₉], Kim <i>et al.</i> (2012) [15], Li, Liu, and Zhu (2015) [10-38], Ma <i>et al.</i> (2015) [T ₉₋₁₇], Shang <i>et al.</i> (2017) [T ₆₋₄₀], Shi <i>et al.</i> (2018) [T ₁₋₄₀], H. Tang <i>et al.</i> (2018) [T ₀₋₄₀], Xiao <i>et al.</i> (2018) [13, M ₁₃₋₃₅], Zhang <i>et al.</i> (2015) [T ₁₀₋₁₉], Zhang <i>et al.</i> (2019) [T ₁₇₋₂₂]	Chen, Liu, and Pan (2018) [T ₈₋₄₀], Han <i>et al.</i> (2017) [T ₄₋₁₆], Liao <i>et al.</i> (2017) [T ₂₋₂₄], Merrer <i>et al.</i> (2012) [12], Pan and Yao (2010) [12, C], Zhang <i>et al.</i> (2016) [13, M ₄₋₁₃]
K band (18–27 GHz)	Bluestone <i>et al.</i> (2015) [20], Jia, Yu, J. Wang <i>et al.</i> (2015) [20], Peng <i>et al.</i> (2017) [T ₇₋₄₀], Xie <i>et al.</i> (2013) [T ₅₋₃₈], X. Xie <i>et al.</i> (2014) [25]	Cai <i>et al.</i> (2012) [20, M ₁₀₋₂₀], Z. Chen <i>et al.</i> (2017) [21, M ₅₋₂₁], J. Chen <i>et al.</i> (2018) [19, M ₂₋₁₉], Chen <i>et al.</i> (2019) [24, M ₁₂₋₂₄], Fedderwitz <i>et al.</i> (2010) [T ₂₁₋₂₂], Y. Jiang <i>et al.</i> (2013) [20], Li, Liu, and Zhu (2015) [T ₉₋₃₈], Liu, Liu <i>et al.</i> (2018) [20, M ₁₀₋₄₀], Pan and Yao (2009) [20, C], Shang <i>et al.</i> (2017) [T ₆₋₄₀], Shi <i>et al.</i> (2018) [T ₁₋₄₀], Suelzer <i>et al.</i> (2017) [T ₁₀₋₄₆], Sung <i>et al.</i> (2009) [20], Teng <i>et al.</i> (2016) [24, M ₃₋₂₄], Wang <i>et al.</i> (2011) [20, M ₁₀₋₂₀], Q. Wang <i>et al.</i> (2014) [25, C], Xiao <i>et al.</i> (2018) [24, M ₁₃₋₃₅], Xu, Jin, and Chi (2013) [20, M ₁₀₋₂₀], C. Zhang <i>et al.</i> (2018) [20, M ₁₀₋₂₀], Zhang <i>et al.</i> (2019) [T ₁₇₋₂₂], Zheng <i>et al.</i> (2015) [20, M ₁₀₋₂₀]	Lee and Song (2017) [20, M ₁₀₋₂₀], C. Li <i>et al.</i> (2016) [24, M ₄₋₂₄], Liao <i>et al.</i> (2017) [T ₂₋₂₄], Yang <i>et al.</i> (2012) [19, M ₉₋₁₉], Yao, Davis, and Maleki (2000) [18, P]
Ka band (27–40 GHz)	Ly <i>et al.</i> (2018) [30, M ₃₀₋₉₀]	Lu <i>et al.</i> (2015) [T ₃₂₋₄₁], Maleki (2011) [30], Pan <i>et al.</i> (2015) [T ₂₈₋₄₁], Shang <i>et al.</i> (2017) [T ₆₋₄₀], Shi <i>et al.</i> (2018) [T ₁₋₄₀], Suelzer <i>et al.</i> (2017) [T ₁₀₋₄₆], H. Tang <i>et al.</i> (2018) [T ₁₋₄₀], Wang, Li, and Zhu (2014) [40, M ₁₀₋₄₀]	Chang <i>et al.</i> (2002) [39], Chen, Li, and Wen (2013) [40, M ₁₀₋₈₀], Chen, Liu, and Pan (2018) [T ₈₋₄₀], Van Dijk <i>et al.</i> (2008) [40], Zhu, Pan, and Ben (2012) [T ₃₂₋₄₃]
V band (40–75 GHz)		Bagnell, Davila-Rodriguez, and Delfyett (2014) [T ₆₋₆₀], Liu, Liu <i>et al.</i> (2018) [40, M ₁₀₋₄₀], Pan <i>et al.</i> (2015) [T ₂₈₋₄₁], Shang <i>et al.</i> (2017) [T ₆₋₄₀]	Chen, Li, and Wen (2013) [60, M ₁₀₋₈₀], Lu <i>et al.</i> (2015) [T ₃₂₋₄₁], Merklein <i>et al.</i> (2016) [T ₅₋₄₀], Suelzer <i>et al.</i> (2017) [T ₁₀₋₄₆]
W band (75–110 GHz)	Ly <i>et al.</i> (2018) [90, M ₃₀₋₉₀]		

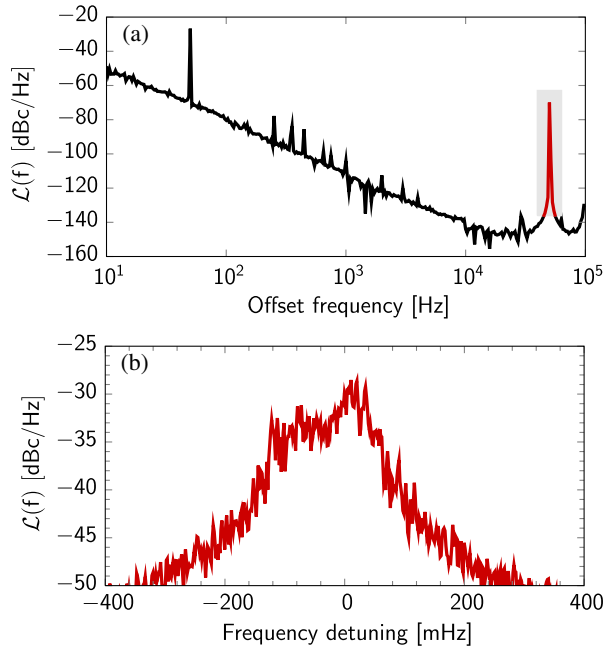


FIG. 28. Typical single-sideband phase noise spectrum for a single-loop OEO oscillating at 10 GHz with a 4-km-long fiber delay line (corresponding to a time delay $T = 20 \mu\text{s}$) in the optical branch, and a narrow bandpass filter with bandwidth $\Delta F = 50 \text{ MHz}$. (a) Experimental phase noise spectrum for a microwave power of 10.5 dBm. The phase noise floor at -148 dBc/Hz is identical to the model prediction. The peak at 50 Hz is a parasite signal originating from the electric mains supply, while the spurious peak around $1/T = 50 \text{ kHz}$ (in red with a gray background) is a ring-cavity mode induced by the fiber delay line. (b) Enlargement of the spectrum around the spurious ring-cavity peak at the offset frequency 50 kHz. Note that its height in (a) is not accurate because of insufficient resolution, while this enlargement provides a more precise measurement. The maximum of this peak is at -28.5 dBc/Hz , corresponding to a height of 119.5 dB from the phase noise floor (the theoretical prediction was 120 dB). Its -3 dB linewidth is around 40 mHz (with a theoretical prediction of 32 mHz). Adapted from Chembo, Volyanskiy *et al.*, 2009.

peaks significantly lengthen buildup of single-mode oscillation in OEO. In fact, they can even lead to a robust multimode dynamics instead of the desired monomode behavior (Chembo *et al.*, 2008). This effect can be efficiently quenched using techniques such as Fourier-domain mode locking (Hao, Cen *et al.*, 2018), and thereby allow for faster buildup.

Despite the presence of the ring-cavity spurious peaks, the basic single-loop topology offers the most competitive phase noise performance for OEOs. The most notable example in this category is the single-loop OEO developed by Eliyahu, Seidel, and Maleki (2008), which featured a 16-km-long delay line and low-noise optoelectronic components. Their oscillator established the record phase noise performance for an OEO, with a spectral purity of -163 dBc/Hz at 6 kHz offset from a 10 GHz carrier, and -157 dBc/Hz at 10 kHz. This is also one of the best performances for a room-temperature microwave oscillator as can be seen in Fig. 26.

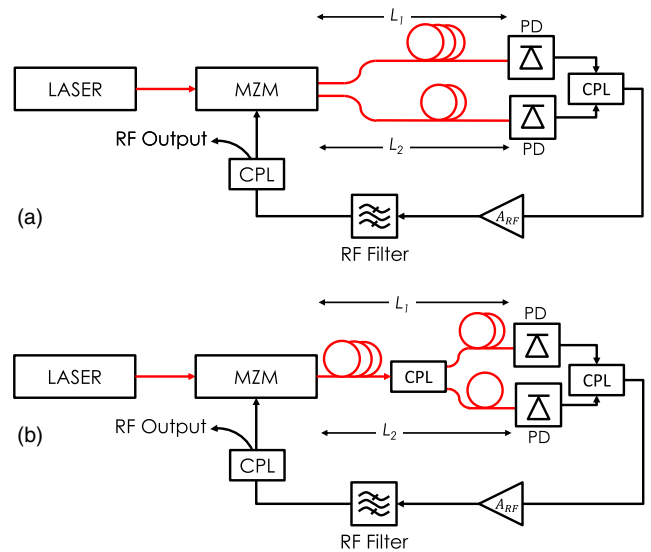


FIG. 29. Common configurations of a dual-loop OEO. CPL: coupler; MZM: Mach-Zehnder modulator; PD: photodiode. (a) OEO with a dual-output Mach-Zehnder modulator; (b) OEO with an optical coupler. From Lelièvre *et al.*, 2017.

The phase noise performance of single-loop OEOs can also be affected by various impairments such as fiber chromatic dispersion (Volyanskiy, Chembo *et al.*, 2010), Brillouin scattering (Saleh, Llopis, and Cibiel, 2013), Rayleigh scattering (Docherty *et al.*, 2013; Okusaga *et al.*, 2013; Cahill *et al.*, 2015), or nonlinear rf amplification (Jahanbakht and Hosseini, 2016).

Finally, note that single-loop OEOs can be implemented with different physical components in the optoelectronic path. For example, instead of the usual lithium niobate intensity modulators, it is possible to use instead a semiconductor-based Mach-Zehnder modulator (Ji, Yao, and Maleki, 1999) or a polarization modulator (Sun *et al.*, 2014). OEOs can also be implemented without a rf amplifier in the electric branch of the feedback loop as demonstrated by Loh *et al.* (2012).

D. Multiloop OEOs

As described in the preceding section, the phase noise spectrum of OEOs is characterized by very sharp and high ring-cavity peaks that are located very close to the carrier ($n \times 50 \text{ kHz}$ for a 4-km fiber delay line, n being an integer). These parasitic peaks are detrimental for most applications as they significantly degrade the spectral purity of the output microwave in the vicinity of these spurs (Liu, Dai, and Xu, 2018). It is also very difficult to filter them out because they are generally too close to the carrier frequency and easily pass through the rf bandpass filter that typically has a multi-MHz bandwidth.

An effective method to reduce the height of these peaks is to consider a multiloop architecture as proposed by Yao and Maleki (2000). In the simplest configuration, the feedback path features a short loop (defining the mode spacing) and a long loop (ensuring the low phase noise), implemented in parallel, as displayed in Fig. 29. This dual-loop feedback permits a strong attenuation of the parasitic peaks via a Vernier

effect, therefore yielding an oscillator with large mode spacing and low phase noise. Such architectures have been thoroughly investigated, using either time-domain (Nguimdo *et al.*, 2012) or frequency-domain approaches (Bánky, Horváth, and Berceli, 2006; Lelièvre *et al.*, 2017). This improved spectral purity is however obtained at the expense of a more complex architecture from the experimental viewpoint.

It is possible to implement multiloop OEOs using multiplexing techniques. The first option is wavelength division multiplexing that is based on multiple loops that are emulated by seeding an intensity modulator with several laser wavelengths (Shumakher and Eisenstein, 2008; Jia, Yu, J. Wang *et al.*, 2015; Charalambous, Perentos, and Iezekiel, 2016). The path followed by each signal is processed using standard wavelength multiplexers and demultiplexers. The second option is polarization multiplexing. In these architectures, the optical signal first passes through a polarization beam splitter, and the polarized output signals are sent in two delay lines (long and short) before being recombined using a polarization beam combiner (Yang *et al.*, 2007). This polarization multiplexing scheme can be combined to other effects such as polarization modulation (Cai *et al.*, 2012), phase modulation (Huang *et al.*, 2017), or even nonlinear effects such as stimulated Brillouin scattering (Han *et al.*, 2017).

Multiloop OEOs have also been developed along other physical and engineering principles, such as optical semiconductor laser injection (Kim *et al.*, 2012), broadband electro-optical frequency combs (X. Xie *et al.*, 2014), or self-phase-locked loops (Zhang *et al.*, 2014). Theoretical research is still ongoing to analyze existing topologies of multiloop OEOs or to propose novel architectures in order to improve both the phase noise performance and the side-mode suppression ratio (García and Gasulla, 2015; Mikitchuk, Chizh, and Malyshev, 2016).

A recent development associated with multiloop OEOs is related to the observation and exploitation of parity-time symmetry in microwave photonics, where microwave oscillation is achieved via a careful adjustment between gain and losses in two competing feedback loops (Y. Liu *et al.*, 2018; Zhang and Yao, 2018).

E. Multifrequency OEOs

Various architectures of OEOs have the capability to output several radio frequencies with ultralow phase noise performance. In general, a nonlinearity of the feedback loop is used to generate harmonic tones with high spectral purity from a fundamental microwave frequency.

Frequency doubling is most commonly achieved using the nonlinearity of a Mach-Zehnder modulator (Wang *et al.*, 2011; Yang *et al.*, 2012; Xu, Jin, and Chi, 2013) or even its polarization sensitivity as proposed by Zheng *et al.* (2015). By combining intensity modulators biased close to their minimum transmission points, the output frequency can be tripled (Z. Chen *et al.*, 2017) and even sextupled (Teng *et al.*, 2016). Frequency sextupling was achieved as well by C. Li *et al.* (2016) using an architecture combining a Mach-Zehnder interferometer and a fiber Bragg grating. More recently, Chen *et al.* (2019) demonstrated a modulatorless approach based on the frequency doubling of the period-one

oscillation of a distributed feedback semiconductor laser with optical feedback.

Multifrequency OEOs can be used to generate nonsinusoidal wave forms in the time domain. Triangular wave-form generators are by far the most common OEOs in that category, and they are based on architectures that have the capability to suppress even-order harmonics [see, for example, Huang *et al.* (2015), W. Yu. Wang *et al.* (2015), T. Wu *et al.* (2016), Zhang *et al.* (2016), and Ma *et al.* (2018)]. OEOs can also generate arbitrary wave forms as demonstrated by Li, Kong, and Yao (2013). Their oscillator cascaded a polarization modulator and a fiber Bragg grating filter, and the output signals were processed in the spectral domain through reconfigurable phase coding or frequency chirping.

F. Tunable OEOs

Frequency tunability is one of the most useful characteristics for a microwave synthesizer, and in general, the main drawback of ultrapure microwave generators (such as quartz oscillators) is that they do not feature this capability. Indeed, in the basic OEO architecture, the oscillation frequency is defined by the rf filter in the electric branch and offers only a limited tunability, typically within the filter bandwidth (a few MHz in the best case). Discontinuous frequency tuning by steps of $1/T$ can be achieved via the selection of any of the ring-cavity modes that fit into the rf filter bandwidth. Continuous frequency tuning is possible as well, as shown by Poinot *et al.* (2002) with an OEO architecture where dispersive feedback could allow for a \sim MHz frequency tuning around various operating frequencies. However, achieving multi-GHz tunability in OEOs while preserving ultrahigh spectral purity is a technological challenge that has been addressed by several research groups in recent years.

An efficient strategy is to implement a tunable microwave photonic filter. Various groups used OEO architectures combining dispersion-compensating fibers and broadband light sources (Li, Li, and Yao, 2012; Liu, Zou, and Chen, 2013; Zhang, Gao, and Yao, 2014). The broadband source can be replaced by a tunable multiwavelength laser as proposed by F. Jiang *et al.* (2013). It is also possible to build the tunable microwave photonic filter using a fiber Bragg grating combined with polarization modulation (Tang *et al.*, 2012; Gao *et al.*, 2013; Wang and Yao, 2013) or intensity modulation (Li and Yao, 2012; Wei *et al.*, 2013; L. Li *et al.*, 2014; C. Li *et al.*, 2018).

Another approach to achieve tunability is based on the current modulation of the seeding laser. A straightforward method is based on directly applying the optoelectronic feedback signal to the rf current modulation electrode of the laser. Various types of lasers have been considered in this scheme, such as distributed-feedback semiconductor lasers (Xiong *et al.*, 2013; G. Chen *et al.*, 2018; Zhang *et al.*, 2019) or AlGaInAs/InP microsquare lasers (Liao *et al.*, 2017). Tunability can also be obtained by combining optoelectronic feedback with external optical feedback (Wishon *et al.*, 2018) or optical injection (Ma *et al.*, 2015; P. Wang *et al.*, 2015; Zhang *et al.*, 2015).

Alternatively, tunability in OEOs can be achieved using other methods such as microwave phase shifting (Fedderwitz

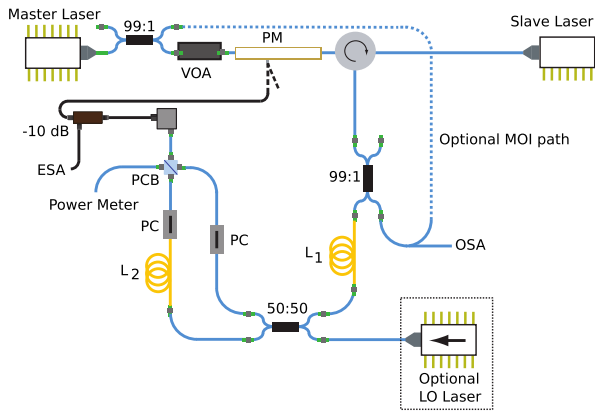


FIG. 30. Tunable OEO for mm-wave generation (10–46 GHz), based on a semiconductor laser subject to optical injection and optoelectronic feedback. The blue (yellow) lines depict (non) polarization-maintaining single-mode optical fiber; the black lines represent rf cables; the dashed lines highlight optional changes to the system’s configuration. VOA: variable optical attenuator; PC: polarization controller; ESA, OSA: electrical or optical spectrum analyzer. From Suelzer *et al.*, 2017.

et al., 2010), dual-frequency lasers (Maxin *et al.*, 2013), injection locking (Fleyer *et al.*, 2016), or yttrium iron garnet (YIG) filters (Xie *et al.*, 2016; Gao *et al.*, 2017; Ustinov *et al.*, 2018; Xiao *et al.*, 2019).

It should also be noted that several OEOs are purposely designed to be tuned up to the millimeter-wave band; see Fig. 30. They are discussed in the next section.

G. Millimeter-wave OEOs

Millimeter waves have a frequency in the 30–300 GHz band, which is also sometimes referred to as the extremely high frequency band. Their short wavelength (1–10 mm) and reduced beamwidth makes them suitable for high-precision radars. These waves are also needed for the next generation of high-capacity wireless networks. Several OEOs have demonstrated their capability to output ultralow phase noise signals in this frequency range.

The first group of mm-wave OEOs corresponds to those oscillating in the Ka band (27–40 GHz). OEOs can output fixed frequencies in that range using different technological devices, such as polymer modulators (Chang *et al.*, 2002), quantum-dash Fabry-Perot lasers with optoelectronic feedback (Van Dijk *et al.*, 2008), frequency quadrupling based on polarization modulation in Sagnac loops (Wang, Li, and Zhu, 2014), or photonic harmonic upconversion (Xiao *et al.*, 2018).

However, most OEOs in the Ka band are in fact widely tunable, typically over the 5–40 GHz frequency range. A first strategy is based on the technique of frequency multiplication. For example, frequency-doubled OEOs have been demonstrated using a tunable optical (Li, Liu, and Zhu, 2015) or microwave (Shang *et al.*, 2017) filter, while a frequency-quadrupled signal was obtained by Chen, Liu, and Pan (2018) with a system based on a dual-polarization QPSK modulator and a phase-shifted fiber Bragg grating. Other efficient mechanisms to achieve tunability up to 40 GHz include semiconductor laser optical injection (Lin *et al.*,

2018) and stimulated Brillouin scattering (Shi *et al.*, 2018; H. Tang *et al.*, 2018).

Note that some of these Ka-band OEOs feature a relatively high spectral purity, particularly when the ~ 40 -GHz-wide tunability range is considered. For example, Merklein *et al.* (2016) developed an oscillator where active narrow-band filtering was performed via stimulated Brillouin scattering, with one of the best close-in phase noise performance for an OEO (approximately -80 dBc/Hz at 10 Hz offset). Along the same line, spectral purity better than -120 dBc/Hz was demonstrated by Xie *et al.* (2013) and Peng *et al.* (2017) using a principle of operation based on tunable optical bandpass filters and stimulated Brillouin scattering, respectively.

Several OEOs have been developed for frequency synthesis in the V band (40–75 GHz). One of the earliest works in that spectral range was performed by Sakamoto, Kawanishi, and Izutsu (2007) with a 52.8 GHz OEO based on the frequency multiplication approach that can be further stabilized such as in the phase-locked frequency-quadrupled OEO proposed by Liu, Liu *et al.* (2018). Tunable OEOs capable of outputting microwaves overlapping the V band have been demonstrated by electrically controlling the central frequency of YIG filters (Zhu, Pan, and Ben, 2012) by varying the injection current applied on dual-mode amplified feedback lasers (Lu *et al.*, 2015; Pan *et al.*, 2015) or by tuning the optical injection of a semiconductor laser with optoelectronic feedback (Suelzer *et al.*, 2017); see Fig. 30. Bagnell, Davila-Rodriguez, and Delfyett (2014) also developed a single-loop OEO based on a Fabry-Perot photonic filter that could output a radio-frequency signal from 6 to 60 GHz.

Finally, OEOs have been developed for the W band as well (75–110 GHz), mainly using frequency multiplication techniques. Millimeter-wave generation up to 80 GHz was demonstrated by Chen, Li, and Wen (2013) using frequency octupling, while Brillouin-assisted frequency decoupling was implemented by Wang, Shan *et al.* (2017) to generate a signal tunable from 88 to 94 GHz. In terms of spectral purity, the work of Ly *et al.* (2018) appeared as particularly noteworthy: their frequency-tripling architecture enabled the generation of a 90 GHz signal with an exceptional phase noise performance, down to -120 dBc/Hz.

H. Optical-pulse OEOs

Several architectures of OEOs have been developed to simultaneously output ultralow jitter optical short pulses and ultrapure microwaves. The specific advantage of this dual-output oscillator is the fact that for being generated by the same feedback loop, the light-wave and microwave signals are mutually coherent and therefore do not need further synchronization. Such OEOs where optical-pulse trains are self-synchronized to GHz microwave signals found numerous applications in areas such as optical communications, optical sampling, lidar technology, and metrology. We refer the reader to Table II for the technical details (repetition rate and pulse width) of the OEOs discussed in this section.

An early architecture of pulsed OEOs was proposed by Davidson *et al.* (1999), with an oscillator that behaved like an harmonic mode-locked laser and could generate nanosecond

TABLE II. Recapitulative table for the pulse width (PW) of all the multi-GHz optical-pulse OEOs discussed in this review whenever available. The attributes in brackets after each reference stand for the repetition rate in GHz, rounded to the nearest integer.

PW < 5 ps	$5 \leq \text{PW} \leq 15$ ps	PW > 15 ps
Chembo, Hmima <i>et al.</i> (2009) [10], Dahan, Shumakher, and Eisenstein (2005) [10], Jia, Yu, Z. Wang <i>et al.</i> (2015) [10], Plascak <i>et al.</i> (2018) [10], Salik, Yu, and Maleki (2007) [9], Yu, Salik, and Maleki (2005) [9]	Dai <i>et al.</i> (2015) [10], Hasegawa, Oikawa, and Nakazawa (2007) [10], Jiang <i>et al.</i> (2007) [10], Koizumi, Yoshida, and Nakazawa (2010) [10], Lasri <i>et al.</i> (2002) [10], Lasri <i>et al.</i> (2004) [10], Lau and Yariv (1984) [1–5], Liu <i>et al.</i> (2012) [10], Yao, Davis, and Maleki (2000) [18], Zhou <i>et al.</i> (2016) [6–15], Zhu, Du, and Pan (2018) [10]	Devgan <i>et al.</i> (2006) [2], Huang <i>et al.</i> (2014) [10], Li, Kong, and Yao (2013) [10–15], Ma <i>et al.</i> (2018) [10], Quinlan <i>et al.</i> (2008) [10], Tang and Shu (2005) [10]

pulses. However, the topic of optical-pulse generation using OEOs gained attention when Yao, Davis, and Maleki (2000) developed the so-called coupled optoelectronic oscillator (COEO). Their system relied on a semiconductor optical amplifier-based ring laser and a semiconductor colliding pulse mode-locked laser. Later on, Dahan, Shumakher, and Eisenstein (2005) reported a COEO using a phototransistor-based microwave oscillator coupled to a fiber cavity OEO with an intracavity fiber parametric amplifier. The COEOs developed by Yu, Salik, and Maleki (2005) and Salik, Yu, and Maleki (2007) involved erbium-doped fiber amplifiers as well. A distinctive property of their oscillators is that beside generating picosecond pulses in the optical domain, they could output X-band microwaves with exceptional spectral purity (phase noise down to -150 dBc/Hz). Other optical sources have also been reported for the implementation of COEOs, such as high-finesse intracavity-etalon lasers (Quinlan *et al.*, 2008) or actively mode-locked fiber ring lasers (Dai *et al.*, 2015). Recently Zhu, Du, and Pan (2018) demonstrated that the stability of COEOs can be improved using enhanced spatial hole burning in an unpumped erbium-doped fiber, thereby leading to a strong spurious side-mode suppression ratio.

Another approach for pulse generation in OEOs relies on direct laser modulation or injection. This strategy was successfully implemented using mode-locked diode lasers (Lasri *et al.*, 2002), or VCSELs (Devgan *et al.*, 2006; Hasegawa, Oikawa, and Nakazawa, 2007; Koizumi, Yoshida, and Nakazawa, 2010). As demonstrated by Zhou *et al.* (2016) with the experimental setup displayed in Fig. 31, optical injection in a semiconductor laser can even permit one to achieve pulse-rate tunability across a multi-GHz frequency range.

The combination of amplitude and phase modulation is also an efficient technique to achieve short pulse generation in OEOs. Jiang *et al.* (2007) proposed an OEO where the rf signal closing the feedback loop was used for optical amplitude modulation via the laser pump current and external phase modulation using a lithium niobate modulator. Time-lens soliton-assisted compression was implemented by Chembo, Hmima *et al.* (2009) to obtain short optical pulses. In their system, sinusoidal prepulses were chirped using phase modulation and then strongly amplified with an erbium-doped fiber amplifier, before being launched in a 4-km-long optical fiber where it underwent soliton compression. The OEO pulse generator introduced by Liu *et al.* (2012) was based on cascaded amplitude and phase modulation, with a dual-loop feedback for spurious mode attenuation. Jia, Yu, Z. Wang

et al. (2015) reported also a dual-loop OEO, characterized by two seeding lasers at different wavelengths. The fed back rf signal was used for the direct modulation of the two lasers and the phase modulation of their multiplexed output.

Pulse generation using OEOs can ultimately be performed with architectures involving a wide variety of physical phenomena, yielding as well a broad range of pulse width performance: for example, we mention stimulated Brillouin scattering in an optical fiber (Tang and Shu, 2005), four-wave mixing in cascaded nonlinear semiconductor optical amplifiers (Huang *et al.*, 2014), or electro-optic combs with optical filtering (Plascak *et al.*, 2018).

Finally, also note that OEOs can be specifically designed to pulse in a regime of very low repetition rate, down to the MHz (Levy and Horowitz, 2011) and even the kHz (Sherman and Horowitz, 2013) frequency range.

I. Whispering-gallery mode resonator OEOs

Whispering-gallery mode (WGM) resonators are axisymmetric dielectric cavities that have the capability to trap photons by total internal reflection. These resonators have found numerous applications in photonics and optoelectronics, particularly when they are driven in the nonlinear regime by a moderate to high pump power [see, for example,

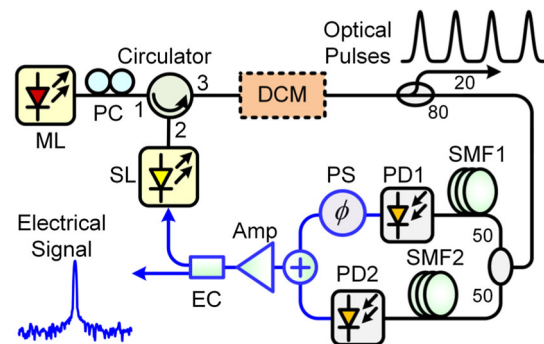


FIG. 31. Schematic diagram of the experimental setup for the OEO pulse generation using an optically injected semiconductor laser. The repetition can be coarsely tuned in the 6.5–15 GHz range. The full width at half maximum of the generated optical pulses can be narrowed down to less than 15 ps. ML: master laser; SL: slave laser; PC: polarization controller; DCM: dispersion compensation module; SMF: single-mode fiber; PD: photodetector; PS: phase shifter; Amp: amplifier; EC: electrical coupler. From Zhou *et al.*, 2016.

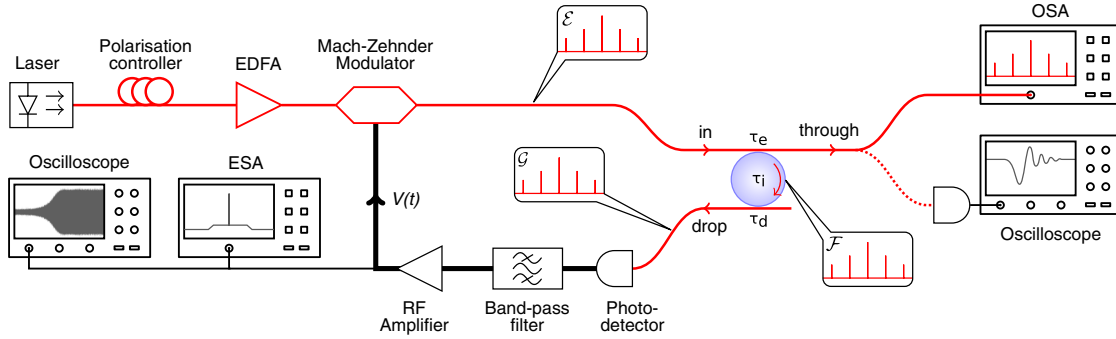


FIG. 32. Experimental setup to investigate the time-domain behavior and dynamical stability of a WGM-based OEO. The optical path is in thin red, while the electric path is in thick black. The insets show the spectra of the optical fields $\mathcal{E}(t)$, $\mathcal{F}(t)$, and $\mathcal{G}(t)$ at the input, interior, and output of the WGM resonator, respectively. The spectral lines are separated by a free-spectral range of the resonator (10.4 GHz for a CaF₂ disk resonator with 3.2 mm radius), which is also the OEO output frequency. In the open-loop configuration (no oscillations), the “through” port can also be used to perform the cavity-ring down measurement, thereby enabling the determination of the intrinsic and coupling loss factors (characterized by $\tau_{i,e,d}$). In the electric branch, a fast oscilloscope enables one to resolve the temporal dynamics of the microwave $V(t)$. EDFA: erbium-doped fiber amplifier; ESA: electrical spectrum analyzer; OSA: optical spectrum analyzer. From Coillet *et al.*, 2013.

Matsko *et al.* (2005), Chiasera *et al.* (2010), Chembo (2016), Strekalov *et al.* (2016), Lin, Coillet, and Chembo (2017), and Pasquazi *et al.* (2018), and references therein]. A typical mm-size WGM disk resonator with a quality factor of 1×10^9 at 1550 nm features a free-spectral range of ~ 10 GHz and a sub-MHz optical linewidth; see Fig. 32. The corresponding photon lifetime is longer than a microsecond, or equivalently, to the photon storage capability of a delay line that is at least 200 m long.

One of the earliest architectures of resonator-based OEOs was proposed by Matsko *et al.* (2003). A lithium niobate WGM resonator played the role of a resonant electro-optical modulator, and the multi-GHz oscillator involved as well a 1 km delay line. As shown by Maleki (2011), this approach where the resonator serves both as the high- Q element and as the modulator in the OEO loop has permitted one to demonstrate one of the smallest and technologically mature OEOs to date, the so-called miniature OEO; see Fig. 33.

When the laser pump power is sufficiently low, the WGM resonators behave quasilinearly and can be inserted into the OEO loop as narrow-band optical filters. In the single-coupler configuration, Volyanskiy, Salzenstein *et al.* (2010) reported a compact WGM OEO where optical filtering was performed by a fused silica disk resonator, while Elyahu *et al.* (2013) demonstrated the wide tunability of WGM OEOs using a tunable optical resonant filter made with a lithium tantalate WGM resonator. On the other hand, using the double-coupling configuration (or add-drop coupling), Merrer *et al.* (2012) presented a single-loop OEO architecture where a calcium fluoride WGM resonator was inserted as a filter in the optical path. A time-domain model to investigate the nonlinear dynamics of these WGM OEOs was proposed by Coillet *et al.* (2013). Using the experimental setup shown in Fig. 32, they performed a full stability analysis for the oscillatory states as a function of the feedback gain and the properties of the WGM filter. The experimental envelope dynamics of the OEO with a calcium fluoride resonator and no delay line was found to be

in excellent agreement with the numerical simulation of the model. Later on, the dynamics and phase noise performance of these WGM OEOs was investigated both experimentally (Saleh *et al.*, 2014) and theoretically (Nguimdo *et al.*, 2015, 2016).

From a broader perspective, research is still ongoing in order to optimize the stability of WGM OEOs, improve their competitiveness with regards to other resonator-based microwave photonic sources (Saleh, Lin, and Chembo, 2015; Saleh and Chembo, 2017), and explore other WGM resonator platforms such as chip-scale (J. Chen *et al.*, 2018) or quasicylindrical microresonators (Jin *et al.*, 2019).

J. Other architectures of narrow-band OEOs

The research related to ultrapure microwave generation with narrow-band OEOs has led to the demonstration of many other original architectures, which involve a wide variety of optical, electro-optical, or electronic phenomena.

Direct laser current modulation using a narrow-band optoelectronic feedback loop is a relatively simple and cost-effective topology for microwave generation. This strategy was successfully implemented by Romeira *et al.* (2011) using a monolithic resonant tunneling diode, and Cho and Sung (2012) using a dual-section distributed-feedback laser.

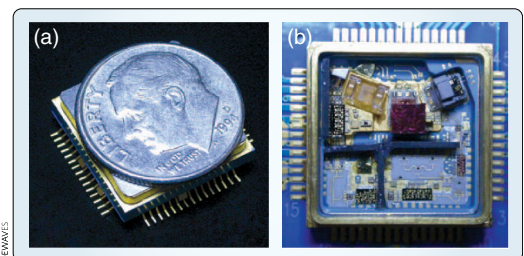


FIG. 33. Miniature OEO based on a lithium niobate WGM resonator. From Maleki, 2011.

Injection locking is also an efficient strategy to improve the phase noise performance of OEOs. Zhou and Blasche (2005) demonstrated an injection-locked dual OEO exhibiting one of the best phase noise performances recorded in the X band, measured at -150 dBc/Hz with a spur reduction of 140 dB. Other injection-based architectures involved heterojunction phototransistors (Lee *et al.*, 2008), edge-emitting lasers (Sung *et al.*, 2009), or Fabry-Perot laser diodes (Y. Jiang *et al.*, 2013). Mutual injection can be used as well as shown by Dai *et al.* (2017) with an OEO where electrical and optical loops are bidirectionally coupled.

Nonlinear optical phenomena can be exploited in OEOs for microwave generation. One of the first architectures in this category was proposed by Yao (1997), and it was based on Brillouin scattering in the optical fiber-delay line. Brillouin scattering was also leveraged in OEOs for the purpose of gain selectivity (B. Wu *et al.*, 2016; Liu, Zheng, and Shu, 2017) or for phase-to-intensity conversion via slow light (Tong *et al.*, 2017). Other nonlinearities such as erbium-doped fiber amplifier saturation were investigated as well for the implementation of all-photonic OEOs (Devgan *et al.*, 2009).

Narrow-band OEOs for microwave generation can also feature even more unconventional topologies. For example, they can be implemented using frequency-shifted feedback (Vallet *et al.*, 2016) or regenerative electronic circuits in order to increase the selectivity of the feedback loop (Bogataj, Vidmar, and Batagelj, 2016). Certain OEO topologies rely on optical instead of radio-frequency filtering, using, for example, Fabry-Perot etalons (Ozdur *et al.*, 2010) or fiber Bragg gratings (Mei *et al.*, 2014; Qu *et al.*, 2015). Recent developments laid a particular emphasis on the chip-scale integration of OEOs, with the promise of delivering competitive performances while fulfilling SWAP-C constraints for a wide array of applications (Hao, Tang *et al.*, 2018; J. Tang *et al.*, 2018; Zhang and Yao, 2018; Xuan, Du, and Aflatouni, 2019).

K. OEOs for signal processing

OEOs have found several applications in the area of high-speed signal processing in both radio and optical communication systems (Devgan, 2013).

One of the earliest areas where the usefulness of OEOs was highlighted is clock recovery in optical fiber networks. The idea here is that under optimal conditions the OEO can lock to the fundamental frequency (that is, the clock) of an incoming stream of binary data and thereby permit its extraction at the receiver end. Yao and Lutes (1996) performed the first experiment on this topic and demonstrated clock recovery for a 4.95 Gbit/s stream of return-to-zero (RZ) binary data. Huo *et al.* (2003) used an OEO for the clock extraction of a 10 Gbit/s NRZ signal, and shortly after clock recovery for 40 Gbit/s RZ signals was also demonstrated (Lasri *et al.*, 2004; Tsuchida and Suzuki, 2005). It was shown later on that frequency-multiplied OEOs could be used as well for clock recovery. The first advantage here is that the data rate limit can be multiplied accordingly, potentially at up to 160 Gbit/s as shown by Pan and Yao (2009). The second advantage is that these architectures permit multichannel optical signal processing alongside clock recovery, such as modulation format conversion and synchronous-modulation-based regeneration

(Pan and Yao, 2010). Along the same line, a frequency-doubling OEO was used by Q. Wang *et al.* (2014) to demonstrate clock recovery for a 4×25 Gbit/s optical time-division-multiplexed signal, for both differential phase-shift keying and on-off keying modulation formats. Recently, Tang *et al.* (2017) also performed clock recovery with a frequency-doubled OEO based on a polarization-sensitive phase modulator for a 25 Gbit/s time-division multiplexed signal. Research is still ongoing in order to gain further understanding into the mechanisms that allow the frequency and/or phase locking of OEOs to external signals (Talla *et al.*, 2015; Mukherjee, Ghosh, and Biswas, 2016; Banerjee *et al.*, 2018; Banerjee, de Britto, and Pacheco, 2019). Also note that beside clock recovery, OEOs can be useful as well for clock division (Lou *et al.*, 2002), clock multiplication (Lu *et al.*, 2011), and even for multi-Gbit/s data stream generation (Chi, Peng, and Lin, 2011).

Efficient photonic upconversion and downconversion is another area where OEOs appear as a pertinent technological solution, particularly in the context of radio-over-fiber networks. Frequency upconversion was performed by Shin and Kumar (2007) with a 1.25 Gbit/s binary signal, by Yang *et al.* (2013) using a 200 Mbit/s signal modulated with the 64 quadrature amplitude modulation format, and by Lee, Jeon, and Song (2019) using a 1 Gbit/s pseudorandom binary sequence. In all cases, the signals were successfully transmitted over several tens of kilometers via optical fiber links. OEOs demonstrated as well the capability to perform the downconversion of Gbit/s signals (Tang, Zhang, and Pan, 2014; Lee and Song, 2017). Radio-over-fiber architectures based on broadband light sources for laser light communications have also been demonstrated with a bandwidth overlapping the mm-wave band (C. Y. Li *et al.*, 2016; Lu *et al.*, 2016). In fact, recent experiments have shown that these particular OEOs can even perform high-speed optical wireless communications at up to 400 Gbit/s (C.-Yi Li *et al.*, 2018).

As far as radio-frequency signal processing is concerned, OEOs have been developed for signal channelization (Urlick *et al.*, 2009), low-power rf detection (Devgan *et al.*, 2010; Shao *et al.*, 2018; Wang *et al.*, 2019; Zhu *et al.*, 2019), complex microwave signal generation (Deng *et al.*, 2017; C. Zhang *et al.*, 2018), or frequency division (Liu *et al.*, 2019).

L. From ultrapure to ultrastable OEOs

The phase noise of an oscillator defines the short-term stability of the output signal, for timescales τ typically shorter than 0.1 s: the long-term stability deals with longer timescales up to several years. As a side note, the timescales are sometimes separated differently in the literature and classified as long term ($\tau > 1$ day), short term ($0.1 \text{ s} < \tau \leq 1$ day), or phase noise ($\tau < 0.1$ s). Stability at the timescale of months or years is also sometimes referred to as *aging*. In all cases, the long-term stability of an oscillator is evaluated in terms of an Allan deviation (or ADEV). This stability indicator is generally noted as $\sigma_y(\tau)$, where τ is the observation time and $y = [\nu(t) - \nu_0]/\nu_0 = \dot{\phi}/2\pi\nu_0$ stands for the fractional frequency, with $\nu(t)$ and ν_0 being the real and nominal frequencies of the oscillator, respectively. More prosaically, $\sigma_y(\tau)$ is the root-mean-square (rms) deviation for fractional

TABLE III. Recapitulative table for the Allan deviation at $\tau = 1$ s (or $\text{ADEV}_{1\text{s}}$) for all the OEO microwave generators discussed in this review whenever available. The attributes in brackets after each reference stand for the oscillation frequency in GHz, rounded to the nearest integer.

$\text{ADEV}_{1\text{s}} < 10^{-11}$	$10^{-11} \leq \text{ADEV}_{1\text{s}} \leq 10^{-9}$	$\text{ADEV}_{1\text{s}} > 10^{-9}$
Bluestone <i>et al.</i> (2015) [3], Hong <i>et al.</i> (2016) [10], Zhang, Hou, and Zhao (2014) [3]	Bagnell, Davila-Rodriguez, and Delfyett (2014) [10], Dai <i>et al.</i> (2018) [10], Fan <i>et al.</i> (2019) [11], Fu <i>et al.</i> (2017) [10], Ji, Yao, and Maleki (1999) [10], Liu, Liu <i>et al.</i> (2018) [10,40], Matsko, Strekalov, and Maleki (2005) [3], Plascak <i>et al.</i> (2018) [10], Romisch <i>et al.</i> (2000) [10], Suelzer <i>et al.</i> (2017) [22], Tseng and Feng (2012) [< 1], Xu <i>et al.</i> (2015) [10], J. Zhao <i>et al.</i> (2016) [3], Zhenghua <i>et al.</i> (2016) [10], Zhu <i>et al.</i> (2016) [10]	Hosseini, Banai, and Kartner (2017) [11], Kim and Cho (2010) [4], Seo and Yim (2017) [3]

frequencies measured at times separated by an interval τ . For instance, an oscillator with nominal frequency $\nu_0 = 10$ GHz that has an Allan deviation of 10^{-10} at $\tau = 1$ s features a rms frequency instability of $\sigma_y(\tau) \times \nu_0 = 1$ Hz between two measurements performed 1 s apart.

We displayed in Table III the Allan deviation performance associated with the various OEOs discussed in this review for an observation time $\tau = 1$ s.

One of the most widespread methods to ensure long-term stability for OEOs is to use feedback control or servosystems. An early research work about the long-term stability of single-loop OEOs along that line was proposed by Romisch *et al.* (2000). Later on, double-loop OEO architectures were proposed to implement various phase- or injection-locking strategies (Tseng and Feng, 2012; Bluestone *et al.*, 2015; Zhu *et al.*, 2016; Fu *et al.*, 2017). Alternative approaches to achieve long-term stability are numerous, and include, for example, phase-lock loops (Xu *et al.*, 2015; Zhenghua *et al.*, 2016), time-delay compensation (Hong *et al.*, 2016; Fan *et al.*, 2019), Sagnac interferometry (Hosseini, Banai, and Kartner, 2017), or frequency-drift compensation (Dai *et al.*, 2018).

Another efficient strategy to achieve high levels of long-term stability in OEOs is to lock them to an atomic clock transition. Strekalov *et al.* (2003) proposed a detailed stability analysis of such OEO architectures and performed as well a preliminary experimental demonstration with a 6.834 GHz OEO locked to a ^{87}Rb clock transition. Kim and Cho (2010) reported later on an OEO stabilized to a Fabry-Perot cavity and to a 3.6 GHz cesium transition. Recent developments in this area include the implementation of 3.035 GHz OEOs locked to the ^{85}Rb atomic transition (Zhang, Hou, and Zhao, 2014; J. Zhao *et al.*, 2016; Seo and Yim, 2017).

Note that an important requirement in order to achieve satisfying levels of long-term stability in OEOs is to ensure an energy-efficient thermal stabilization. An interesting solution is to replace the usual solid-core single-mode fibers by hollow-core photonic crystal fibers in the delay line, as the latter feature a smaller sensitivity to thermal fluctuations because part of the light propagates into the microstructured holes and does not contribute to heat transfers (Kaba *et al.*, 2006; Beck *et al.*, 2012). This improvement in thermal sensitivity was accurately measured by Mutugala *et al.* (2017) using the hollow-core OEO presented in Fig. 34, and they found that it was reduced by a factor of up to ≈ 15 .

In general, the Allan deviation can be determined from the phase noise spectrum (Rubiola, 2010), and a clear indication of ultrastability is ultralow phase noise at offset frequencies very close to the carrier (typically below ~ 1 Hz). For instance, in Fig. 26, the phase noise of the best OEO at 1 Hz offset is not available, but can be projected to be around -40 dBc/Hz. However, the optical frequency division oscillator from Fortier *et al.* (2011) and the optical frequency comb oscillator from Xie *et al.* (2017) display a phase noise lower than -100 dBc/Hz at 1 Hz offset. It is therefore not surprising that they feature exceptional stability performances, with Allan deviations of the order of 10^{-16} at 1 s, significantly better than the most stable OEOs that have a stability of the order of 10^{-12} . However, note that, on the one hand, OEOs are characterized by relatively simple and robust architectures that are optimal for short-term stability, while, on the other hand, the microwaves displaying the highest long-term stability are

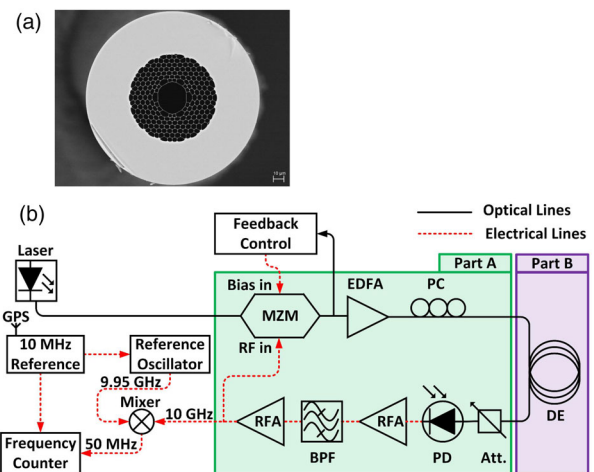


FIG. 34. Architecture of a 10 GHz OEO using a 860-m-long hollow-core photonic band-gap fiber delay line. The temperature stability of the OEO was improved by a factor ≈ 15 , as compared to a standard optical fiber delay line. (a) Cross sectional scanning electron microscope image of the hollow-core fiber. (b) Experimental OEO setup. MZM: Mach-Zehnder modulator; PC: polarization controller; DE: delay element; PD: photodiode; RFA: rf amplifier; EDFA: erbium-doped fiber amplifier; Att: attenuator; BPF: bandpass filter; GPS: global positioning system. From Mutugala *et al.*, 2017.

obtained with significantly more complex and delicate experimental setups, which yield metrological performances approaching the absolute limits set by the fundamental laws of physics.

VI. OEO SENSING APPLICATIONS

Narrow-band OEOs have the capability to operate in ultralow noise oscillatory states, as discussed in Sec. V. As a consequence, narrow-band OEOs can be implemented for the purpose of sensing, the main idea being that physical quantities (temperature, pressure, strain, etc.) can modify the optical path length of the light-wave feedback signal or the microwave resonance frequency, thereby inducing a measurable frequency shift for the output rf oscillation (Grigor'yants *et al.*, 1985; Zou *et al.*, 2016; Yao, 2017). Most of these sensors do not systematically aim at outperforming the competition in terms of sensitivity: instead, their usefulness mainly depends on technological context of the microwave photonics supra-system in which they are embedded. The scientific literature has reported several architectures of OEO sensors, and an overview of these systems is provided hereafter.

A. Magnetic field and refraction index sensing

One of the first OEO sensors was described by Matsko, Strekalov, and Maleki (2005), and it aimed at the high-accuracy measurement of magnetic fields. The main element of this OEO magnetometer is an atomic cell filled with ^{87}Rb isotope vapor, whose atomic transitions at 6.834 GHz depend on the surrounding magnetic field via their magneto-optical constant ($7 \text{ kHz}/\mu\text{T}$ for ^{87}Rb). This atomic transition matches the second harmonic of the OEO oscillation frequency ($\approx 3.42 \text{ GHz}$), which could therefore be used to measure the magnetic field around the atomic cell. They performed static magnetic field measurements and achieved a resolution of 0.02 nT with a dynamical range of 0.1–100 μT (to be compared with the magnetic field of the Earth at $\sim 50 \mu\text{T}$).

One of the earliest OEO-based refraction index sensors was developed by Nguyen, Nakatani, and Journet (2010), and it had a resolution of $\sim 10^{-2}$. The optical branch of the OEO included a free-space portion where a transparent material could be placed and a variation of a refraction index induced a variation of an optical path for the laser signal, that is, a variation of the time delay T resulting in a measurable shift of the microwave oscillation frequency.

B. Load and strain sensing

Load and strain sensing based on narrow-band OEOs is usually performed by sending a dual-wavelength signal on the fiber-delay line and monitor the frequency separation as a function of a stress exerted on the fiber. The first advantage of this method is that the thermal environmental fluctuations affect equally both wavelengths and are therefore canceled in the base-band beat-note signal. The second advantage is that the frequency sensing approach generally allows these systems to operate in real time. Applications are mainly related to structural monitoring in civil, aerospace, and mechanical engineering.

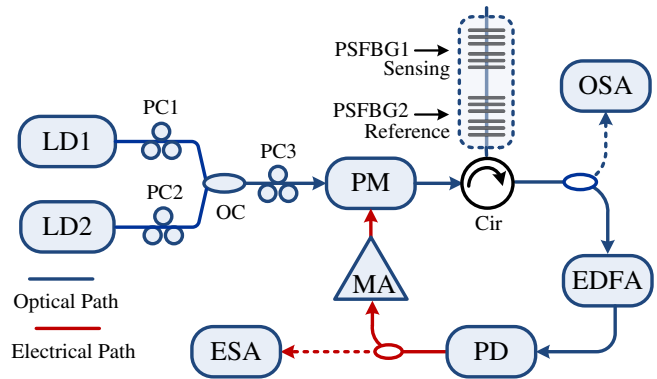


FIG. 35. Schematic representation of an OEO strain sensor. LD: laser diode; PC: polarization controller; OC: optical coupler; PM: phase modulator; PSFBG: phase-shifted fiber Bragg gratings; Cir: circulator; OSA: optical spectrum analyzer; EDFA: erbium-doped fiber amplifier; PD: photodiode; MA: microwave amplifier; ESA: electrical spectrum analyzer. From Xu *et al.*, 2017.

The first architecture was proposed by Kong, Li, and Yao (2013), who demonstrated that OEOs could sense transverse loads. In their system, the load is applied to a phase-shifted fiber Bragg grating and introduces a birefringence leading to two oscillating frequencies whose beat note is a function of the load. The sensitivity of the OEO was $9.7 \text{ GHz}/(\text{N}/\text{mm})$, with a minimal detectable load of $2 \times 10^{-4} \text{ N}/\text{mm}$. The strain sensor demonstrated by Xu *et al.* (2017) relied on a dual-frequency and single-loop OEO architecture; see Fig. 35. Two phase-shifted fiber Bragg gratings with different passbands are incorporated into the OEO optical branch, one of them being a reference and the other being submitted to strain. The beat note between the central frequencies of the filters will shift according to the applied strain, thereby providing a sensing mechanism, with a resolution of $0.8 \mu\epsilon$, and a sensitivity of $120 \text{ MHz}/\mu\epsilon$. Fan *et al.* (2017) introduced a multiplexed and dual OEO for strain sensing, with two slightly mismatched laser signals being multiplexed in a common and long optical fiber, before being demultiplexed toward the sensing and reference paths. The strain in the sensing path is proportional to the frequency shift obtained by mixing the light-wave signals of the two OEOs. The experimental setup achieved a measurement range of $600 \mu\epsilon$, with an error of $\pm 0.3 \mu\epsilon$.

C. Temperature and pressure sensing

Narrow-band OEOs can be used for the high-sensitivity measurement of thermodynamical quantities such as temperature and pressure. These sensors are generally based on the thermal or barometric variation of a photonic device (fiber, resonator, grating, etc.) in the optical path of the OEO feedback loop that leads to a measurable oscillation frequency shift.

Zhu *et al.* (2014) proposed and experimentally demonstrated an OEO for which the shift of the oscillation frequency was inversely proportional to the variation of temperature. Their OEO sensor featured a very short delay line (12 m) in order to optimize its tunability. The system achieved a sensitivity of $44 \text{ kHz}/^\circ\text{C}$, with an accuracy of 0.1°C in the

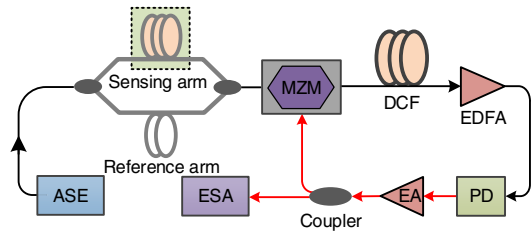


FIG. 36. Schematic representation of an OEO for temperature sensing. ASE: amplified spontaneous emission; MZM: Mach-Zehnder modulator; DCF: dispersion compensating fiber; EDFA: erbium-doped fiber amplifier; PD: photodetector; EA: electrical amplifier; ESA: electrical spectrum analyzer. From Wang, Zhang, and Yao, 2016.

20–240 °C temperature range. The OEO temperature sensor developed by Wang, Zhang, and Yao (2016) was based on a broadband light source seeding an imbalanced Mach-Zehnder fiber interferometer, with one arm performing the sensing while the other served as reference; see Fig. 36. The signal was then sent in a dispersion compensating fiber before being photodetected, and this chain behaved as a tunable microwave photonic filter, with a temperature dependent central frequency that defines the oscillation frequency of the OEO. The system achieved a sensitivity of 3.7 MHz/°C for temperatures ranging from 25 to 75 °C. Chew *et al.* (2017) proposed an OEO temperature sensor based on a silicon-on-insulator microresonator that was the temperature-sensitive element performing bandpass filtering in the feedback loop. They demonstrated a sensitivity of 7.7 GHz/°C with a precision of 0.02 °C in the 23.5–25.5 °C temperature range. A consistent trend with OEO temperature sensors is that increasing the sensitivity is generally achieved at the expense of the detection range. However, it should also be emphasized that the needs for temperature sensing are quite diverse depending on the field application, so that this versatility in detection ranges and sensitivity can in fact be viewed as a key advantage of OEO-based temperature sensors.

Wang, Wang *et al.* (2017) demonstrated that pressure can also be measured with OEOs, as shown in Fig. 37. They

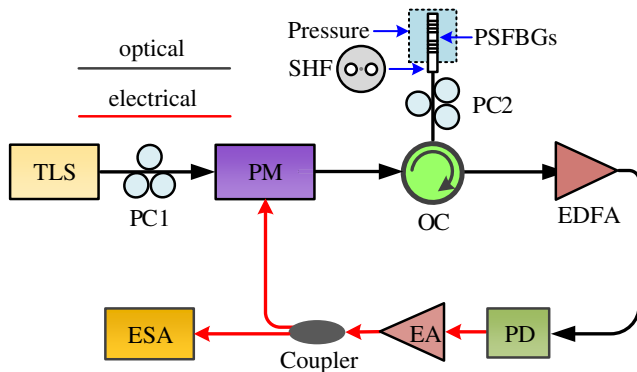


FIG. 37. Schematic representation of an OEO pressure sensor. TLS: tunable laser source; PM: phase modulator; OC: optical circulator; EDFA: erbium-doped fiber amplifier; PD: photodetector; EA: electrical amplifier; ESA: electrical spectrum analyzer; PC: polarization controller; SHF: side-hole fiber; PSFBG: phase-shifted fiber Bragg gratings. From Wang, Wang *et al.*, 2017.

introduced two phase-shifted fiber Bragg gratings made with side-hole fibers to serve as reference and sensing devices in an OEO oscillation loop. The frequency shift between the central frequency of these two optical filters was pressure dependent, and their system achieved a sensitivity of 420 MHz/MPa in the 0–4 MPa range (to be compared to the atmospheric pressure of ~0.1 MPa).

D. Distance, rotation, and vibration sensing

The measurement of distances using narrow-band OEOs generally relies on phase or frequency shifts induced by a feedback loop delay variation.

As far as long-distance sensing is concerned, Zhang *et al.* (2013) proposed an OEO architecture where the optical branch features a variable free-space portion. The output signal was multiplexed with an intensity-modulated signal in the ultralong optical fiber-delay line of the OEO. The method allowed one to measure distances with a standard deviation of 15 μm and potentially down to $\pm 4 \mu\text{m}$ with averaging. The system developed by J. Wang *et al.* (2014) was intended for long-range and high-precision absolute distance measurement. It was based on a dual-OEO architecture where two pump signals are multiplexed in the same feedback loop, while two electric branches process the baseband signal and perform the distance-to-frequency conversion. They demonstrated a maximum error of 1.5 μm at an emulated distance of 3.35 km, and the relative precision of their system could be as low as 4.5×10^{-10} . The recent distance sensing setup reported by Cui *et al.* (2018) was based on the association of an optical frequency comb and an OEO locked to a Rb atomic clock, achieving the measurement of km-long distances with sub-micron precision (relative stability of $\sim 10^{-10}$).

For short-distance sensing, Zou *et al.* (2014) proposed a system involving two OEOs seeded with an incoherent light source. They showed that the optical distance variation was translated to a microwave frequency shift. The first OEO had a resolution of 3.6 nm and a sensitivity of -28 kHz/cm (-480 kHz/cm) when the oscillation frequency was 490 MHz (29 MHz), while the second OEO featured a sensitivity of -14 kHz/cm with a 57 MHz microwave, yielding a nm-scale resolution. A distance sensor including an acousto-optical modulator and an intraloop Michelson interferometer was later on reported by Lee *et al.* (2016). Their system translated the distance to an optical frequency shift, unlike most OEO sensors where the measured quantity is proportional to a microwave frequency shift. This setup permitted a distance measurement with subnanometer precision.

OEOs have also been developed to perform acoustic and vibration sensing. Jin *et al.* (2017) performed vibration sensing with an OEO capable of highly sensitive phase demodulation. Their single-loop OEO was built with a dual-output Mach-Zehnder modulator, with one of the output fibered arms being convolved around a piezoelectric vibration sensor. The vibration-induced optical phase variation was converted to a microwave, and while the performance of the system depended on the phase noise of the signal, it was independent of its frequency. The minimum detectable optical phase shift was set to $0.2 \mu\text{rad}/\sqrt{\text{Hz}}$ at 10 kHz, proving the

potential of this OEO sensor for extremely weak vibration detection. Fleyer and Horowitz (2018) demonstrated that OEOs can operate as acoustic and vibration sensors as well, when driven by a forcing signal that changes the overall delay time in the feedback loop.

Finally, as initially proposed by Konopsky (1996), OEOs can be used for angular velocity sensing if the fiber-delay line is wrapped in a Sagnac loop configuration. An experimental demonstration of this generic concept was implemented by J. Zhang *et al.* (2018), with an OEO where the optical carrier and the first-order sidebands propagated in opposite directions. The rotation angular velocity was proportional to the phase difference between counterpropagating signals that was translated to a measurable microwave frequency shift with a sensitivity of 52 kHz/(rad/s). Using a coupled OEO architecture, Ye *et al.* (2019) achieved a sensitivity of 172 kHz/(rad/s) with a minimally detectable angular velocity of 1.2°/h, which is quite close to the performance required for tactical applications (0.1–1°/h).

E. Multiphysics sensing

The concepts behind OEO-based sensing can be implemented for different physical variables in the same system, which can thereby become a versatile, multipurpose sensor.

Yin *et al.* (2017) designed a dual-frequency OEO sensor incorporating fiber Bragg gratings and Fabry-Perot filters for simultaneous strain and temperature sensing. This system achieved a sensitivity of 100 MHz/ $\mu\epsilon$ for strain sensing, and -41 MHz/ $^{\circ}\text{C}$ for temperature sensing. Liu *et al.* (2017) proposed a strain and temperature OEO sensor based on a phase-shifted fiber Bragg grating. The optical filters generate two microwave signals exhibiting different sensitivities for strain (54.3 and 58.5 MHz/ $\mu\epsilon$) and temperature (1.52 and 1.34 GHz/ $^{\circ}\text{C}$). Yang *et al.* (2018) reported an ultrafast high-sensitivity refractive index and temperature OEO sensor that included a Fabry-Perot fiber Bragg grating setup featuring a narrow notch in the reflection spectrum. The microwave generated by the OEO varied with both refraction index and temperature, with sensitivities of 414 MHz/mRIU (one-thousandth of refraction index unit) and 2.5 GHz/ $^{\circ}\text{C}$, respectively. Simultaneous temperature and refractive index measurements using a chip sensor were demonstrated by Liu, Deng *et al.* (2018), based on OEO with a dual-passband microwave photonic filter. The interrogation resolution for the temperature and refraction index sensing was $\sim 10^{-5}$ $^{\circ}\text{C}$ and ~ 0.1 μRIU , respectively, with MHz interrogation speeds. Wu *et al.* (2018) recently proposed a dual-frequency OEO based on a magnetostrictive alloy-fiber Bragg grating to evidence magnetic field and temperature sensing with sensitivities of -38.4 MHz/Oe and -1.23 GHz/ $^{\circ}\text{C}$, respectively. Finally, note that beyond sensing, OEOs can also be useful to measure important optical fiber parameters such as chromatic dispersion (Y. Tang *et al.*, 2018; Terra, 2019a), or thermo-optic coefficients (Terra, 2019b).

VII. CONCLUSION AND PERSPECTIVES

OEOs have been the focus of a particularly broad set of research activities in the last decades. This unwavering interest

is principally rooted in the conceptually simple, but still complex and versatile nature of these systems.

The early architectures of OEOs were mostly devoted to solve technical problems such as the laser stabilization, or to create novel functionalities like optoelectronic switches. The introduction of the time delay opened the possibility of complex behaviors, which were initially explored from the nonlinear dynamics viewpoint, before being investigated from an application perspective.

Fundamental research in time-delayed OEO has essentially focused on the understanding of their dynamical properties. Initially, the road map was based on the ideas introduced by Ikeda on the complexity induced by the interplay between time delay and nonlinearity. Ikeda-like OEOs can be driven in various dynamical states that mainly include fixed points, limit cycles, and chaos, regardless of the broad- or narrow-band nature of the feedback loop. However, it was shown that hybrid states such as chaotic breathers or chimera states can emerge as well, depending on the parameters of the system. In the case of semiconductor lasers with optoelectronic feedback, the route to chaos appeared to feature a different phenomenology, where the dynamical state of the system depended strongly on the interplay between the feedback gain, the free-spectral range, and the relaxation oscillation frequency of the laser. These systems could output different types of oscillatory signals that could be periodically or chaotically pulsating. The OEO idea can also be extended to spatio-temporal systems, where the spatial dimension is emulated by a two-dimensional optical device. Several groups have investigated quantum effects in OEOs, in order, for example, to explore the single-photon regime of Ikeda-like OEOs, or to study the cavity quantum electrodynamics effects in an OEO where the laser and the photodetector are cooled down to cryogenic temperatures.

A powerful drive in OEO research has been the plethora of technological applications associated with this concept. In the broad bandwidth configuration, OEOs can be driven in the chaotic state where synchronization opens the way for chaos communication applications. Several field experiments have demonstrated the high level of performance for these communications schemes. Still in that regime, other applications such as random number generation and broadband radar or lidar have been investigated by various research groups. Broadband OEOs have also permitted the experimental implementation of neuromorphic computers with performances matching the state of the art, for various tasks, such as spoken digit classification or nonlinear time-series prediction. As far as narrow-band OEOs are concerned, ultrapure microwave generation has been the key that allowed them to emerge as some of the most studied systems in microwave photonics. They have fulfilled the promise of frequency versatility and high phase noise performance at room temperature, while allowing for numerous variations that permitted one to adapt this system for other applications, such as clock extraction or optical-pulse generation. Several architectures of narrow-band OEOs have also been successfully developed for the purpose of sensing, via a calibration that allows for high-precision and high-speed measurements of various physical quantities via a linear microwave frequency shift from an arbitrarily defined reference.

Future research on OEOs will have to address several challenges that are either of scientific or technological nature.

From a scientific perspective, major insights have already been provided by OEOs for a better understanding of delayed dynamical systems. However, even though they inherently feature an infinite dimensionality, the stable attractors are generally finite dimensional, with a topological structure that remains in some cases unclear, such as for chaotic breathers and chimera states. The full characterization of these high-dimensional attractors as a function of the OEO parameters is still an open problem that deserves further study. It should also be noted that complex nonlinear behaviors have mainly been investigated in the asymptotic case of narrow-band and broadband bandwidth OEOs. The intermediate configuration is a continuum in terms of timescales that has not been explored yet, even though of high interest from a dynamical point of view. Another open field for research is the interaction between noise and time delay that can be investigated using Langevin delay-differential equations. Indeed, this topic appeared to be highly relevant for the theoretical analysis of phase noise in OEO microwave generators. It can be anticipated that the stochastic analysis of OEOs will be required in order to investigate phenomena such as excitability or stochastic resonance, for example. As far as spatiotemporal OEOs are concerned, it is expected that new phenomenologies will be unveiled once the time delay will be accounted for in the feedback process, with possible applications in image processing. The understanding of quantum effects in time-delayed optoelectronic systems also emerges as one of the most fascinating challenge in OEO science, particularly for the analysis of quantum properties such as nonlocality in systems featuring time-delay separation with past states. In this regard, the generation of entangled states using electro-optical phase modulators emerges as a relevant paradigm that can be efficiently translated to the context of OEOs (Galmès *et al.*, 2019).

From the application viewpoint, the aim of OEOs essentially remains the same, that is, to leverage on the benefits provided by optical and electronic systems: broad bandwidth on the one hand, controllability on the other hand. OEOs have already permitted the implementation of several proof-of-concept experiments with state-of-the-art performances. A key technological challenge is now to demonstrate that beyond performance, these OEOs are competitive solutions when other constraints are considered, such as robustness, size, weight, power, and cost. The most advanced application in this regard is undoubtedly ultrapure microwave generation, which has achieved the maximum technological readiness level and ultimately the commercial stage. It is expected that some key features of these OEOs—most notably tunability, mm-wave range, and capability to handle light-wave and microwave signals at both input and output—could be uniquely suited to process *natively* high-throughput data at the nodes of the upcoming generation of densely interconnected optical fiber and wireless communication networks. One can expect as well OEO sensors, neuromorphic computers, and communication systems to reach the highest level of maturity in the short or midterm. In particular, chip-scale integration (see, for example, Fig. 38) appears as one of the most important steps ahead for OEOs to meet the constraint of

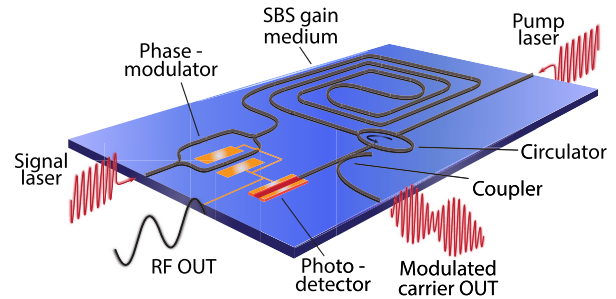


FIG. 38. An artistic view of a fully integrated OEO based on stimulated Brillouin scattering (SBS). A partially integrated version of this OEO has permitted the demonstration of ultrapure microwave generation with a close-in phase noise of only -80 dBc/Hz at 10 Hz offset from a signal in the 5–40 GHz band. From Merklein *et al.*, 2016.

mass production leading to a scale reduction of cost and improved reliability.

Research on the topic of optoelectronic oscillators with time-delayed feedback has already been very fruitful. However, their potential to contribute to our understanding of fundamental aspects of complexity and to inspire cutting-edge applications remains intact. The trend leading to better or novel optoelectronic components at lower cost also appears as a key element suggesting that OEOs will still play a major role in nonlinear, microwave, and quantum photonics in the years to come.

ACKNOWLEDGMENTS

The authors acknowledge fruitful interactions with several colleagues in relation to the topics discussed in this review, particularly P. Colet, J. Dudley, T. Erneux, I. Fischer, J.-P. Goedgebuer, P. Kumar, C. R. Menyuk, J.-M. Merolla, C. R. Mirasso, T. Murphy, R. Roy, E. Rubiola, M. San Miguel, V. Udaltsov, P. Wofo, and N. Yu. Y. K. C. thanks the Georgia Tech-CNRS Joint International Laboratory in Atlanta, Georgia, USA, where part of this work was completed. He acknowledges funding from the European Research Council through the projects NextPhase (StG 278616) and Versyt (PoC 632108), the Centre National d’Etudes Spatiales (CNES) through the project SHYRO, and the University of Maryland. The authors acknowledge support from the EIPHI Graduate School (Engineering and Innovation through Physical sciences, High-technologies, and cross-disciplinary research, ANR-17-EURE-0002) and the BiPhoProc project (ANR-14-OHRI-0002-02).

REFERENCES

- Abarbanel, H. D. I., M. B. Kennel, L. Illing, S. Tang, H. F. Chen, and J. M. Liu, 2001, “Synchronization and communication using semiconductor lasers with optoelectronic feedback,” *IEEE J. Quantum Electron.* **37**, 1301–1311.
- Abraham, E., and S. D. Smith, 1982, “Optical bistability and related devices,” *Rep. Prog. Phys.* **45**, 815–885.
- Ai, J., L. Wang, and J. Wang, 2017, “Secure communications of CAP-4 and OOK signals over MMF based on electro-optic chaos,” *Opt. Lett.* **42**, 3662–3665.

- Antonik, P., F. Duport, M. Hermans, A. Smerieri, M. Haelterman, and S. Massar, 2017, "Online training of an opto-electronic reservoir computer applied to real-time channel equalization," *IEEE Trans. Neural Netw. Learn. Syst.* **28**, 2686–2698.
- Antonik, P., M. Haelterman, and S. Massar, 2017, "Brain-inspired photonic signal processor for generating periodic patterns and emulating chaotic systems," *Phys. Rev. Applied* **7**, 054014.
- Appeltant, L., M. C. Soriano, G. Van der Sande, J. Danckaert, S. Massar, J. Dambre, B. Schrauwen, C. R. Mirasso, and I. Fischer, 2011, "Information processing using a single dynamical node as complex system," *Nat. Commun.* **2**, 468.
- Arecchi, F. T., G. Giacomelli, A. Lapucci, and R. Meucci, 1992, "Two-dimensional representation of a delayed dynamical system," *Phys. Rev. A* **45**, R4225–R4228.
- Arecchi, F. T., G. L. Lippi, G. P. Puccioni, and J. R. Tredicce, 1984, "Deterministic chaos in laser with injected signal," *Opt. Commun.* **51**, 308–314.
- Argyris, A., D. Syvridis, L. Larger, V. Annovazzi-Lodi, P. Colet, I. Fischer, J. García-Ojalvo, C. R. Mirasso, L. Pesquera, and K. A. Shore, 2005, "Chaos-based communications at high bit rates using commercial fibre-optic links," *Nature (London)* **438**, 343–346.
- Bagnell, M., J. Davila-Rodriguez, and P. J. Delfyett, 2014, "Millimeter-wave generation in an optoelectronic oscillator using an ultrahigh finesse etalon as a photonic filter," *J. Lightwave Technol.* **32**, 1063–1067.
- Banerjee, A., L. A. D. de Britto, and G. M. Pacheco, 2019, "Analysis of injection locking and pulling in single-loop optoelectronic oscillator," *IEEE Trans. Microwave Theory Tech.* **67**, 2087–2094.
- Banerjee, A., J. Sarkar, N. Das, and B. Biswas, 2018, "Phase-locking dynamics in optoelectronic oscillator," *Opt. Commun.* **414**, 119–127.
- Bányk, T., B. Horváth, and T. Bercei, 2006, "Optimum configuration of multiloop optoelectronic oscillators," *J. Opt. Soc. Am. B* **23**, 1371.
- Bao, Y., E. Banyas, and L. Illing, 2018, "Periodic and quasiperiodic dynamics of optoelectronic oscillators with narrow-band time-delayed feedback," *Phys. Rev. E* **98**, 062207.
- Beck, G., L. Bigot, G. Bouwmans, A. Kudlinski, J. P. Vilcot, and M. Douay, 2012, "Benefits of photonic bandgap fibers for the thermal stabilization of optoelectronic oscillators," *IEEE Photonics J.* **4**, 789–794.
- Blakely, J. N., L. Illing, and D. J. Gauthier, 2004, "High-speed chaos in an optical feedback system with flexible timescales," *IEEE J. Quantum Electron.* **40**, 299–305.
- Bluestone, A., D. T. Spencer, S. Srinivasan, D. Guerra, J. E. Bowers, and L. Theogarajan, 2015, "An ultra-low phase-noise 20-ghz PLL utilizing an optoelectronic voltage-controlled oscillator," *IEEE Trans. Microwave Theory Tech.* **63**, 1046–1052.
- Bogataj, L., M. Vidmar, and B. Batagelj, 2016, "Opto-electronic oscillator with quality multiplier," *IEEE Trans. Microwave Theory Tech.* **64**, 663–668.
- Bogris, A., A. Argyris, and D. Syvridis, 2007, "Analysis of the optical amplifier noise effect on electrooptically generated hyperchaos," *IEEE J. Quantum Electron.* **43**, 552–559.
- Bonifacio, R., and L. A. Lugiato, 1978a, "Bistable absorption in a ring cavity," *Lett. Nuovo Cimento* **21**, 505–509.
- Bonifacio, R., and L. A. Lugiato, 1978b, "Instabilities for a coherently driven absorber in a ring cavity," *Lett. Nuovo Cimento* **21**, 510–516.
- Brunner, D., B. Penkovsky, B. A. Marquez, M. Jacquot, I. Fischer, and L. Larger, 2018, "Tutorial: Photonic neural networks in delay systems," *J. Appl. Phys.* **124**, 152004.
- Brunner, D., M. C. Soriano, C. R. Mirasso, and I. Fischer, 2013, "Parallel photonic information processing at gigabyte per second data rates using transient states," *Nat. Commun.* **4**, 1364.
- Cahill, J. P., O. Okusaga, W. Zhou, C. R. Menyuk, and G. M. Carter, 2015, "Superlinear growth of Rayleigh scattering-induced intensity noise in single-mode fibers," *Opt. Express* **23**, 6400–6407.
- Cai, S., S. Pan, D. Zhu, Z. Tang, P. Zhou, and X. Chen, 2012, "Coupled frequency-doubling optoelectronic oscillator based on polarization modulation and polarization multiplexing," *Opt. Commun.* **285**, 1140–1143.
- Callan, K. E., L. Illing, Z. Gao, D. J. Gauthier, and E. Schöll, 2010, "Broadband chaos generated by an optoelectronic oscillator," *Phys. Rev. Lett.* **104**, 113901.
- Chan, S.-C., G.-Q. Xia, and J.-M. Liu, 2007, "Optical generation of a precise microwave frequency comb by harmonic frequency locking," *Opt. Lett.* **32**, 1917–1919.
- Chang, D. H., H. R. Fetterman, H. Erilig, H. Zhang, A. C. Oh, C. Zhang, and W. H. Steier, 2002, "39-GHz optoelectronic oscillator using broad-band polymer electrooptic modulator," *IEEE Photonics Technol. Lett.* **14**, 191–193.
- Charalambous, G., G. K. M. Hasanuzzaman, A. Perentos, and S. Iezekiel, 2017, "High-Q wavelength division multiplexed optoelectronic oscillator based on a cascaded multi-loop topology," *Opt. Commun.* **387**, 361–365.
- Charalambous, G., A. Perentos, and S. Iezekiel, 2016, "High-Q optoelectronic oscillator based on active recirculating delay line and dual-loop topology," *IEEE Photonics Technol. Lett.* **28**, 2850–2853.
- Chembo, Y. K., 2016, "Kerr optical frequency combs: Theory, applications and perspectives," *Nanophotonics* **5**, 214–230.
- Chembo, Y. K., 2017, "Laser-based optoelectronic generation of narrowband microwave chaos for radars and radio-communication scrambling," *Opt. Lett.* **42**, 3431–3434.
- Chembo, Y. K., A. Hmima, P.-A. Lacourt, L. Larger, and J. M. Dudley, 2009, "Generation of ultralow jitter optical pulses using optoelectronic oscillators with time-lens soliton-assisted compression," *J. Lightwave Technol.* **27**, 5160–5167.
- Chembo, Y. K., M. Jacquot, J. M. Dudley, and L. Larger, 2016, "Ikeda-like chaos on a dynamically filtered supercontinuum light source," *Phys. Rev. A* **94**, 023847.
- Chembo, Y. K., L. Larger, R. Bendoula, and P. Colet, 2008, "Effects of gain and bandwidth on the multimode behavior of optoelectronic microwave oscillators," *Opt. Express* **16**, 9067–9072.
- Chembo, Y. K., L. Larger, and P. Colet, 2008, "Nonlinear dynamics and spectral stability of optoelectronic microwave oscillators," *IEEE J. Quantum Electron.* **44**, 858–866.
- Chembo, Y. K., L. Larger, H. Tavernier, R. Bendoula, E. Rubiola, and P. Colet, 2007, "Dynamic instabilities of microwaves generated with optoelectronic oscillators," *Opt. Lett.* **32**, 2571–2573.
- Chembo, Y. K., K. Volyanskiy, L. Larger, E. Rubiola, and P. Colet, 2009, "Determination of phase noise spectra in optoelectronic microwave oscillators: A Langevin approach," *IEEE J. Quantum Electron.* **45**, 178–186.
- Chen, G., D. Lu, L. Guo, W. Zhao, Y. Huang, and L. Zhao, 2018, "Frequency-tunable OEO using a DFB laser at period-one oscillations with optoelectronic feedback," *IEEE Photonics Technol. Lett.* **30**, 1593–1596.
- Chen, G., D. Lu, L. Guo, W. Zhao, Y. Huang, and L. Zhao, 2019, "Optoelectronic oscillation of the second harmonic of a period-one oscillating distributed feedback laser," *Optik (Stuttgart)* **180**, 313–317.

- Chen, J., Y. Zheng, C. Xue, C. Zhang, and Y. Chen, 2018, "Filtering effect of SiO₂ optical waveguide ring resonator applied to optoelectronic oscillator," *Opt. Express* **26**, 12638–12647.
- Chen, J.-J., Z.-M. Wu, T. Deng, X. Tang, X. Yang, and G.-Q. Xia, 2017, "Current- and feedback-induced state bistability in a 1550 nm-VCSEL with negative optoelectronic feedback," *IEEE Photonics J.* **9**, 1500310.
- Chen, Y., W. Li, and A. Wen, 2013, "Frequency-multiplying optoelectronic oscillator with a tunable multiplication factor," *IEEE Trans. Microwave Theory Tech.* **61**, 3479–3485.
- Chen, Y., S. Liu, and S. Pan, 2018, "Multi-format signal generation using a frequency-tunable optoelectronic oscillator," *Opt. Express* **26**, 4933–4941.
- Chen, Z., J. Dai, Y. Zhou, F. Yin, T. Zhang, J. Li, Y. Dai, and K. Xu, 2017, "Triple band frequency generator based on an optoelectronic oscillator with low phase noise," *Opt. Express* **25**, 20749–20756.
- Cheng, M., L. Deng, X. Gao, H. Li, M. Tang, S. Fu, P. Shum, and D. Liu, 2015, "Security-enhanced OFDM-PON using hybrid chaotic system," *IEEE Photonics Technol. Lett.* **27**, 326–329.
- Cheng, M., L. Deng, H. Li, and D. Liu, 2014, "Enhanced secure strategy for electro-optic chaotic systems with delayed dynamics by using fractional fourier transformation," *Opt. Express* **22**, 5241–5251.
- Chengui, G. R. G., A. F. Talla, J. H. Talla Mbé, A. Coillet, K. Saleh, L. Larger, P. Woaf, and Y. K. Chembo, 2014, "Theoretical and experimental study of slow-scale Hopf limit-cycles in laser-based wideband optoelectronic oscillators," *J. Opt. Soc. Am. B* **31**, 2310–2316.
- Chengui, G. R. G., J. H. Talla Mbé, A. F. Talla, P. Woaf, and Y. K. Chembo, 2018, "Dynamics of optoelectronic oscillators with electronic and laser nonlinearities," *IEEE J. Quantum Electron.* **54**, 5000207.
- Chengui, G. R. G., P. Woaf, and Y. K. Chembo, 2016, "The simplest laser-based optoelectronic oscillator: An experimental and theoretical study," *J. Lightwave Technol.* **34**, 873–878.
- Chew, S. X., X. Yi, W. Yang, C. Wu, L. Li, L. Nguyen, and R. Minasian, 2017, "Optoelectronic oscillator based sensor using an on-chip sensing probe," *IEEE Photonics J.* **9**, 5500809.
- Chi, Y.-C., P.-C. Peng, and G.-Ru Lin, 2011, "Clock-free RZ-BPSK data generation using self-starting optoelectronic oscillator," *J. Lightwave Technol.* **29**, 1702.
- Chiang, H.-P., C.-H. Huang, C.-Y. Cheng, and D.-W. Huang, 2002, "Chaos in wavelength of tunable semiconductor laser diode with time-delayed Fabry-Perot feedback," *Electron. Lett.* **38**, 1440–1441.
- Chiarello, F., L. Ursini, and M. Santagiustina, 2011, "Securing wireless infrared communications through optical chaos," *IEEE Photonics Technol. Lett.* **23**, 564–566.
- Chiasera, A., Y. Dumeige, P. Feron, M. Ferrari, Y. Jestin, G. Nunzi Conti, S. Pelli, S. Soria, and G. C. Righini, 2010, "Spherical whispering-gallery-mode microresonators," *Laser Photonics Rev.* **4**, 457–482.
- Cho, J.-H., and H.-K. Sung, 2012, "Simple optoelectronic oscillators using direct modulation of dual-section distributed feedback lasers," *IEEE Photonics Technol. Lett.* **24**, 2172–2174.
- Cohen, A. B., B. Ravoori, T. E. Murphy, and R. Roy, 2008, "Using synchronization for prediction of high-dimensional chaotic dynamics," *Phys. Rev. Lett.* **101**, 154102.
- Coillet, A., R. Henriet, P. Salzenstein, K. P. Huy, L. Larger, and Y. K. Chembo, 2013, "Time-domain dynamics and stability analysis of optoelectronic oscillators based on whispering-gallery mode resonators," *IEEE J. Sel. Top. Quantum Electron.* **19**, 1–12.
- Colet, P., and R. Roy, 1994, "Digital communication with synchronized chaotic lasers," *Opt. Lett.* **19**, 2056–2058.
- Courtial, J., J. Leach, and M. J. Padgett, 2001, "Fractals in pixellated video feedback," *Nature (London)* **414**, 864.
- Crutchfield, J. P., 1984, "Space-time dynamics in video feedback," *Physica D (Amsterdam)* **10**, 229–245.
- Crutchfield, J. P., 1988, "Spatio-temporal complexity in nonlinear image processing," *IEEE Trans. Circuit Syst.* **35**, 770–780.
- Cuenot, J.-B., L. Larger, J.-P. Goedgebuer, and W. T. Rhodes, 2001, "Chaos shift keying with an optoelectronic encryption system using chaos in wavelength," *IEEE J. Quantum Electron.* **37**, 849–855.
- Cui, P., L. Yang, Y. Guo, J. Lin, Y. Liu, and J. Zhu, 2018, "Absolute distance measurement using an optical comb and an optoelectronic oscillator," *IEEE Photonics Technol. Lett.* **30**, 744–747.
- Cuomo, K. M., and A. V. Oppenheim, 1993, "Circuit implementation of synchronized chaos with applications to communications," *Phys. Rev. Lett.* **71**, 65–68.
- Dahan, D., E. Shumakher, and G. Eisenstein, 2005, "Self-starting ultralow-jitter pulse source based on coupled optoelectronic oscillators with an intracavity fiber parametric amplifier," *Opt. Lett.* **30**, 1623.
- Dai, J., A. Liu, J. Liu, T. Zhang, Y. Zhou, F. Yin, Y. Dai, Y. Liu, and K. Xu, 2017, "Supermode noise suppression with mutual injection locking for coupled optoelectronic oscillator," *Opt. Express* **25**, 27060–27066.
- Dai, J., Z. Zhao, Y. Zeng, J. Liu, A. Liu, T. Zhang, F. Yin, Y. Zhou, Y. Liu, and K. Xu, 2018, "Stabilized optoelectronic oscillator with enlarged frequency-drift compensation range," *IEEE Photonics Technol. Lett.* **30**, 1289–1292.
- Dai, Y., R. Wang, F. Yin, J. Dai, L. Yu, J. Li, and K. Xu, 2015, "Sidemode suppression for coupled optoelectronic oscillator by optical pulse power feedforward," *Opt. Express* **23**, 27589.
- Damen, T. C., and M. A. Duguay, 1980, "Optoelectronic regenerative pulser," *Electron. Lett.* **16**, 166–167.
- Davidson, T., P. Goldgeier, G. Eisenstein, and M. Orenstein, 1999, "High spectral purity CW oscillation and pulse generation in optoelectronic microwave oscillator," *Electron. Lett.* **35**, 1260–1261.
- Deng, H., J. Zhang, X. Chen, and J. Yao, 2017, "Photonic generation of a phase-coded chirp microwave waveform with increased TBWP," *IEEE Photonics Technol. Lett.* **29**, 1420–1423.
- Deng, T., G.-Q. Xia, L.-P. Cao, J.-G. Chen, X.-D. Lin, and Z.-M. Wu, 2009, "Bidirectional chaos synchronization and communication in semiconductor lasers with optoelectronic feedback," *Opt. Commun.* **282**, 2243–2249.
- Devgan, P., 2013, "A review of optoelectronic oscillators for high speed signal processing applications," *ISRN Electron.* **2013**, 401969.
- Devgan, P., D. Serkland, G. Keeler, K. Geib, and P. Kumar, 2006, "An optoelectronic oscillator using an 850-nm VCSEL for generating low jitter optical pulses," *IEEE Photonics Technol. Lett.* **18**, 685–687.
- Devgan, P. S., M. W. Pruessner, V. J. Urick, and K. J. Williams, 2010, "Detecting low-power RF signals using a multimode optoelectronic oscillator and integrated optical filter," *IEEE Photonics Technol. Lett.* **22**, 152–154.
- Devgan, P. S., V. J. Urick, J. F. Diehl, and K. J. Williams, 2009, "Improvement in the phase noise of a 10 GHz optoelectronic oscillator using all-photonic gain," *J. Lightwave Technol.* **27**, 3189–3193.

- Docherty, A., C. R. Menyuk, J. P. Cahill, O. Okusaga, and W. Zhou, 2013, “Rayleigh-scattering-induced RIN and amplitude-to-phase conversion as a source of length-dependent phase noise in OEOs,” *IEEE Photonics J.* **5**, 5500514.
- Dorizzi, B., B. Grammaticos, M. Le Berre, Y. Pomeau, E. Ressayre, and A. Tallet, 1987, “Statistics and dimension of chaos in differential delay systems,” *Phys. Rev. A* **35**, 328–339.
- Drzewietzki, L., S. Breuer, and W. Elsasser, 2013, “Timing phase noise reduction of modelocked quantum-dot lasers by time-delayed optoelectronic feedback,” *Electron. Lett.* **49**, 557–559.
- Duport, F., A. Smerieri, A. Akrouit, M. Haelterman, and S. Massar, 2016a, “Fully analogue photonic reservoir computer,” *Sci. Rep.* **6**, 22381.
- Duport, F., A. Smerieri, A. Akrouit, M. Haelterman, and S. Massar, 2016b, “Virtualization of a photonic reservoir computer,” *J. Lightwave Technol.* **34**, 2085–2091.
- Eliyahu, D., W. Liang, E. Dale, A. A. Savchenkov, V. S. Ilchenko, A. B. Matsko, D. Seidel, and L. Maleki, 2013, “Resonant widely tunable opto-electronic oscillator,” *IEEE Photonics Technol. Lett.* **25**, 1535–1538.
- Eliyahu, D., D. Seidel, and L. Maleki, 2008, “Phase noise of a high performance OEO and an ultra low noise floor cross-correlation microwave photonic homodyne system,” *2008 IEEE International Frequency Control Symposium*, pp. 811–814 [<https://ieeexplore.ieee.org/document/4623111>].
- Elsonbaty, A., S. F. Hegazy, and S. S. A. Obayya, 2015, “Simultaneous suppression of time-delay signature in intensity and phase of dual-channel chaos communication,” *IEEE J. Quantum Electron.* **51**, 2400309.
- Erneux, T., 2009, *Applied Delay Differential Equations* (Springer, New York).
- Erneux, T., L. Larger, M. W. Lee, and J.-P. Goedgebuer, 2004, “Ikeda Hopf bifurcation revisited,” *Physica D (Amsterdam)* **194**, 49–64.
- Essevaz-Roulet, B., P. Petitjeans, M. Rosen, and J. E. Wesfreid, 2000, “Farey sequences of spatiotemporal patterns in video feedback,” *Phys. Rev. E* **61**, 3743–3749.
- Fan, Z., Q. Qiu, J. Su, and T. Zhang, 2019, “Tunable low-drift spurious-free optoelectronic oscillator based on injection locking and time delay compensation,” *Opt. Lett.* **44**, 534–537.
- Fan, Z., J. Su, T. Zhang, N. Yang, and Q. Qiu, 2017, “High-precision thermal-insensitive strain sensor based on optoelectronic oscillator,” *Opt. Express* **25**, 27037–27050.
- Fang, X., B. Wetzell, J.-M. Merolla, J. M. Dudley, L. Larger, C. Guyeux, and J. M. Bahi, 2014, “Noise and chaos contributions in fast random bit sequence generated from broadband optoelectronic entropy sources,” *IEEE Trans. Circuits Syst. I* **61**, 888–901.
- Farhat, N. H., D. Psaltis, A. Prata, and E. Paek, 1985, “Optical implementation of the Hopfield model,” *Appl. Opt.* **24**, 1469–1475.
- Fedderwitz, S., A. Stöhr, S. Babieli, V. Rymanov, and D. Jager, 2010, “Optoelectronic K-band oscillator with gigahertz tuning range and low phase noise,” *IEEE Photonics Technol. Lett.* **22**, 1497–1499.
- Feigenbaum, M. J., 1980, “Universal behavior in nonlinear systems,” *Los Alamos Sci.*, 4–27 [<https://lib-www.lanl.gov/lascience01.shtml>].
- Feldman, A., 1978, “Ultralinear bistable electro-optic polarization modulator,” *Appl. Phys. Lett.* **33**, 243–245.
- Fleyer, M., and M. Horowitz, 2018, “Phase measurement by using a forced delay-line oscillator and its application for an acoustic fiber sensor,” *Opt. Express* **26**, 9107–9133.
- Fleyer, M., A. Sherman, M. Horowitz, and M. Namer, 2016, “Wideband-frequency tunable optoelectronic oscillator based on injection locking to an electronic oscillator,” *Opt. Lett.* **41**, 1993–1996.
- Fortier, T. M., *et al.*, 2011, “Generation of ultrastable microwaves via optical frequency division,” *Nat. Photonics* **5**, 425–429.
- Fu, R., X. Jin, Y. Zhu, X. Jin, X. Yu, S. Zheng, H. Chi, and X. Zhang, 2017, “Frequency stability optimization of an OEO using phase-locked-loop and self-injection-locking,” *Opt. Commun.* **386**, 27–30.
- Galmès, B., K. Phan-Huy, L. Furfaro, Y. K. Chembo, and J.-M. Merolla, 2019, “Nine-frequency-path quantum interferometry over 60 km of optical fiber,” *Phys. Rev. A* **99**, 033805.
- Gao, B., F. Zhang, P. Zhou, and S. Pan, 2017, “A frequency-tunable two-tone RF signal generator by polarization multiplexed optoelectronic oscillator,” *IEEE Microwave Wireless Compon. Lett.* **27**, 192–194.
- Gao, L., M. Wang, X. Chen, and J. Yao, 2013, “Frequency- and phase-tunable optoelectronic oscillator,” *IEEE Photonics Technol. Lett.* **25**, 1011–1013.
- Gao, X., F. Xie, and H. Hu, 2015, “Enhancing the security of electro-optic delayed chaotic system with intermittent time-delay modulation and digital chaos,” *Opt. Commun.* **352**, 77–83.
- García, S., and I. Gasulla, 2015, “Multi-cavity optoelectronic oscillators using multicore fibers,” *Opt. Express* **23**, 2403.
- Garmire, E., S. D. Allen, J. Marburger, and C. M. Verber, 1978, “Multimode integrated optical bistable switch,” *Opt. Lett.* **3**, 69–71.
- Garmire, E., J. H. Marburger, and S. D. Allen, 1978, “Incoherent mirrorless bistable optical devices,” *Appl. Phys. Lett.* **32**, 320–321.
- Garmire, E., J. H. Marburger, S. D. Allen, and H. G. Winful, 1979, “Transient response of hybrid bistable optical devices,” *Appl. Phys. Lett.* **34**, 374–376.
- Gastaud, N., S. Poinot, L. Larger, J.-M. Merolla, M. Hanna, J.-P. Goedgebuer, and F. Malassenet, 2004, “Electro-optical chaos for multi-10 Gbit/s optical transmissions,” *Electron. Lett.* **40**, 898–899.
- Genin, E., L. Larger, J.-P. Goedgebuer, M. W. Lee, R. Ferrière, and X. Bavard, 2004, “Chaotic oscillations of the optical phase for multigigahertz-bandwidth secure communications,” *IEEE J. Quantum Electron.* **40**, 294–298.
- Giacomelli, G., M. Calzavara, and F. T. Arecchi, 1989, “Instabilities in a semiconductor laser with delayed optoelectronic feedback,” *Opt. Commun.* **74**, 97–101.
- Gibbs, H. M., F. A. Hopf, D. L. Kaplan, and R. L. Shoemaker, 1981, “Observation of chaos in optical bistability,” *Phys. Rev. Lett.* **46**, 474–477.
- Goedgebuer, J.-P., L. Larger, and H. Porte, 1998, “Optical cryptosystem based on synchronization of hyperchaos generated by a delayed feedback tunable laser diode,” *Phys. Rev. Lett.* **80**, 2249–2252.
- Goedgebuer, J.-P., L. Larger, H. Porte, and F. Delorme, 1998, “Chaos in wavelength with a feedback tunable laser diode,” *Phys. Rev. E* **57**, 2795–2798.
- Goedgebuer, J.-P., P. Levy, L. Larger, C.-C. Chen, and W. T. Rhodes, 2002, “Optical communication with synchronized hyperchaos generated electrooptically,” *IEEE J. Quantum Electron.* **38**, 1178–1183.
- Grapinet, M., V. Udaltsov, M. Jacquot, P.-A. Lacourt, J. M. Dudley, and L. Larger, 2008a, “Experimental chaotic map generated by picosecond laser pulse-seeded electro-optic nonlinear delay dynamics,” *Chaos* **18**, 013110.
- Grapinet, M., V. Udaltsov, M. Jacquot, P.-A. Lacourt, J. M. Dudley, and L. Larger, 2008b, “Synchronisation and communication with regularly clocked optoelectronic discrete time chaos,” *Electron. Lett.* **44**, 764–766.
- Grigorieva, E. V., H. Haken, and S. A. Kaschenko, 1999, “Theory of quasiperiodicity in model of lasers with delayed optoelectronic feedback,” *Opt. Commun.* **165**, 279–292.

- Grigor'yants, V. V., A. A. Dvornikov, Y. B. Il'in, V. N. Konstantinov, V. A. Prokof'iev, and G. M. Utkin, 1985, "A laser diode with feedback using a fibre delay line as a stable-frequency signal generator and potential fibre sensor," *Opt. Quantum Electron.* **17**, 263–267.
- Hagerstrom, A. M., T. E. Murphy, and R. Roy, 2015, "Harvesting entropy and quantifying the transition from noise to chaos in a photon-counting feedback loop," *Proc. Natl. Acad. Sci. U.S.A.* **112**, 9258–9263.
- Hagerstrom, A. M., T. E. Murphy, R. Roy, P. Hövel, I. Omelchenko, and E. Schöll, 2012, "Experimental observation of chimeras in coupled-map lattices," *Nat. Phys.* **8**, 658–661.
- Han, X., L. Ma, Y. Shao, Q. Ye, Y. Gu, and M. Zhao, 2017, "Polarization multiplexed dual-loop optoelectronic oscillator based on stimulated Brillouin scattering," *Opt. Commun.* **383**, 138–143.
- Hao, T., Q. Cen, Y. Dai, J. Tang, W. Li, J. Yao, N. Zhu, and M. Li, 2018, "Breaking the limitation of mode building time in an optoelectronic oscillator," *Nat. Commun.* **9**, 1839.
- Hao, T., J. Tang, D. Domenech, W. Li, N. Zhu, J. Capmany, and M. Li, 2018, "Toward monolithic integration of OEOs: From systems to chips," *J. Lightwave Technol.* **36**, 4565–4582.
- Hart, J. D., D. C. Schmadel, T. E. Murphy, and R. Roy, 2017, "Experiments with arbitrary networks in time-multiplexed delay systems," *Chaos* **27**, 121103.
- Hart, J. D., Y. Zhang, R. Roy, and A. E. Motter, 2019, "Topological control of synchronization patterns: Trading symmetry for stability," *Phys. Rev. Lett.* **122**, 058301.
- Hasegawa, H., Y. Oikawa, and M. Nakazawa, 2007, "A 10-GHz optoelectronic oscillator at 850 nm using a single-mode VCSEL and a photonic crystal fiber," *IEEE Photonics Technol. Lett.* **19**, 1451–1453.
- Häusler, G., G. Seckmeyer, and T. Weiss, 1986, "Chaos and cooperation in nonlinear pictorial feedback systems. 1: Experiments," *Appl. Opt.* **25**, 4656–4663.
- Häusler, G., and M. Simon, 1978, "Generation of space and time picture oscillations by active incoherent feedback," *Opt. Acta* **25**, 327–336.
- Hayasaki, Y., E. Hikosaka, H. Yamamoto, and N. Nishida, 2005, "Optical image processing using an optoelectronic feedback system with electronic distortion correction," *Opt. Express* **13**, 4657–4665.
- Hermans, M., P. Antonik, M. Haelterman, and S. Massar, 2016, "Embodiment of learning in electro-optical signal processors," *Phys. Rev. Lett.* **117**, 128301.
- Hizanidis, J., S. Deligiannidis, A. Bogris, and D. Syvridis, 2010, "Enhancement of chaos encryption potential by combining all-optical and electrooptical chaos generators," *IEEE J. Quantum Electron.* **46**, 1642–1649.
- Hong, J., W. He, S. Yao, X. Wang, Z. Hu, and Z. Li, 2016, "New structure for high-performance opto-electronic oscillator," *Optik* **127**, 8431–8435.
- Hosseini, S. E., A. Banai, and F. X. Kartner, 2017, "Tunable low-jitter low-drift spurious-free transposed-frequency optoelectronic oscillator," *IEEE Trans. Microw. Theory Techn.* **65**, 2625–2635.
- Hu, G., Y. Zhang, H. A. Cerdeira, and S. Chen, 2000, "From low-dimensional synchronous chaos to high-dimensional desynchronous spatiotemporal chaos in coupled systems," *Phys. Rev. Lett.* **85**, 3377–3380.
- Hu, H., S. Shi, and F. Xie, 2017, "Electro-optic intensity chaotic system with an extra optical feedback," *Opt. Commun.* **402**, 140–146.
- Hu, H., W. Su, L. Liu, and Z. Yu, 2014, "Electro-optic intensity chaotic system with varying parameters," *Phys. Lett. A* **378**, 184–190.
- Huang, L., D. Chen, P. Wang, T. Zhang, P. Xiang, Y. Zhang, T. Pu, and X. Chen, 2015, "Generation of triangular pulses based on an optoelectronic oscillator," *IEEE Photonics Technol. Lett.* **27**, 2500–2503.
- Huang, L., *et al.*, 2017, "Novel dual-loop optoelectronic oscillator based on self-polarization-stabilization technique," *Opt. Express* **25**, 21993–22003.
- Huang, N., M. Li, Y. Deng, and N. H. Zhu, 2014, "Optical pulse generation based on an optoelectronic oscillator with cascaded nonlinear semiconductor optical amplifiers," *IEEE Photonics J.* **6**, 5500208.
- Huang, Y., H. Hu, F. Xie, and J. Zheng, 2018, "An innovative electro-optical chaotic system using electrical mutual injection with nonlinear transmission function," *IEEE Photonics J.* **10**, 7900112.
- Huggett, G. R., 1968, "Modelocking of CW lasers by regenerative RF feedback," *Appl. Phys. Lett.* **13**, 186–187.
- Huo, L., Y. Dong, C. Lou, and Y. Z. Gao, 2003, "Clock extraction using an optoelectronic oscillator from high-speed NRZ signal and NRZ-to-RZ format transformation," *IEEE Photonics Technol. Lett.* **15**, 981–983.
- Ikeda, K., 1979, "Multiple-valued stationary state and its instability of the transmitted light by a ring cavity system," *Opt. Commun.* **30**, 257–261.
- Ikeda, K., H. Daido, and O. Akimoto, 1980, "Optical turbulence: chaotic behavior of transmitted light from a ring cavity," *Phys. Rev. Lett.* **45**, 709–712.
- Illing, L., and D. J. Gauthier, 2005, "Hopf bifurcations in time-delay systems with band-limited feedback," *Physica D (Amsterdam)* **210**, 180–202.
- Illing, L., C. D. Panda, and L. Shareshian, 2011, "Isochronal chaos synchronization of delay-coupled optoelectronic oscillators," *Phys. Rev. E* **84**, 016213.
- Ito, H., Y. Ogawa, and H. Inaba, 1979, "Integrated bistable optical device using Mach-Zehnder interferometric optical waveguide," *Electron. Lett.* **15**, 283–285.
- Ito, H., Y. Ogawa, and H. Inaba, 1981, "Analyses and experiments on integrated optical multivibrators using electrooptically controlled bistable optical devices," *IEEE J. Quantum Electron.* **17**, 325–331.
- Ivanov, E. N., and M. E. Tobar, 2009, "Low phase-noise sapphire crystal microwave oscillators: Current status," *IEEE Trans. Ultrason. Ferroelectr. Freq. Control* **56**, 263–269.
- Jaeger, H., and H. Haas, 2004, "Harnessing nonlinearity: Predicting chaotic systems and saving energy in wireless communication," *Science* **304**, 78–80.
- Jahanbakht, S., and S. E. Hosseini, 2016, "Frequency domain noise analysis of optoelectronic oscillators considering the nonlinearity of the RF amplifier," *J. Opt. Soc. Am. B* **33**, 548–557.
- Ji, Y., X. S. Yao, and L. Maleki, 1999, "Compact optoelectronic oscillator with ultra-low phase noise performance," *Electron. Lett.* **35**, 1554–1555.
- Jia, S., J. Yu, J. Wang, W. Wang, Q. Wu, G. Huang, and E. Yang, 2015, "A novel optoelectronic oscillator based on wavelength multiplexing," *IEEE Photonics Technol. Lett.* **27**, 213–216.
- Jia, S., J. Yu, Z. Wang, J. Wang, W. Wang, B. Chen, and Y. Yu, 2015, "A novel highly stable dual-wavelength short optical pulse source based on a dual-loop optoelectronic oscillator with two wavelengths," *IEEE Photonics J.* **7**, 1502611.
- Jiang, F., J. H. Wong, H. Q. Lam, J. Zhou, S. Aditya, P. H. Lim, K. E. K. Lee, P. P. Shum, and X. Zhang, 2013, "An optically tunable wideband optoelectronic oscillator based on a bandpass microwave photonic filter," *Opt. Express* **21**, 16381–16389.
- Jiang, Y., G. Bai, L. Hu, H. Li, Z. Zhou, J. Xu, and S. Wang, 2013, "Frequency locked single-mode optoelectronic oscillator by using

- low frequency RF signal injection,” *IEEE Photonics Technol. Lett.* **25**, 382–384.
- Jiang, Y., J.-L. Yu, H. Hu, W.-R. Wang, Y.-T. Wang, and E.-Z. Yang, 2007, “Phase-modulator-based optoelectronic oscillator for generating short optical pulse and microwave signal,” *Opt. Eng. (N.Y.)* **46**, 090502.
- Jin, X., M. Wang, K. Wang, Y. Dong, and L. Yu, 2019, “High spectral purity electromagnetically induced transparency-based microwave optoelectronic oscillator with a quasi-cylindrical microcavity,” *Opt. Express* **27**, 150–165.
- Jin, X., Y. Zhu, J. Guo, X. Jin, X. Yu, S. Zheng, H. Chi, and X. Zhang, 2017, “Highly sensitive demodulation of a vibration-induced phase shift based on a low-noise OEO,” *Opt. Lett.* **42**, 4052–4054.
- Jin, Y., Q. Zhao, H. Yin, and H. Yue, 2015, “Handwritten numeral recognition utilizing reservoir computing subject to optoelectronic feedback,” *Proceedings of the IEEE International Conference on Natural Computation (ICNC)*, pp. 1165–1169 [<https://ieeexplore.ieee.org/document/7378156>].
- Joiner, K. L., F. Palmero, and R. Carretero-Gonzalez, 2016, “Optoelectronic chaos in a simple light activated feedback circuit,” *Int. J. Bifurcation Chaos Appl. Sci. Eng.* **26**, 1650080.
- Juan, Y.-S., and F.-Y. Lin, 2009, “Ultra broadband microwave frequency combs generated by an optical pulse-injected semiconductor laser,” *Opt. Express* **17**, 18596–18605.
- Kaba, M., H. W. Li, A. S. Daryoush, J. P. Vilcot, D. Decoster, J. Chazelas, G. Bouwmans, Y. Quiquempois, and F. Deborgies, 2006, “Improving thermal stability of opto-electronic oscillators,” *IEEE Microw. Mag.* **7**, 38–47.
- Kaplan, A. E., 1981, “Bistable reflection of light by an electro-optically driven interface,” *Appl. Phys. Lett.* **38**, 67–69.
- Ke, J., L. Yi, G. Xia, and W. Hu, 2018, “Chaotic optical communications over 100-km fiber transmission at 30-Gb/s bit rate,” *Opt. Lett.* **43**, 1323–1326.
- Kersten, R. T., 1978, “Ein optisches nachrichtensystem mit bauelementen der integrierten optik für die übertragung hoher bitraten,” *Archiv für Elektrotechnik* **60**, 353–359.
- Kim, J. M., and D. Cho, 2010, “Optoelectronic oscillator stabilized to an intra-loop Fabry-Perot cavity by a dual servo system,” *Opt. Express* **18**, 14905–14912.
- Kim, J.-Y., J.-H. Jo, W.-Y. Choi, and H.-K. Sung, 2012, “Dual-loop dual-modulation optoelectronic oscillators with highly suppressed spurious tones,” *IEEE Photonics Technol. Lett.* **24**, 706–708.
- Kingni, S. T., G. Van der Sande, I. V. Ermakov, and J. Danckaert, 2015, “Theoretical analysis of semiconductor ring lasers with short and long time-delayed optoelectronic and incoherent feedback,” *Opt. Commun.* **341**, 147–154.
- Koizumi, K., M. Yoshida, and M. Nakazawa, 2010, “A 10-GHz optoelectronic oscillator at 1.1 μm using a single-mode VCSEL and a photonic crystal fiber,” *IEEE Photonics Technol. Lett.* **22**, 293–295.
- Kong, F., W. Li, and J. Yao, 2013, “Transverse load sensing based on a dual-frequency optoelectronic oscillator,” *Opt. Lett.* **38**, 2611–2613.
- Konopsky, V. N., 1996, “A new type of optical gyro via electro-optical oscillator,” *Opt. Commun.* **126**, 236–239.
- Kouomou, Y. C., P. Colet, N. Gastaud, and L. Larger, 2004, “Effect of parameter mismatch on the synchronization of chaotic semiconductor lasers with electro-optical feedback,” *Phys. Rev. E* **69**, 056226.
- Kouomou, Y. C., P. Colet, L. Larger, and N. Gastaud, 2005a, “Chaotic breathers in delayed electro-optical systems,” *Phys. Rev. Lett.* **95**, 203903.
- Kouomou, Y. C., P. Colet, L. Larger, and N. Gastaud, 2005b, “Mismatch-induced bit error rate in optical chaos communications using semiconductor lasers with electrooptical feedback,” *IEEE J. Quantum Electron.* **41**, 156–163.
- Kouomou, Y. C., and P. Wofo, 2003a, “Cluster synchronization in coupled chaotic semiconductor lasers and application to switching in chaos-secured communication networks,” *Opt. Commun.* **223**, 283–293.
- Kouomou, Y. C., and P. Wofo, 2003b, “Transitions from spatio-temporal chaos to cluster and complete synchronization states in a shift-invariant set of coupled nonlinear oscillators,” *Phys. Rev. E* **67**, 046205.
- Lachinova, S. L., and W. Lu, 2001, “Domain coexistence in nonlinear optical pattern formation,” *Phys. Rev. E* **64**, 026207.
- Lang, R., and K. Kobayashi, 1980, “External optical feedback effects on semiconductor injection laser properties,” *IEEE J. Quantum Electron.* **16**, 347–355.
- Larger, L., 2013, “Complexity in electro-optic delay dynamics: Modelling, design and applications,” *Phil. Trans. R. Soc. A* **371**, 20120464.
- Larger, L., A. Baylón-Fuentes, R. Martinenghi, V. S. Udaltsov, Y. K. Chembo, and M. Jacquot, 2017, “High-speed photonic reservoir computing using a time-delay-based architecture: Million words per second classification,” *Phys. Rev. X* **7**, 011015.
- Larger, L., and J. M. Dudley, 2010, “Optoelectronic chaos,” *Nature (London)* **465**, 41–42.
- Larger, L., J.-P. Goedgebuer, and F. Delorme, 1998, “Optical encryption system using hyperchaos generated by an optoelectronic wavelength oscillator,” *Phys. Rev. E* **57**, 6618–6624.
- Larger, L., J.-P. Goedgebuer, and J.-M. Merolla, 1998, “Chaotic oscillator in wavelength: A new setup for investigating differential difference equations describing nonlinear dynamics,” *IEEE J. Quantum Electron.* **34**, 594–601.
- Larger, L., P.-A. Lacourt, S. Poinot, and M. Hanna, 2005, “From flow to map in an experimental high-dimensional electro-optic nonlinear delay oscillator,” *Phys. Rev. Lett.* **95**, 043903.
- Larger, L., M. W. Lee, J.-P. Goedgebuer, W. Elflein, and T. Erneux, 2001, “Chaos in coherence modulation: bifurcations of an oscillator generating optical delay fluctuations,” *J. Opt. Soc. Am. B* **18**, 1063–1068.
- Larger, L., B. Penkovsky, and Y. Maistrenko, 2015, “Laser chimeras as a paradigm for multistable patterns in complex systems,” *Nat. Commun.* **6**, 7752.
- Larger, L., M. C. Soriano, D. Brunner, L. Appeltant, J. M. Gutierrez, L. Pesquera, C. R. Mirasso, and I. Fischer, 2012, “Photonic information processing beyond Turing: an optoelectronic implementation of reservoir computing,” *Opt. Express* **20**, 3241–3249.
- Lasri, J., A. Bilenca, D. Dahan, V. Sidorov, G. Eisenstein, D. Ritter, and K. Yvind, 2002, “A self-starting hybrid optoelectronic oscillator generating ultra low jitter 10-GHz optical pulses and low phase noise electrical signals,” *IEEE Photonics Technol. Lett.* **14**, 1004–1006.
- Lasri, J., P. Devgan, R. Tang, and P. Kumar, 2004, “Ultralow timing jitter 40-Gb/s clock recovery using a self-starting optoelectronic oscillator,” *IEEE Photonics Technol. Lett.* **16**, 263–265.
- Lau, K. Y., and A. Yariv, 1984, “Self-sustained picosecond pulse generation in a GaAlAs laser at an electrically tunable repetition rate by optoelectronic feedback,” *Appl. Phys. Lett.* **45**, 124–126.
- Lavrov, R., M. Jacquot, and L. Larger, 2010, “Nonlocal nonlinear electro-optic phase dynamics demonstrating 10 Gb/s chaos communications,” *IEEE J. Quantum Electron.* **46**, 1430–1435.
- Lavrov, R., M. Peil, M. Jacquot, L. Larger, V. Udaltsov, and J. Dudley, 2009, “Electro-optic delay oscillator with nonlocal

- nonlinearity: Optical phase dynamics, chaos, and synchronization,” *Phys. Rev. E* **80**, 026207.
- Lee, C.-H., S.-Y. Shin, and S.-Y. Lee, 1988, “Optical short-pulse generation using diode lasers with negative optoelectronic feedback,” *Opt. Lett.* **13**, 464–466.
- Lee, J., S. Park, D. H. Seo, S. H. Yim, S. Yoon, and D. Cho, 2016, “Displacement measurement using an optoelectronic oscillator with an intra-loop Michelson interferometer,” *Opt. Express* **24**, 21910–21920.
- Lee, J.-Y., M.-S. Jeon, and J.-I. Song, 2019, “Remote optical frequency up-converter based on optoelectronic oscillator,” *IEEE Photonics Technol. Lett.* **31**, 50–53.
- Lee, J.-Y., and J.-I. Song, 2017, “Photonic frequency down-converter based on a frequency-doubling OEO using two cascaded EAMs,” *IEEE Photonics Technol. Lett.* **29**, 1529–1532.
- Lee, K. H., J. Y. Kim, W. Y. Choi, H. Kamitsuna, M. Ida, and K. Kurishima, 2008, “Low-cost optoelectronic self-injection-locked oscillators,” *IEEE Photonics Technol. Lett.* **20**, 1151–1153.
- Lee, M. W., L. Larger, and J.-P. Goedgebuer, 2003, “Transmission system using chaotic delays between lightwaves,” *IEEE J. Quantum Electron.* **39**, 931–935.
- Lelièvre, O., *et al.*, 2017, “A model for designing ultralow noise single- and dual-loop 10-GHz optoelectronic oscillators,” *J. Lightwave Technol.* **35**, 4366–4374.
- Levy, E. C., and M. Horowitz, 2011, “Single-cycle radio-frequency pulse generation by an optoelectronic oscillator,” *Opt. Express* **19**, 17599.
- Levy, E. C., O. Okusaga, M. Horowitz, C. R. Menyuk, W. Zhou, and G. M. Carter, 2010, “Comprehensive computational model of single- and dual-loop optoelectronic oscillators with experimental verification,” *Opt. Express* **18**, 21461–21476.
- Lewis, M. F., 1992, “Novel RF oscillator using optical components,” *Electron. Lett.* **28**, 31–32.
- Li, C., J. Mao, R. Dai, X. Zhou, and J. Jiang, 2016, “Frequency-sextupling optoelectronic oscillator using a Mach-Zehnder interferometer and an FBG,” *IEEE Photonics Technol. Lett.* **28**, 1356–1359.
- Li, C., Y. Wang, W. Y. Wang, Z. Xu, B. Zhao, H. Wang, and D. Tang, 2018, “Widely tunable optoelectronic oscillator using a dispersion-induced single bandpass MPF,” *IEEE Photonics Technol. Lett.* **30**, 7–10.
- Li, C. Y., H. H. Lu, T. T. Shih, M. T. Cheng, C. M. Ho, X. Y. Lin, Z. Y. Yang, and S. J. Huang, 2016, “A bidirectional fiber-wireless and fiber-IVLLC convergence system with a dual-polarization modulation scheme and an MZM-OEO-based BLS,” *IEEE Photonics J.* **8**, 7200408.
- Li, C.-Yi, H.-H. Lu, Y.-N. Chen, C.-W. Su, Y.-R. Wu, Z.-H. Wang, and Y.-P. Lin, 2018, “A high-speed and long-reach PAM4 optical wireless communication system,” *IEEE Photonics J.* **10**, 7906109.
- Li, L., L. Paolino, X. Yi, and T. Huang, 2014, “Shifted dispersion-induced RF-fading based continuously tunable optoelectronic oscillator,” *Electron. Lett.* **50**, 1079–1081.
- Li, M., Y. Hong, Y. Song, and X. Zhang, 2018, “Effect of controllable parameter synchronization on the ensemble average bit error rate of space-to-ground downlink chaos laser communication system,” *Opt. Express* **26**, 2954–2964.
- Li, M., W. Li, and J. Yao, 2012, “Tunable optoelectronic oscillator incorporating a high-Q spectrum-sliced photonic microwave transversal filter,” *IEEE Photonics Technol. Lett.* **24**, 1251–1253.
- Li, N., and J. Wei, 2019, “Bifurcation analysis in a nonlinear electro-optical oscillator with delayed bandpass feedback,” *Nonlinear Dyn.* **96**, 483–496.
- Li, W., F. Kong, and J. Yao, 2013, “Arbitrary microwave waveform generation based on a tunable optoelectronic oscillator,” *J. Lightwave Technol.* **31**, 3780–3786.
- Li, W., J. G. Liu, and N. H. Zhu, 2015, “A widely and continuously tunable frequency doubling optoelectronic oscillator,” *IEEE Photonics Technol. Lett.* **27**, 1461–1464.
- Li, W., and J. Yao, 2012, “A wideband frequency tunable optoelectronic oscillator incorporating a tunable microwave photonic filter based on phase-modulation to intensity-modulation conversion using a phase-shifted fiber Bragg grating,” *IEEE Trans. Microwave Theory Tech.* **60**, 1735–1742.
- Liao, J.-F., and J.-Q. Sun, 2013, “Polarization dynamics and chaotic synchronization in unidirectionally coupled VCSELs subjected to optoelectronic feedback,” *Opt. Commun.* **295**, 188–196.
- Liao, M.-L., Y.-Z. Huang, H.-Z. Weng, J.-Y. Han, Z.-X. Xiao, J.-L. Xiao, and Y.-D. Yang, 2017, “Narrow-linewidth microwave generation by an optoelectronic oscillator with a directly modulated microsquare laser,” *Opt. Lett.* **42**, 4251–4254.
- Lin, F.-Y., and J.-M. Liu, 2003, “Nonlinear dynamics of a semiconductor laser with delayed negative optoelectronic feedback,” *IEEE J. Quantum Electron.* **39**, 562–568.
- Lin, F.-Y., and J.-M. Liu, 2004, “Chaotic lidar,” *IEEE J. Sel. Top. Quantum Electron.* **10**, 991–997.
- Lin, F.-Y., and M.-C. Tsai, 2007, “Chaotic communication in radio-over-fiber transmission based on optoelectronic feedback semiconductor lasers,” *Opt. Express* **15**, 302–311.
- Lin, G., A. Coillet, and Y. K. Chembo, 2017, “Nonlinear photonics with high-Q whispering-gallery-mode resonators,” *Adv. Opt. Photonics* **9**, 828–890.
- Lin, X.-D., Z.-M. Wu, T. Deng, X. Tang, L. Fan, Z.-Y. Gao, and G.-Q. Xia, 2018, “Generation of widely tunable narrow-linewidth photonic microwave signals based on an optoelectronic oscillator using an optically injected semiconductor laser as the active tunable microwave photonic filter,” *IEEE Photonics J.* **10**, 5502209.
- Lin, Y. S., 2012, “Theory of stability and bifurcation in a multi-quantum well laser with opto-electronic delayed feedback,” *Opt. Laser Technol.* **44**, 83–91.
- Liu, A., J. Dai, and K. Xu, 2018, “Stable and low-spurs optoelectronic oscillators: A review,” *Appl. Sci.* **8**, 2623.
- Liu, C., W. Zou, and J. Chen, 2013, “An optoelectronic oscillator based on carrier-suppression-effect-free single bandpass microwave photonic filter,” *IEEE Photonics J.* **5**, 5501807.
- Liu, J., H. Deng, W. Zhang, and J. Yao, 2018, “On-chip sensor for simultaneous temperature and refractive index measurements based on a dual-passband microwave photonic filter,” *J. Lightwave Technol.* **36**, 4099–4105.
- Liu, J., G. S. Kanter, S. X. Wang, and P. Kumar, 2012, “10 GHz ultra-stable short optical pulse generation via phase-modulation enhanced dual-loop optoelectronic oscillator,” *Opt. Commun.* **285**, 1035–1038.
- Liu, J., A. Liu, Z. Wu, Y. Gao, J. Dai, Y. Liu, and K. Xu, 2018, “Frequency-demultiplication OEO for stable millimeter-wave signal generation utilizing phase-locked frequency-quadrupling,” *Opt. Express* **26**, 27358–27367.
- Liu, J., M. Wang, Y. Tang, Y. Yang, Y. Wu, W. Jin, and S. Jian, 2017, “Switchable optoelectronic oscillator using an FM-PS-FBG for strain and temperature sensing,” *IEEE Photonics Technol. Lett.* **29**, 2008–2011.
- Liu, J., B. Zheng, and C. Shu, 2017, “Self-oscillating optical frequency comb based on a Raman-pumped Brillouin optoelectronic oscillator,” *IEEE Photonics Technol. Lett.* **29**, 1003–1006.

- Liu, J.-M., H.-F. Chen, and S. Tang, 2002, “Synchronized chaotic optical communications at high bit rates,” *IEEE J. Quantum Electron.* **38**, 1184–1196.
- Liu, L., J. Lin, and S. Miao, 2017, “Bubbling effect in the electro-optic delayed feedback oscillator coupled network,” *Opt. Commun.* **387**, 310–315.
- Liu, L., S. Miao, M. Cheng, and X. Gao, 2016, “A new switching parameter varying optoelectronic delayed feedback model with computer simulation,” *Sci. Rep.* **6**, 22295.
- Liu, S., K. Lv, J. Fu, L. Wu, W. Pan, and S. Pan, 2019, “Wideband microwave frequency division based on an optoelectronic oscillator,” *IEEE Photonics Technol. Lett.* **31**, 389–392.
- Liu, X., W. Pan, X. Zou, L. Yan, B. Luo, and B. Lu, 2014, “Investigation on tunable modulation index in the polarization-modulator-based optoelectronic oscillator,” *IEEE J. Quantum Electron.* **50**, 68–73.
- Liu, Y., P. Davis, and T. Aida, 2001, “Synchronized chaotic mode hopping in DBR lasers with delayed opto-electric feedback,” *IEEE J. Quantum Electron.* **37**, 337–352.
- Liu, Y., T. Hao, W. Li, J. Capmany, N. Zhu, and M. Li, 2018, “Observation of parity-time symmetry in microwave photonics,” *Light Sci. Applications* **7**, 38.
- Liu, Y., and J. Ohtsubo, 1992, “Chaos in an active interferometer,” *J. Opt. Soc. Am. B* **9**, 261–265.
- Loh, W., S. Yegnanarayanan, J. Klamkin, S. M. Duff, J. J. Plant, F. J. O’Donnell, and P. W. Juodawlkis, 2012, “Amplifier-free slab-coupled optical waveguide optoelectronic oscillator systems,” *Opt. Express* **20**, 19589–98.
- Lou, C., L. Huo, G. Chang, and Y. Z. Gao, 2002, “Experimental study of clock division using the optoelectronic oscillator,” *IEEE Photonics Technol. Lett.* **14**, 1178–1180.
- Lu, D., B. Pan, H. Chen, and L. Zhao, 2015, “Frequency-tunable optoelectronic oscillator using a dual-mode amplified feedback laser as an electrically controlled active microwave photonic filter,” *Opt. Lett.* **40**, 4340–4343.
- Lu, D., X. Zhao, C. Lou, and L. Huo, 2011, “Synchronized clock multiplication through optical subharmonic injection locking of an optoelectronic oscillator,” *Opt. Commun.* **284**, 2742–2746.
- Lu, H.-H., C.-Y. Li, T.-C. Lu, C.-J. Wu, C.-A. Chu, A. Shiva, and T. Mochii, 2016, “Bidirectional fiber-wireless and fiber-VLLC transmission system based on an OEO-based BLS and a RSOA,” *Opt. Lett.* **41**, 476–479.
- Ly, A., V. Auroux, R. Khayat-zadeh, N. Gutierrez, A. Fernandez, and O. Llopis, 2018, “Highly spectrally pure 90-GHz signal synthesis using a coupled optoelectronic oscillator,” *IEEE Photonics Technol. Lett.* **30**, 1313–1316.
- Ma, C., J. Yu, J. Wang, Y. Yu, T. Xie, E. Yang, and Y. Jiang, 2018, “Photonic generation of microwave waveforms based on a dual-loop optoelectronic oscillator,” *Opt. Commun.* **426**, 158–163.
- Ma, X.-W., Y.-Z. Huang, L.-X. Zou, B.-W. Liu, H. Long, H.-Z. Weng, Y.-D. Yang, and J.-L. Xiao, 2015, “Narrow-linewidth microwave generation using AlGaInAs/InP microdisk lasers subject to optical injection and optoelectronic feedback,” *Opt. Express* **23**, 20321.
- Maass, W., T. Natschläger, and H. Markram, 2002, “Real-time computing without stable states: A new framework for neural computation based on perturbations,” *Neural Comput.* **14**, 2531–2560.
- Maleki, L., 2011, “The optoelectronic oscillator,” *Nat. Photonics* **5**, 728–730.
- Maleki, L., D. Eliyahu, and A. B. Matsko, 2011, “Optoelectronic oscillator,” in *Broadband Optical Modulators: Science, Technology, and Applications*, edited by A. Chen and E. J. Murphy, Chap. 21 (CRC Press, Boca Raton), pp. 467–487.
- Marino, F., M. Ciszak, S. F. Abdalah, K. Al-Naimee, R. Meucci, and F. T. Arecchi, 2011, “Mixed-mode oscillations via canard explosions in light-emitting diodes with optoelectronic feedback,” *Phys. Rev. E* **84**, 047201.
- Marino, F., G. Giacomelli, and S. Barland, 2014, “Front pinning and localized states analogues in long-delayed bistable systems,” *Phys. Rev. Lett.* **112**, 103901.
- Marquez, B. A., L. Larger, D. Brunner, Y. K. Chembo, and M. Jacquot, 2016, “Interaction between Liénard and Ikeda dynamics in a nonlinear electro-optical oscillator with delayed bandpass feedback,” *Phys. Rev. E* **94**, 062208.
- Márquez, B. A., J. J. Suárez-Vargas, and J. A. Ramírez, 2014, “Polynomial law for controlling the generation of n-scroll chaotic attractors in an optoelectronic delayed oscillator,” *Chaos* **24**, 033123.
- Martinenghi, R., S. Rybalko, M. Jacquot, Y. K. Chembo, and L. Larger, 2012, “Photonic nonlinear transient computing with multiple-delay wavelength dynamics,” *Phys. Rev. Lett.* **108**, 244101.
- Matsko, A., A. Savchenkov, D. Strekalov, V. Ilchenko, and L. Maleki, 2005, “Review of applications of whispering-gallery mode resonators in photonics and nonlinear optics,” *IPN Prog. Rep.* **42**, 1–51 [<https://ipnpr.jpl.nasa.gov/>].
- Matsko, A. B., L. Maleki, A. A. Savchenkov, and V. S. Ilchenko, 2003, “Whispering gallery mode based optoelectronic microwave oscillator,” *J. Mod. Opt.* **50**, 2523–2542.
- Matsko, A. B., D. Strekalov, and L. Maleki, 2005, “Magnetometer based on the opto-electronic microwave oscillator,” *Opt. Commun.* **247**, 141–148.
- Maxin, J., G. Pillet, B. Steinhauser, L. Morvan, O. Llopis, and D. Dolfi, 2013, “Widely tunable opto-electronic oscillator based on a dual frequency laser,” *J. Lightwave Technol.* **31**, 2919–2925.
- May, R. M., 1976, “Simple mathematical models with very complicated dynamics,” *Nature (London)* **261**, 459–467.
- McCall, S. L., 1978, “Instability and regenerative pulsation phenomena in Fabry-Perot nonlinear optic media devices,” *Appl. Phys. Lett.* **32**, 284–286.
- Mei, Y., T. Jin, H. Chi, S. Zheng, X. Jin, and X. Zhang, 2014, “Optoelectronic oscillator with phase-shifted fiber Bragg grating,” *Opt. Commun.* **319**, 117–120.
- Merklein, M., B. Stiller, I. V. Kabakova, U. S. Mutugala, K. Vu, S. J. Madden, B. J. Eggleton, and R. Slavik, 2016, “Widely tunable, low phase noise microwave source based on a photonic chip,” *Opt. Lett.* **41**, 4633–4636.
- Merrer, P.-H., K. Saleh, O. Llopis, S. Berneschi, F. Cosi, and G. Nunzi Conti, 2012, “Characterization technique of optical whispering gallery mode resonators in the microwave frequency domain for optoelectronic oscillators,” *Appl. Opt.* **51**, 4742.
- Mikitchuk, K., A. Chizh, and S. Malyshev, 2016, “Modeling and design of delay-line optoelectronic oscillators,” *IEEE J. Quantum Electron.* **52**, 5000108.
- Miscuglio, M., A. Mehrabian, Z. Hu, S. I. Azzam, J. George, A. V. Kildishev, M. Pelton, and V. J. Sorger, 2018, “All-optical nonlinear activation function for photonic neural networks,” *Opt. Mater. Express* **8**, 3851–3863.
- Mu, P., W. Pan, S. Xiang, N. Li, X. Liu, and X. Zou, 2015, “Fast physical and pseudo random number generation based on a nonlinear optoelectronic oscillator,” *Mod. Phys. Lett. B* **29**, 1550142.
- Mukherjee, A., D. Ghosh, and B. Biswas, 2016, “On the effect of combining an external synchronizing signal feeding the

- Mach-Zehnder modulator in an optoelectronic oscillator,” *Optik* **127**, 3576–3581.
- Munnely, P., B. Lingnau, M. M. Karow, T. Heindel, M. Kamp, S. Höfling, K. Lüdge, C. Schneider, and S. Reitzenstein, 2017, “On-chip optoelectronic feedback in a micropillar laser-detector assembly,” *Optica* **4**, 303–306.
- Murphy, T. E., A. B. Cohen, B. Ravoori, K. R. B. Schmitt, A. V. Setty, F. Sorrentino, C. R. S. Williams, E. Ott, and R. Roy, 2010, “Complex dynamics and synchronization of delayed-feedback nonlinear oscillators,” *Phil. Trans. R. Soc. A* **368**, 343–366.
- Murphy, T. E., and R. Roy, 2008, “Chaotic lasers: The world’s fastest dice,” *Nat. Photonics* **2**, 714–715.
- Mutugala, U. S., *et al.*, 2017, “Optoelectronic oscillator incorporating hollow-core photonic bandgap fiber,” *Opt. Lett.* **42**, 2647–2650.
- Nakazawa, M., T. Nakashima, and M. Tokuda, 1984, “An optoelectronic self-oscillatory circuit with an optical fiber delayed feedback and its injection locking technique,” *J. Lightwave Technol.* **2**, 719–730.
- Nakazawa, M., M. Tokuda, and N. Uchida, 1981, “Self-sustained intensity oscillation of a laser diode introduced by a delayed electrical feedback using an optical fiber and an electrical amplifier,” *Appl. Phys. Lett.* **39**, 379–381.
- Neyer, A., and E. Voges, 1981, “Nonlinear electrooptic oscillator using an integrated interferometer,” *Opt. Commun.* **37**, 169–174.
- Neyer, A., and E. Voges, 1982a, “Dynamics of electrooptic bistable devices with delayed feedback,” *IEEE J. Quantum Electron.* **18**, 2009–2015.
- Neyer, A., and E. Voges, 1982b, “High-frequency electro-optic oscillator using an integrated interferometer,” *Appl. Phys. Lett.* **40**, 6–8.
- Neyer, A., and E. Voges, 1982c, “Hybrid electro-optical multivibrator operating by finite feedback delay,” *Electron. Lett.* **18**, 59–60.
- Nguimdo, R. M., Y. K. Chembo, P. Colet, and L. Larger, 2012, “On the phase noise performance of nonlinear double-loop optoelectronic microwave oscillators,” *IEEE J. Quantum Electron.* **48**, 1415–1423.
- Nguimdo, R. M., P. Colet, L. Larger, and L. Pesquera, 2011, “Digital key for chaos communication performing time delay concealment,” *Phys. Rev. Lett.* **107**, 034103.
- Nguimdo, R. M., R. Lavrov, P. Colet, M. Jacquot, Y. K. Chembo, and L. Larger, 2010, “Effect of fiber dispersion on broadband chaos communications implemented by electro-optic nonlinear delay phase dynamics,” *IEEE J. Quantum Electron.* **28**, 2688–2696.
- Nguimdo, R. M., V. Lecocq, Y. K. Chembo, and T. Erneux, 2016, “Effect of time delay on the stability of optoelectronic oscillators based on whispering-gallery mode resonators,” *IEEE J. Quantum Electron.* **52**, 6500107.
- Nguimdo, R. M., K. Saleh, A. Coillet, G. Lin, R. Martinenghi, and Y. K. Chembo, 2015, “Phase noise performance of optoelectronic oscillators based on whispering-gallery mode resonators,” *IEEE J. Quantum Electron.* **51**, 6500308.
- Nguyen, L. D., K. Nakatani, and B. Journet, 2010, “Refractive index measurement by using an optoelectronic oscillator,” *IEEE Photonics Technol. Lett.* **22**, 857–859.
- Nietzke, R., J. Sacher, W. Elsasser, and E. O. Gobel, 1990, “Mode locking of a semiconductor laser by self-synchronising optoelectronic feedback of the longitudinal mode beats,” *Electron. Lett.* **26**, 1016–1018.
- Nourine, M., Y. K. Chembo, and L. Larger, 2011, “Wideband chaos generation using a delayed oscillator and a two-dimensional nonlinearity induced by a quadrature phase-shift-keying electro-optic modulator,” *Opt. Lett.* **36**, 2833–2835.
- Oden, J., R. Lavrov, Y. K. Chembo, and L. Larger, 2017, “Multi-Gbit/s optical phase chaos communications using a time-delayed optoelectronic oscillator with a three-wave interferometer nonlinearity,” *Chaos* **27**, 114311.
- Okada, M., and K. Takizawa, 1979, “Optical multistability in the mirrorless electrooptic device with feedback,” *IEEE J. Quantum Electron.* **15**, 82–85.
- Okada, M., and K. Takizawa, 1980, “Optical regenerative oscillation and monostable pulse generation in electrooptic bistable devices,” *IEEE J. Quantum Electron.* **16**, 770–776.
- Okada, M., and K. Takizawa, 1981, “Instability of an electrooptic bistable device with a delayed feedback,” *IEEE J. Quantum Electron.* **17**, 2135–2140.
- Okusaga, O., J. P. Cahill, A. Docherty, C. R. Menyuk, W. Zhou, and G. M. Carter, 2013, “Suppression of Rayleigh-scattering-induced noise in OEOs,” *Opt. Express* **21**, 22255–22262.
- Oliver, N., L. Larger, and I. Fischer, 2016, “Consistency in experiments on multistable driven delay systems,” *Chaos* **26**, 103115.
- Ortín, S., M. C. Soriano, L. Pesquera, D. Brunner, D. San-Martín, I. Fischer, C. R. Mirasso, and J. M. Gutiérrez, 2015, “A unified framework for reservoir computing and extreme learning machines based on a single time-delayed neuron,” *Sci. Rep.* **5**, 14945.
- Ozdur, I., D. Mandridis, N. Hoghooghi, and P. J. Delfyett, 2010, “Low noise optically tunable opto-electronic oscillator with Fabry-Perot etalon,” *J. Lightwave Technol.* **28**, 3100–3106.
- Pallavisini, A., L. Larger, V. S. Udaltsov, J.-M. Merolla, R. Quéré, N. Butterlin, and J.-P. Goedgebuer, 2007, “Rf-interferences generate chaotic GHz FM-carrier for communications,” *IEEE J. Quantum Electron.* **43**, 426–433.
- Pan, B., D. Lu, L. Zhang, and L. Zhao, 2015, “A widely tunable optoelectronic oscillator based on directly modulated dual-mode laser,” *IEEE Photonics J.* **7**, 1400707.
- Pan, S., and J. Yao, 2009, “Optical clock recovery using a polarization-modulator-based frequency-doubling optoelectronic oscillator,” *J. Lightwave Technol.* **27**, 3531–3539.
- Pan, S., and J. Yao, 2010, “Multichannel optical signal processing in NRZ systems based on a frequency-doubling optoelectronic oscillator,” *IEEE J. Sel. Top. Quantum Electron.* **16**, 1460–1468.
- Paoli, T. L., and J. E. Ripper, 1970a, “Frequency stabilization and narrowing of optical pulses from CW GaAs injection lasers,” *IEEE J. Quantum Electron.* **6**, 335–339.
- Paoli, T. L., and J. E. Ripper, 1970b, “Self-stabilization and narrowing of optical pulses from GaAs junction lasers by injection current feedback,” *Appl. Phys. Lett.* **16**, 96–97.
- Paquot, Y., F. Duport, A. Smerieri, J. Dambre, B. Schrauwen, M. Haelterman, and S. Massar, 2012, “Optoelectronic reservoir computing,” *Sci. Rep.* **2**, 287.
- Pasquazi, A., *et al.*, 2018, “Micro-combs: A novel generation of optical sources,” *Phys. Rep.* **729**, 1–81.
- Paulus, P., R. Langenhorst, and D. Jäger, 1987, “Stable pulsations of semiconductor lasers by optoelectronic feedback with avalanche photodiodes,” *Electron. Lett.* **23**, 471–472.
- Pecora, L. M., and T. L. Carroll, 1990, “Synchronization in chaotic systems,” *Phys. Rev. Lett.* **64**, 821–824.
- Pecora, L. M., F. Sorrentino, A. M. Hagerstrom, T. E. Murphy, and R. Roy, 2014, “Cluster synchronization and isolated desynchronization in complex networks with symmetries,” *Nat. Commun.* **5**, 4079.
- Peil, M., M. Jacquot, Y. K. Chembo, L. Larger, and T. Erneux, 2009, “Routes to chaos and multiple time scale dynamics in broadband bandpass nonlinear delay electro-optic oscillators,” *Phys. Rev. E* **79**, 026208.

- Peil, M., L. Larger, and I. Fischer, 2007, “Versatile and robust chaos synchronization phenomena imposed by delayed shared feedback coupling,” *Phys. Rev. E* **76**, 045201.
- Peng, H., *et al.*, 2017, “Wideband tunable optoelectronic oscillator based on the deamplification of stimulated Brillouin scattering,” *Opt. Express* **25**, 10287.
- Pieroux, D., T. Erneux, A. Gavrielides, and V. Kovanis, 2000, “Hopf bifurcation subject to a large delay in a laser system,” *SIAM J. Appl. Math.* **61**, 966–982.
- Plaschak, M. E., R. B. Ramirez, K. Bagnell, and P. J. Delfyett, 2018, “Tunable broadband electro-optic comb generation using an optically filtered optoelectronic oscillator,” *IEEE Photonics Technol. Lett.* **30**, 335–338.
- Poinsot, S., H. Porte, J.-P. Goedgebuer, W. T. Rhodes, and B. Boussert, 2002, “Continuous radio-frequency tuning of an optoelectronic oscillator with dispersive feedback,” *Opt. Lett.* **27**, 1300–1302.
- Qin, J., Q. Zhao, H. Yin, Y. Jin, and C. Liu, 2017, “Numerical simulation and experiment on optical packet header recognition utilizing reservoir computing based on optoelectronic feedback,” *IEEE Photonics J.* **9**, 7901311.
- Qu, S., T. Jin, H. Chi, G. Tong, F. Ren, and X. Zhao, 2015, “An optoelectronic oscillator using an FBG and an FBG-based Fabry-Perot filter,” *Opt. Commun.* **342**, 141–143.
- Quinlan, F., C. Williams, S. Ozharar, S. Gee, and P. J. Delfyett, 2008, “Self-stabilization of the optical frequencies and the pulse repetition rate in a coupled optoelectronic oscillator,” *J. Lightwave Technol.* **26**, 2571–2577.
- Ravoori, B., A. B. Cohen, J. Sun, A. E. Motter, T. E. Murphy, and R. Roy, 2011, “Robustness of optimal synchronization in real networks,” *Phys. Rev. Lett.* **107**, 034102.
- Rogers, E. A., R. Kalra, R. D. Schroll, A. Uchida, D. P. Lathrop, and R. Roy, 2004, “Generalized synchronization of spatiotemporal chaos in a liquid crystal spatial light modulator,” *Phys. Rev. Lett.* **93**, 084101.
- Romeira, B., R. Avó, J. M. L. Figueiredo, S. Barland, and J. Javaloyes, 2016, “Regenerative memory in time-delayed neuromorphic photonic resonators,” *Sci. Rep.* **6**, 19510.
- Romeira, B., J. M. L. Figueiredo, and J. Javaloyes, 2017, “Delay dynamics of neuromorphic optoelectronic nanoscale resonators: Perspectives and applications,” *Chaos* **27**, 114323.
- Romeira, B., F. Kong, W. Li, J. M. L. Figueiredo, J. Javaloyes, and J. Yao, 2014, “Broadband chaotic signals and breather oscillations in an optoelectronic oscillator incorporating a microwave photonic filter,” *J. Lightwave Technol.* **32**, 3933–3942.
- Romeira, B., K. Seunarine, C. N. Ironside, A. E. Kelly, and J. M. L. Figueiredo, 2011, “A self-synchronized optoelectronic oscillator based on an RTD photodetector and a laser diode,” *IEEE Photonics Technol. Lett.* **23**, 1148–1150.
- Romisch, S., J. Kitching, E. Ferre-Pikal, L. Hollberg, and F. L. Walls, 2000, “Performance evaluation of an optoelectronic oscillator,” *IEEE Trans. Ultrason. Ferroelectr. Freq. Control* **47**, 1159–1165.
- Rontani, D., A. Locquet, M. Sciamanna, D. S. Citrin, and A. Uchida, 2011, “Generation of orthogonal codes with chaotic optical systems,” *Opt. Lett.* **36**, 2287–2289.
- Rosin, D. P., K. E. Callan, D. J. Gauthier, and E. Schöll, 2011, “Pulse-train solutions and excitability in an optoelectronic oscillator,” *Europhys. Lett.* **96**, 34001.
- Rubiola, E., 2010, *Phase Noise and Frequency Stability in Oscillators* (Cambridge University Press, Cambridge, England).
- Sakamoto, T., T. Kawanishi, and M. Izutsu, 2007, “Optoelectronic oscillator employing reciprocating optical modulator for millimetre-wave generation,” *Electron. Lett.* **43**, 1031–1033.
- Saleh, K., and Y. K. Chembo, 2017, “Phase noise performance comparison between microwaves generated with Kerr optical frequency combs and optoelectronic oscillators,” *Electron. Lett.* **53**, 264–266.
- Saleh, K., R. Henriët, S. Diallo, G. Lin, R. Martinenghi, I. V. Balakireva, P. Salzenstein, A. Coillet, and Y. K. Chembo, 2014, “Phase noise performance comparison between optoelectronic oscillators based on optical delay lines and whispering gallery mode resonators,” *Opt. Express* **22**, 32158.
- Saleh, K., G. Lin, and Y. K. Chembo, 2015, “Effect of laser coupling and active stabilization on the phase noise performance of optoelectronic microwave oscillators based on whispering-gallery-mode resonators,” *IEEE Photonics J.* **7**, 5500111.
- Saleh, K., O. Llopis, and G. Cibiel, 2013, “Optical scattering induced noise in fiber ring resonators and optoelectronic oscillators,” *J. Lightwave Technol.* **31**, 1433–1446.
- Salik, E., N. Yu, and L. Maleki, 2007, “An ultralow phase noise coupled optoelectronic oscillator,” *IEEE Photonics Technol. Lett.* **19**, 444–446.
- Schlaak, H. F., A. Neyer, and W. Sohler, 1980, “Electrooptical oscillator using an integrated cutoff modulator,” *Opt. Commun.* **32**, 72–74.
- Schlaak, H. F., and R. Th. Kersten, 1981, “Integrated optical oscillators and their applications to optical communication systems,” *Opt. Commun.* **36**, 186–188.
- Schnapper, A., M. Papuchon, and C. Puech, 1979, “Optical bistability using an integrated two arm interferometer,” *Opt. Commun.* **29**, 364–368.
- Sciamanna, M., and K. A. Shore, 2015, “Physics and applications of laser diode chaos,” *Nat. Photonics* **9**, 151–162.
- Seo, D. H., and S. H. Yim, 2017, “Frequency pulling effect of an intraloop atomic filter in an optoelectronic oscillator,” *Appl. Opt.* **56**, 666–670.
- Shahverdiev, E. M., R. A. Nuriev, R. H. Hashimov, and K. A. Shore, 2005, “Parameter mismatches, variable delay times and synchronization in time-delayed systems,” *Chaos Solitons Fractals* **25**, 325–331.
- Shang, S., A. Wen, Y. Gao, and W. Zhang, 2017, “Tunable frequency-doubled optoelectronic oscillator based on a phase modulator in a Sagnac loop,” *Optik* **145**, 617–622.
- Shao, Y., X. Han, M. Li, and M. Zhao, 2018, “RF signal detection by a tunable optoelectronic oscillator based on a PS-FBG,” *Opt. Lett.* **43**, 1199–1202.
- Shapiro, J. H., G. Saplakoglu, S.-T. Ho, P. Kumar, B. E. A. Saleh, and M. C. Teich, 1987, “Theory of light detection in the presence of feedback,” *J. Opt. Soc. Am. B* **4**, 1604–1620.
- Sherman, A., and M. Horowitz, 2013, “Ultralow-repetition-rate pulses with ultralow jitter generated by passive mode-locking of an optoelectronic oscillator,” *J. Opt. Soc. Am. B* **30**, 2980.
- Shi, M., L. Yi, W. Wei, and W. Hu, 2018, “Generation and phase noise analysis of a wide optoelectronic oscillator with ultra-high resolution based on stimulated Brillouin scattering,” *Opt. Express* **26**, 16113–16124.
- Shin, M., and P. Kumar, 2007, “Optical microwave frequency up-conversion via a frequency-doubling optoelectronic oscillator,” *IEEE Photonics Technol. Lett.* **19**, 1726–1728.
- Shumaker, E., and G. Eisenstein, 2008, “A novel multiloop optoelectronic oscillator,” *IEEE Photonics Technol. Lett.* **20**, 1881–1883.
- Smith, P., E. Turner, and P. Maloney, 1978, “Electrooptic nonlinear Fabry-Pérot devices,” *IEEE J. Quantum Electron.* **14**, 207–212.

- Smith, P. W., I. P. Kaminow, P. J. Maloney, and L. W. Stulz, 1978, "Integrated bistable optical devices," *Appl. Phys. Lett.* **33**, 24–26.
- Smith, P. W., and E. H. Turner, 1977, "A bistable Fabry-Perot resonator," *Appl. Phys. Lett.* **30**, 280–281.
- Smith, P. W., E. H. Turner, and B. B. Mumford, 1978, "Nonlinear electro-optic Fabry-Perot devices using reflected-light feedback," *Opt. Lett.* **2**, 55–57.
- Sohler, W., 1980, "Optical bistable device as electro-optical multi-vibrator," *Appl. Phys. Lett.* **36**, 351–353.
- Soriano, M. C., J. García-Ojalvo, C. R. Mirasso, and I. Fischer, 2013, "Complex photonics: Dynamics and applications of delay-coupled semiconductor lasers," *Rev. Mod. Phys.* **85**, 421–470.
- Soriano, M. C., S. Ortín, D. Brunner, L. Larger, C. R. Mirasso, I. Fischer, and L. Pesquera, 2013, "Optoelectronic reservoir computing: tackling noise-induced performance degradation," *Opt. Express* **21**, 12–20.
- Stekalov, D., D. Aveline, N. Yu, R. Thompson, A. B. Matsko, and L. Maleki, 2003, "Stabilizing an optoelectronic microwave oscillator with photonic filters," *J. Lightwave Technol.* **21**, 3052–3061.
- Stekalov, D. V., C. Marquardt, A. B. Matsko, H. G. Schwefel, and G. Leuchs, 2016, "Nonlinear and quantum optics with whispering gallery resonators," *J. Opt.* **18**, 123002.
- Suelzer, J. S., T. B. Simpson, P. Devgan, and N. G. Usechak, 2017, "Tunable, low-phase-noise microwave signals from an optically injected semiconductor laser with opto-electronic feedback," *Opt. Lett.* **42**, 3181.
- Sun, W. H., W. Li, W. T. Wang, J. G. Liu, and N. H. Zhu, 2014, "Reconfigurable microwave photonic filter with negative coefficient based on an optoelectronic oscillator," *Opt. Commun.* **321**, 73–77.
- Sung, H.-K., X. Zhao, E. K. Lau, D. Parekh, C. J. Chang-Hasnain, and M. C. Wu, 2009, "Optoelectronic oscillators using direct-modulated semiconductor lasers under strong optical injection," *IEEE J. Sel. Top. Quantum Electron.* **15**, 572–577.
- Takizawa, T., Y. Liu, and J. Ohtsubo, 1994, "Chaos in a feedback Fabry-Perot interferometer," *IEEE J. Quantum Electron.* **30**, 334–338.
- Talla, A. F., R. Martinenghi, G. R. G. Chengui, J. H. T. Mbé, K. Saleh, A. Coillet, G. Lin, P. Woaf, and Y. K. Chembo, 2015, "Analysis of phase-locking in narrow-band optoelectronic oscillators with intermediate frequency," *IEEE J. Quantum Electron.* **51**, 5000108.
- Talla, A. F., R. Martinenghi, P. Woaf, and Y. K. Chembo, 2016, "Breather and pulse-package dynamics in multilinear electro-optical systems with delayed feedback," *IEEE Photonics J.* **8**, 7803608.
- Talla Mbé, J. H., J. S. D. Kamaha, Y. K. Chembo, and P. Woaf, 2019, "Dynamics of wideband time-delayed optoelectronic oscillators with nonlinear filters," *IEEE J. Quantum Electron.* **55**, 5000106.
- Talla Mbé, J. H., A. F. Talla, G. R. G. Chengui, A. Coillet, L. Larger, P. Woaf, and Y. K. Chembo, 2015, "Mixed-mode oscillations in slow-fast delayed optoelectronic systems," *Phys. Rev. E* **91**, 012902.
- Talla Mbé, J. H., P. Woaf, and Y. K. Chembo, 2019, "A normal form method for the determination of oscillations characteristics near the primary Hopf bifurcation in bandpass optoelectronic oscillators: Theory and experiment," *Chaos* **29**, 033104.
- Tang, H., Y. Yu, Z. Wang, L. Xu, and X. Zhang, 2018, "Wideband tunable optoelectronic oscillator based on a microwave photonic filter with an ultra-narrow passband," *Opt. Lett.* **43**, 2328–2331.
- Tang, J., T. Hao, W. Li, D. Domenech, R. Baños, P. Muñoz, N. Zhu, J. Capmany, and M. Li, 2018, "Integrated optoelectronic oscillator," *Opt. Express* **26**, 12257–12265.
- Tang, S., and J. M. Liu, 2001a, "Chaotic pulsing and quasi-periodic route to chaos in a semiconductor laser with delayed optoelectronic feedback," *IEEE J. Quantum Electron.* **37**, 329–336.
- Tang, S., and J. M. Liu, 2001b, "Message encoding-decoding at 2.5 Gbits/s through synchronization of chaotic pulsing semiconductor lasers," *Opt. Lett.* **26**, 1843–1845.
- Tang, S., and J. M. Liu, 2001c, "Synchronization of high-frequency chaotic optical pulses," *Opt. Lett.* **26**, 596–598.
- Tang, S., and J. M. Liu, 2003, "Experimental verification of anticipated and retarded synchronization in chaotic semiconductor lasers," *Phys. Rev. Lett.* **90**, 194101.
- Tang, S., R. Vicente, M. C. Chiang, C. R. Mirasso, and J.-M. Liu, 2004, "Nonlinear dynamics of semiconductor lasers with mutual optoelectronic coupling," *IEEE J. Sel. Top. Quantum Electron.* **10**, 936–943.
- Tang, W. W., and C. Shu, 2005, "Self-starting picosecond optical pulse source using stimulated Brillouin scattering in an optical fiber," *Opt. Express* **13**, 171–174.
- Tang, Y., M. Wang, J. Sun, B. Wu, J. Zhang, Q. Ding, and T. Li, 2017, "Multifold clock recovery and demultiplexing based on a polarization-dependent phase modulator incorporated frequency-doubling optoelectronic oscillator," *Opt. Commun.* **403**, 304–311.
- Tang, Y., M. Wang, B. Wu, J. Zhang, Q. Ding, H. Mu, B. Yin, J. Sun, and F. Yan, 2018, "Chromatic dispersion measurement based on a high-Q optoelectronic oscillator incorporating cascaded FIR and IIR filters," *Continuum Mech. Thermodyn.* **1**, 1205–1214.
- Tang, Z., S. Pan, D. Zhu, R. Guo, Y. Zhao, M. Pan, D. Ben, and J. Yao, 2012, "Tunable optoelectronic oscillator based on a polarization modulator and a chirped FBG," *IEEE Photonics Technol. Lett.* **24**, 1487–1489.
- Tang, Z., F. Zhang, and S. Pan, 2014, "Photonic microwave down-converter based on an optoelectronic oscillator using a single dual-drive Mach-Zehnder modulator," *Opt. Express* **22**, 305.
- Taubman, M. S., H. Wiseman, D. E. McClelland, and H.-A. Bachor, 1995, "Intensity feedback effects on quantum-limited noise," *J. Opt. Soc. Am. B* **12**, 1792–1800.
- Teng, Y., Y. Chen, B. Zhang, J. Li, L. Lu, Y. Zhu, and P. Zhang, 2016, "Generation of low phase-noise frequency-sextupled signals based on multimode optoelectronic oscillator and cascaded Mach-Zehnder modulators," *IEEE Photonics J.* **8**, 7803708.
- Terra, O., 2019a, "Chromatic dispersion measurement in optical fibers using optoelectronic oscillations," *Opt. Laser Technol.* **115**, 292–297.
- Terra, O., 2019b, "Optoelectronic oscillations for thermo-optic coefficient measurement of optical fibers," *Meas. Sci. Technol.* **30**, 035205.
- Tezuka, M., K. Kanno, and M. Bunsen, 2016, "Reservoir computing with a slowly modulated mask signal for preprocessing using a mutually coupled optoelectronic system," *Jpn. J. Appl. Phys.* **55**, 08RE06.
- Tian, W., L. Zhang, J. Ding, S. Shao, X. Fu, and L. Yang, 2018, "Ultrafast physical random bit generation from a chaotic oscillator with a silicon modulator," *Opt. Lett.* **43**, 4839–4842.
- Tong, G., T. Jin, H. Chi, X. Zhu, T. Lai, and X. Wu, 2017, "A novel optoelectronic oscillator based on Brillouin-induced slow light effect," *IEEE Photonics Technol. Lett.* **29**, 1375–1378.
- Totz, J. F., J. Rode, M. R. Tinsley, K. Showalter, and H. Engel, 2018, "Spiral wave chimera states in large populations of coupled chemical oscillators," *Nat. Phys.* **14**, 282–285.

- Tseng, W.-H., and K.-M. Feng, 2012, "Enhancing long-term stability of the optoelectronic oscillator with a probe-injected fiber delay monitoring mechanism," *Opt. Express* **20**, 1597–1607.
- Tsuchida, H., and M. Suzuki, 2005, "40-Gb/s optical clock recovery using an injection-locked optoelectronic oscillator," *IEEE Photonics Technol. Lett.* **17**, 211–213.
- Uchida, A., K. Mizumura, and S. Yoshimori, 2006, "Chaotic dynamics and synchronization in microchip solid-state lasers with optoelectronic feedback," *Phys. Rev. E* **74**, 066206.
- Uchida, A., F. Rogister, J. García-Ojalvo, and R. Roy, 2005, "Synchronization and communication with chaotic laser systems," in *Progress in Optics*, Vol. 48, edited by E. Wolf (Elsevier, New York), pp. 203–341.
- Uchida, A., *et al.*, 2008, "Fast physical random bit generation with chaotic semiconductor lasers," *Nat. Photonics* **2**, 728–732.
- Udaltsov, V. S., J.-P. Goedgebuer, L. Larger, J.-B. Cuenot, P. Levy, and W. T. Rhodes, 2003, "Cracking chaos-based encryption systems ruled by nonlinear time delay differential equations," *Phys. Lett. A* **308**, 54–60.
- Udaltsov, V. S., J.-P. Goedgebuer, L. Larger, and W. T. Rhodes, 2001, "Dynamics of non-linear feedback systems with short time-delays," *Opt. Commun.* **195**, 187–196.
- Urick, V. J., P. S. Devgan, J. D. McKinney, F. Bucholtz, and K. J. Williams, 2009, "Channelisation of radio-frequency signals using optoelectronic oscillator," *Electron. Lett.* **45**, 1242–1244.
- Ustinov, A. B., A. A. Nikitin, V. V. Lebedev, A. A. Serebrennikov, A. V. Shamray, A. V. Kondrashov, and B. A. Kalinikos, 2018, "A low phase noise tunable microwave spin wave optoelectronic oscillator," *J. Phys. Conf. Ser.* **1038**, 012033.
- Vallée, R., and C. Delisle, 1985, "Mode description of the dynamical evolution of an acousto-optic bistable device," *IEEE J. Quantum Electron.* **21**, 1423–1428.
- Vallet, M., M. Romanelli, G. Loas, F. Van Dijk, and M. Alouini, 2016, "Self-stabilized optoelectronic oscillator using frequency-shifted feedback and a delay line," *IEEE Photonics Technol. Lett.* **28**, 1088–1091.
- Van der Sande, G., D. Brunner, and M. C. Soriano, 2017, "Advances in photonic reservoir computing," *Nanophotonics* **6**, 561–576.
- Van Dijk, F., A. Enard, X. Buet, F. Lelarge, and G.-H. Duan, 2008, "Phase noise reduction of a quantum dash mode-locked laser in a millimeter-wave coupled opto-electronic oscillator," *J. Lightwave Technol.* **26**, 2789–2794.
- VanWiggeren, G. D., and R. Roy, 1998a, "Communication with chaotic lasers," *Science* **279**, 1198–1200.
- VanWiggeren, G. D., and R. Roy, 1998b, "Optical communication with chaotic waveforms," *Phys. Rev. Lett.* **81**, 3547–3550.
- Verstraeten, D., B. Schrauwen, M. D'Haene, and D. Strooband, 2007, "An experimental unification of reservoir computing methods," *Neural Netw.* **20**, 391–403.
- Vicente, R., J. Dauden, P. Colet, and R. Toral, 2005, "Analysis and characterization of the hyperchaos generated by a semiconductor laser subject to a delayed feedback loop," *IEEE J. Quantum Electron.* **41**, 541–548.
- Volyanskiy, K., Y. K. Chembo, L. Larger, and E. Rubiola, 2010, "Contribution of laser frequency and power fluctuations to the microwave phase noise of optoelectronic oscillators," *J. Lightwave Technol.* **28**, 2730–2735.
- Volyanskiy, K., P. Salzenstein, H. Tavernier, M. Pogurmirskiy, Y. K. Chembo, and L. Larger, 2010, "Compact optoelectronic microwave oscillators using ultra-high Q whispering gallery mode disk-resonators and phase modulation," *Opt. Express* **18**, 22358–22363.
- Vorontsov, M. A., G. W. Carhart, and R. Dou, 2000, "Spontaneous optical pattern formation in a large array of optoelectronic feedback circuits," *J. Opt. Soc. Am. B* **17**, 266–274.
- Wang, G., T. Hao, W. Li, N. Zhu, and M. Li, 2019, "Detection of wideband low-power RF signals using a stimulated Brillouin scattering-based optoelectronic oscillator," *Opt. Commun.* **439**, 133–136.
- Wang, J., J. Yu, W. Miao, B. Sun, S. Jia, W. Wang, and Q. Wu, 2014, "Long-range, high-precision absolute distance measurement based on two optoelectronic oscillators," *Opt. Lett.* **39**, 4412–4415.
- Wang, L., N. Zhu, W. Li, and J. Liu, 2011, "A frequency-doubling optoelectronic oscillator based on a dual-parallel Mach-Zehnder modulator and a chirped fiber Bragg grating," *IEEE Photonics Technol. Lett.* **23**, 1688–1690.
- Wang, L. X., N. H. Zhu, J. Y. Zheng, J. G. Liu, and W. Li, 2012, "Chaotic ultra-wideband radio generator based on an optoelectronic oscillator with a built-in microwave photonic filter," *Appl. Opt.* **51**, 2935–2940.
- Wang, M., and J. Yao, 2013, "Tunable optical frequency comb generation based on an optoelectronic oscillator," *IEEE Photonics Technol. Lett.* **25**, 2035–2038.
- Wang, P., *et al.*, 2015, "Frequency tunable optoelectronic oscillator based on a directly modulated DFB semiconductor laser under optical injection," *Opt. Express* **23**, 20450.
- Wang, Q., L. Huo, Y. Xing, D. Wang, X. Chen, C. Lou, and B. Zhou, 2014, "Gaussian-like dual-wavelength prescaled clock recovery with simultaneous frequency-doubled clock recovery using an optoelectronic oscillator," *Opt. Express* **22**, 2798.
- Wang, W. T., W. Li, and N. H. Zhu, 2014, "Frequency quadrupling optoelectronic oscillator using a single polarization modulator in a Sagnac loop," *Opt. Commun.* **318**, 162–165.
- Wang, W. Yu., W. Li, W. H. Sun, W. Wang, J. G. Liu, and N. H. Zhu, 2015, "Triangular microwave waveforms generation based on an optoelectronic oscillator," *IEEE Photonics Technol. Lett.* **27**, 522–525.
- Wang, Y., Y. Shan, L. Pan, X. Wang, C. Meng, W. Dong, and X. Zhang, 2017, "A tunable frequency-decouple optoelectronic oscillator based on frequency comb and stimulated Brillouin scattering," *Opt. Quantum Electron.* **49**, 253.
- Wang, Y., M. Wang, W. Xia, X. Ni, and D. Wu, 2017, "Optical fiber Bragg grating pressure sensor based on dual-frequency optoelectronic oscillator," *IEEE Photonics Technol. Lett.* **29**, 1864–1867.
- Wang, Y., J. Zhang, and J. Yao, 2016, "An optoelectronic oscillator for high sensitivity temperature sensing," *IEEE Photonics Technol. Lett.* **28**, 1458–1461.
- Wei, Z., R. Wang, T. Pu, G. Sun, T. Fang, and J. Zheng, 2013, "A tunable optoelectronic oscillator based on a tunable microwave attenuator," *Opt. Fiber Technol.* **19**, 383–386.
- Weicker, L., T. Erneux, O. D'Huys, J. Danckaert, M. Jacquot, Y. Chembo, and L. Larger, 2012, "Strongly asymmetric square waves in a time-delayed system," *Phys. Rev. E* **86**, 055201.
- Weicker, L., T. Erneux, O. D'Huys, J. Danckaert, M. Jacquot, Y. Chembo, and L. Larger, 2013, "Slow-fast dynamics of a time-delayed electro-optic oscillator," *Phil. Trans. R. Soc. A* **371**, 20120459.
- Weicker, L., T. Erneux, M. Jacquot, Y. Chembo, and L. Larger, 2012, "Crenelated fast oscillatory outputs of a two-delay electro-optic oscillator," *Phys. Rev. E* **85**, 026206.
- Williams, C. R. S., T. E. Murphy, R. Roy, F. Sorrentino, T. Dahms, and E. Schöll, 2013, "Experimental observations of group synchrony in a system of chaotic optoelectronic oscillators," *Phys. Rev. Lett.* **110**, 064104.

- Wishon, M. J., D. Choi, T. Niebur, N. Webster, Y. K. Chembo, E. A. Viktorov, D. S. Citrin, and A. Locquet, 2018, “Low-noise X-band tunable microwave generator based on a semiconductor laser with feedback,” *IEEE Photonics Technol. Lett.* **30**, 1597–1600.
- Woods, D., and T. J. Naughton, 2012, “Photonic neural networks,” *Nat. Phys.* **8**, 257–259.
- Wu, B., M. Wang, Y. Dong, Y. Tang, H. Mu, H. Li, B. Yin, F. Yan, and Z. Han, 2018, “Magnetic field sensor based on a dual-frequency optoelectronic oscillator using cascaded magnetostrictive alloy-fiber Bragg grating-Fabry Perot and fiber Bragg grating-Fabry Perot filters,” *Opt. Express* **26**, 27628–27638.
- Wu, B., M. Wang, J. Sun, B. Yin, H. Chen, T. Li, and S. Jian, 2016, “Frequency- and phase-tunable optoelectronic oscillator based on a DPMZM and SBS effect,” *Opt. Commun.* **363**, 123–127.
- Wu, T., Y. Jiang, C. Ma, Z. Jia, G. Bai, Y. Zi, and F. Huang, 2016, “Simultaneous triangular waveform signal and microwave signal generation based on dual-loop optoelectronic oscillator,” *IEEE Photonics J.* **8**, 7805610.
- Wu, W.-T., Y.-H. Liao, and F.-Y. Lin, 2010, “Noise suppressions in synchronized chaos lidars,” *Opt. Express* **18**, 26155–26162.
- Xia, G.-Q., Z.-M. Wu, and J.-F. Liao, 2009, “Theoretical investigations of cascaded chaotic synchronization and communication based on optoelectronic negative feedback semiconductor lasers,” *Opt. Commun.* **282**, 1009–1015.
- Xiao, K., X. Jin, X. Jin, X. Yu, Q. Tan, and G. Wang, 2019, “Tunable OEO-based photonic RF receiver with image frequency rejection,” *Appl. Opt.* **58**, 2127–2131.
- Xiao, X., S. Li, Z. Xie, S. Peng, D. Wu, X. Xue, X. Zheng, and B. Zhou, 2018, “Photonic harmonic up-converter based on a self-oscillating optical frequency comb using a DP-DPMZM,” *Opt. Commun.* **413**, 48–53.
- Xie, X., T. Sun, H. Peng, C. Zhang, P. Guo, L. Zhu, W. Hu, and Z. Chen, 2014, “Low-noise and broadband optical frequency comb generation based on an optoelectronic oscillator,” *Opt. Lett.* **39**, 785–788.
- Xie, X., C. Zhang, T. Sun, P. Guo, X. Zhu, L. Zhu, W. Hu, and Z. Chen, 2013, “Wideband tunable optoelectronic oscillator based on a phase modulator and a tunable optical filter,” *Opt. Lett.* **38**, 655–7.
- Xie, X., *et al.*, 2017, “Photonic microwave signals with zeptosecond-level absolute timing noise,” *Nat. Photonics* **11**, 44–48.
- Xie, Y.-Y., H.-J. Che, W.-L. Zhao, Y.-X. Huang, W.-H. Xu, X. Li, Q. Kan, and J.-C. Li, 2014, “Dynamics of 1550-nm VCSELs with positive optoelectronic feedback: Theory and experiments,” *IEEE Photonics J.* **6**, 1502508.
- Xie, Z., S. Li, H. Yan, X. Xiao, X. Zheng, and B. Zhou, 2016, “Tunable dual frequency optoelectronic oscillator with low intermodulation based on dual-parallel Mach-Zehnder modulator,” *Opt. Express* **24**, 30282.
- Xiong, J., R. Wang, T. Fang, T. Pu, D. Chen, L. Lu, P. Xiang, J. Zheng, and J. Zhao, 2013, “Low-cost and wideband frequency tunable optoelectronic oscillator based on a directly modulated distributed feedback semiconductor laser,” *Opt. Lett.* **38**, 4128.
- Xu, O., J. Zhang, H. Deng, and J. Yao, 2017, “Dual-frequency optoelectronic oscillator for thermal-insensitive interrogation of a FBG strain sensor,” *IEEE Photonics Technol. Lett.* **29**, 357–360.
- Xu, W., T. Jin, and H. Chi, 2013, “Frequency multiplying optoelectronic oscillator based on nonlinearly-coupled double loops,” *Opt. Express* **21**, 32516.
- Xu, X., J. Dai, Y. Dai, F. Yin, Y. Zhou, J. Li, J. Yin, Q. Wang, and K. Xu, 2015, “Broadband and wide-range feedback tuning scheme for phase-locked loop stabilization of tunable optoelectronic oscillators,” *Opt. Lett.* **40**, 5858.
- Xuan, Z., L. Du, and F. Aflatouni, 2019, “Frequency locking of semiconductor lasers to RF oscillators using hybrid-integrated opto-electronic oscillators with dispersive delay lines,” *Opt. Express* **27**, 10729–10737.
- Yamamoto, Y., N. Imoto, and S. Machida, 1986, “Amplitude squeezing in a semiconductor laser using quantum nondemolition measurement and negative feedback,” *Phys. Rev. A* **33**, 3243–3261.
- Yanchuk, S., and G. Giacomelli, 2017, “Spatio-temporal phenomena in complex systems with time delays,” *J. Phys. A* **50**, 103001.
- Yang, B., X. Jin, Y. Chen, H. Chi, X. Zhang, S. Zheng, E. Tangdiongga, and T. Koonen, 2013, “Photonic microwave up-conversion of vector signals based on an optoelectronic oscillator,” *IEEE Photonics Technol. Lett.* **25**, 1758–1761.
- Yang, B., X. Jin, H. Chi, X. Zhang, S. Zheng, S. Zou, and H. Chen, 2012, “Optically tunable frequency-doubling Brillouin optoelectronic oscillator with carrier phase-shifted double sideband modulation,” *IEEE Photonics Technol. Lett.* **24**, 1051–1053.
- Yang, J., Y. Jin-Long, W. Yao-Tian, Z. Li-Tai, and Y. En-Ze, 2007, “An optical domain combined dual-loop optoelectronic oscillator,” *IEEE Photonics Technol. Lett.* **19**, 807–809.
- Yang, Y., *et al.*, 2018, “Refractive index and temperature sensing based on an optoelectronic oscillator incorporating a Fabry-Perot fiber bragg grating,” *IEEE Photonics J.* **10**, 6800309.
- Yao, J., 2017, “Optoelectronic oscillators for high speed and high resolution optical sensing,” *J. Lightwave Technol.* **35**, 3489–3497.
- Yao, T., D. Zhu, D. Ben, and S. Pan, 2015, “Distributed MIMO chaotic radar based on wavelength-division multiplexing technology,” *Opt. Lett.* **40**, 1631–1634.
- Yao, X. S., 1997, “High-quality microwave signal generation by use of Brillouin scattering in optical fibers,” *Opt. Lett.* **22**, 1329–1331.
- Yao, X. S., L. Davis, and L. Maleki, 2000, “Coupled optoelectronic oscillators for generating both RF signal and optical pulses,” *J. Lightwave Technol.* **18**, 73–78.
- Yao, X. S., and G. Lutes, 1996, “A high-speed photonic clock and carrier recovery device,” *IEEE Photonics Technol. Lett.* **8**, 688–690.
- Yao, X. S., and L. Maleki, 1994, “High frequency optical subcarrier generator,” *Electron. Lett.* **30**, 1525–1526.
- Yao, X. S., and L. Maleki, 1996a, “Converting light into spectrally pure microwave oscillation,” *Opt. Lett.* **21**, 483–485.
- Yao, X. S., and L. Maleki, 1996b, “Optoelectronic microwave oscillator,” *J. Opt. Soc. Am. B* **13**, 1725–1735.
- Yao, X. S., and L. Maleki, 1996c, “Optoelectronic oscillator for photonic systems,” *IEEE J. Quantum Electron.* **32**, 1141–1149.
- Yao, X. S., and L. Maleki, 2000, “Multiloop optoelectronic oscillator,” *IEEE J. Quantum Electron.* **36**, 79–84.
- Yaowen, L., L. Haibin, Z. Hong, and W. Yinghai, 1999, “Self-similarity in a system with a short-time delayed feedback,” *Phys. Lett. A* **256**, 166–172.
- Ye, L., Y. Ma, W. Wang, J. Wang, J. Yu, and K. Song, 2019, “High-sensitivity angular velocity measurement based on bidirectional coupled optoelectronic oscillator,” *Opt. Commun.* **440**, 201–206.
- Yin, B., M. Wang, S. Wu, Y. Tang, S. Feng, and H. Zhang, 2017, “High sensitivity axial strain and temperature sensor based on dual-frequency optoelectronic oscillator using PMFBG Fabry-Perot filter,” *Opt. Express* **25**, 14106–14113.
- Youn, S.-H., W. Jhe, J.-H. Lee, and J.-S. Chang, 1994, “Effect of vacuum fluctuations on the quantum-mechanical amplitude noise of a laser diode in feedback systems,” *J. Opt. Soc. Am. B* **11**, 102–108.

- Yu, N., E. Salik, and L. Maleki, 2005, "Ultralow-noise mode-locked laser with coupled optoelectronic oscillator configuration," *Opt. Lett.* **30**, 1231–1233.
- Zhang, C., X. Jin, X. Jin, X. Yu, L. Feng, H. Yang, H. Chi, and X. Zhang, 2018, "Photonic vector signal generation based on OEO and optical coherent QPSK modulation," *IEEE Photonics Technol. Lett.* **30**, 1711–1714.
- Zhang, F., B. Gao, P. Zhou, and S. Pan, 2016, "Triangular pulse generation by polarization multiplexed optoelectronic oscillator," *IEEE Photonics Technol. Lett.* **28**, 1645–1648.
- Zhang, J., L. Gao, and J. Yao, 2014, "Tunable optoelectronic oscillator incorporating a single passband microwave photonic filter," *IEEE Photonics Technol. Lett.* **26**, 326–329.
- Zhang, J., M. Wang, Y. Tang, Q. Ding, B. Wu, Y. Yang, H. Mu, B. Yin, and S. Jian, 2018, "High-sensitivity measurement of angular velocity based on an optoelectronic oscillator with an intra-loop Sagnac interferometer," *Opt. Lett.* **43**, 2799–2802.
- Zhang, J., and J. Yao, 2018, "Parity-time-symmetric optoelectronic oscillator," *Sci. Adv.* **4**, eaar6782.
- Zhang, L., A. K. Poddar, U. L. Rohde, and A. S. Daryoush, 2014, "Comparison of optical self-phase locked loop techniques for frequency stabilization of oscillators," *IEEE Photonics J.* **6**, 7903015.
- Zhang, T., J. Xiong, P. Wang, J. Zheng, F. Zhang, T. Pu, and X. Chen, 2015, "Tunable optoelectronic oscillator using FWM dynamics of an optical-injected DFB Laser," *IEEE Photonics Technol. Lett.* **27**, 1313–1316.
- Zhang, T., J. Zhu, T. Guo, J. Wang, and S. Ye, 2013, "Improving accuracy of distance measurements based on an optoelectronic oscillator by measuring variation of fiber delay," *Appl. Opt.* **52**, 3495–3499.
- Zhang, W., and J. Yao, 2018, "Silicon photonic integrated optoelectronic oscillator for frequency-tunable microwave generation," *J. Lightwave Technol.* **36**, 4655–4663.
- Zhang, W. L., W. Pan, B. Luo, X. F. Li, X. H. Zuo, and M. Y. Wang, 2007, "Theoretical study on polarization dynamics of VCSELs with negative optoelectronic feedback," *Appl. Opt.* **46**, 7262–7266.
- Zhang, X., J. Zheng, T. Pu, Y. Zhang, Y. Shi, J. Li, Y. Li, H. Zhu, and X. Chen, 2019, "Simple frequency-tunable optoelectronic oscillator using integrated multi-section distributed feedback semiconductor laser," *Opt. Express* **27**, 7036–7046.
- Zhang, Y., D. Hou, and J. Zhao, 2014, "Long-term frequency stabilization of an optoelectronic oscillator using phase-locked loop," *J. Lightwave Technol.* **32**, 2408–2414.
- Zhao, J., Y. Zhang, H. Lu, D. Hou, S. Zhang, and Z. Wang, 2016, "Chip scale atomic resonator frequency stabilization system with ultra-low power consumption for optoelectronic oscillators," *IEEE Trans. Ultrason. Ferroelectr. Freq. Control* **63**, 1022–1027.
- Zhao, Q., H. Yin, W. Shi, D. Huang, and F. Liu, 2016, "Identification and suppression of the time delay signature of wavelength chaos," *Opt. Rev.* **23**, 689–694.
- Zhao, Q., H. Yin, and H. Zhu, 2018, "Simultaneous recognition of two channels of optical packet headers utilizing reservoir computing subject to mutual-coupling optoelectronic feedback," *Optik* **157**, 951–956.
- Zheng, J., W. Sun, W. Wang, Y. Tong, W. Y. Wang, X. Wang, H. Yuan, J. Liu, and N. Zhu, 2015, "Frequency-doubling OEO using the polarization property of LiNbO₃ modulator," *IEEE Photonics Technol. Lett.* **27**, 1864–1867.
- Zheng, J., H. Wang, J. Fu, L. Wei, S. Pan, L. Wang, J. Liu, and N. Zhu, 2014, "Fiber-distributed ultra-wideband noise radar with steerable power spectrum and colorless base station," *Opt. Express* **22**, 4896–4907.
- Zheng, Y. G., and Z. H. Wang, 2009, "Stability and Hopf bifurcations of an optoelectronic time-delay feedback system," *Nonlinear Dyn.* **57**, 125–134.
- Zhenghua, Z., Y. Chun, C. Zhewei, C. Yuhua, and L. Xianghua, 2016, "An ultra-low phase noise and highly stable optoelectronic oscillator utilizing IL-PLL," *IEEE Photonics Technol. Lett.* **28**, 516–519.
- Zhou, P., F. Zhang, B. Gao, and S. Pan, 2016, "Optical pulse generation by an optoelectronic oscillator with optically injected semiconductor laser," *IEEE Photonics Technol. Lett.* **28**, 1827–1830.
- Zhou, W., and G. Blasche, 2005, "Injection-locked dual optoelectronic oscillator with ultra-low phase noise and ultra-low spurious level," *IEEE Trans. Microwave Theory Tech.* **53**, 929–933.
- Zhu, D., T. Du, and S. Pan, 2018, "A coupled optoelectronic oscillator with performance improved by enhanced spatial hole burning in an erbium-doped fiber," *J. Lightwave Technol.* **36**, 3726–3732.
- Zhu, D., S. Pan, and D. Ben, 2012, "Tunable frequency-quadrupling dual-loop optoelectronic oscillator," *IEEE Photonics Technol. Lett.* **24**, 194–196.
- Zhu, X., M. Cheng, L. Deng, X. Jiang, C. Ke, M. Zhang, S. Fu, M. Tang, P. Shum, and D. Liu, 2017, "An optically coupled electro-optic chaos system with suppressed time-delay signature," *IEEE Photonics J.* **9**, 6601009.
- Zhu, Y., X. Jin, H. Chi, S. Zheng, and X. Zhang, 2014, "High-sensitivity temperature sensor based on an optoelectronic oscillator," *Appl. Opt.* **53**, 5084–5087.
- Zhu, Y., X. Jin, X. Jin, X. Yu, S. Zheng, H. Chi, and X. Zhang, 2016, "A novel scheme of microwave generation based on heterodyne phase locking of an OEO," *IEEE Photonics Technol. Lett.* **28**, 2637–2640.
- Zhu, Z., M. Merklein, D.-Y. Choi, K. Vu, P. Ma, S. J. Madden, and B. J. Eggleton, 2019, "Highly sensitive, broadband microwave frequency identification using a chip-based Brillouin optoelectronic oscillator," *Opt. Express* **27**, 12855–12868.
- Zou, X., M. Li, W. Pan, B. Luo, L. Yan, and L. Shao, 2014, "Optical length change measurement via RF frequency shift analysis of incoherent light source based optoelectronic oscillator," *Opt. Express* **22**, 11129–11139.
- Zou, X., X. Liu, W. Li, P. Li, W. Pan, L. Yan, and L. Shao, 2016, "Optoelectronic oscillators (OEOs) to sensing, measurement, and detection," *IEEE J. Quantum Electron.* **52**, 0601116.